Stent Location Measurement in the Human Body Using Flexible Antenna

by

Yifan Zhang

B.E. in Energy and Power Engine, Hohai University, 2013

Submitted to the Graduate Faculty of

Swanson School of Engineering in partial fulfillment

of the requirements for the degree of

Master of Science in Mechanical Engineering

University of Pittsburgh

2019

UNIVERSITY OF PITTSBURGH

SWANSON SCHOOL OF ENGINEERING

This thesis was presented

by

Yifan Zhang

It was defended on

May 3, 2019

and approved by

William W. Clark, Ph.D., Professor
Director of the Innovation, Product Design, and Entrepreneurship Program
Department of Mechanical Engineering and Materials Science

Jeffrey S. Vipperman, Ph.D., Professor
Department of Mechanical Engineering and Materials Science
Department of Bioengineering

Bryan W. Tillman, M.D., Ph.D., Assistant Professor
Division of Vascular Surgery
University of Pittsburgh Medical Center

Thesis Advisor: William W. Clark, Ph.D., Professor
Department of Mechanical Engineering and Materials Science

Stent Location Measurement in the Human Body Using Flexible Antenna

Yifan Zhang, M.S.

University of Pittsburgh, 2019

Artery injury related hemorrhage is the leading cause of death for soldiers on the battlefield. To save their lives, a perfusion stent has been developed for hemostasis by covering the wound while the blood could still flush through. One basic requirement for such a stent is to place it at marked position where the stent only covers the trauma, while vital vessel branches are not blocked.

This idea is achieved by radio frequency devices, basically including an active radiator called transmitter, and a passive receiver. When the transmitter and the receiver are fixed at certain positions, there would be a unique curve depicting the power magnitude varying with frequency. For preparation, we regularly move the receiver to several positions and record the power curve related with the relative position between the transmitter and the receiver. In field test, when the transmitter is provided with the same frequency scope, if the power curve pattern is matched with one of the recorded patterns, we determine the relative position related with the matched pattern. To realize this purpose, this thesis first focusses on how to improve the circuit structure so that a radiation power is strong enough to be detected. Lots of modeling simulations are included in this part. Next, neural network is applied for the pattern classifying. Though the algorithm for neural network is not the concern of this thesis.

Table of Contents

List of Tables

List of Figures

Preface

This is the thesis for me to obtain the master's degree in mechanical engineering and graduate from the University of Pittsburgh. After engaged in this project for one year.

First, I would like to thank Dr. Clark for always give me guidance when I encounter difficulties. Without his help, I can never make such an impressing achievement. It makes me feel satisfied when I have the chance to save the patients' lives by applying my knowledge learned from the University of Pittsburgh.

I also sincerely appreciate the help from the other faculty members, including Yicheng Ding, who realized the basic idea for this project by developing the first version of antenna. Ryan Naugle, who contributed in auxiliary devices and data collection. Andrew Plesniak, the auto-RF reader developer. And medical school faculties Catherine Go and Jenna Kuhn, who helped me to carry the tests in necropsy.

Though we have achieved our fundamental purpose, there is still a long way to go to make our devices practically available because of some serious drawbacks. Thus, I wish anyone read this thesis could raise their idea for further improvement. Together we can make a significant difference.

Yifan Zhang

Pittsburgh, April 7, 2019

1.0 Introduction

1.1 Background and Motivation

Bleeding caused by various kinds of injuries is a very common occurrence, which can in many cases be stopped effectively by pressing with a finger or bandage on the wounded area. However, for more serious wounds, particularly when the trauma is deep within the body, like aorta injuries caused by bullet or shrapnel on the battlefield, or violent collision in a car accident, external pressure cannot stop bleeding. In cases such as these, hemorrhage can be the leading cause of death if it cannot be readily stopped.

To save the lives of patients in cases such as these, the covered rescue stent has been developed. For example, one kind of self-expanding covered nitinol stent has been a useful tool in treating common carotid artery blowout. (Kim et al, 2006) A stent is a tubular structure that could be placed in a blood vessel, and normally functions as the support to hold the passageway open. For the convenience of deployment, most stents are compressible so that they can be collected into a sheath and advanced smoothly within the artery. After reaching the desired position, it can be expanded and start to take effect. The working state of the stent under these two conditions is shown in Figure 1. Because of this structural property, stents are widely used as the treatment for vascular disease such as angiostenosis and angiemphraxis.

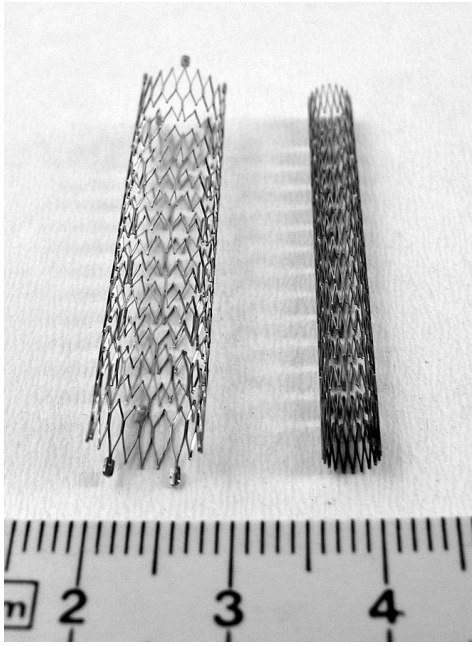

Figure 1 Expanded and compressed artery stent (Müller, 2006).

The idea of achieving hemostasis with a stent is achieved by covering the stent with a material that is impermeable to blood. In the referenced work, the covering material is Polytetrafluoroethylene (PTFE), which is widely used as a gasket material because of its superior resistance to high temperature and aggressive chemicals, as it shown in Figure 2. To stop hemorrhage, the diameter between stent and vessel should be close to each other, so that the PTFE layer could be held by the expanded stent to seal the wound. In fact, the stent should expand so that the covering layer is pressed tightly against the vessel wall. The length of the stent is designed to cover a relatively long distance in the vessel so that it can be effective on wounds in many locations. Though the covered stent has been proved useful in hemostasis, it would cause immediate or delayed cerebral ischemia if it stays permanently in the artery. (Kim et al, 2006) To deal with this problem, a retrievable stent which could temporarily stabilize the patient has been developed at the University of Pittsburgh. (Chun, 2017)

Figure 2 The stent covered with PTFE (ARAN Biomedical)

Placing the stent within human body places special requirements on the design. First, the device must be small enough to fit in the diameter of human arteries, limited by the arteries in the lower limbs where entry occurs. The materials in the stent cannot be harmful to the patient. The device must be easy to operate and be made such that it can be quickly removed when the patient reaches a hospital. Finally, the reliability of the device must be guaranteed.

The stent is designed for emergency use when imaging tools are not available for use to properly place the stent within the body. As a result, the original stent design, shown in Figure 3, was made long enough to cover most parts of the artery for hemostasis. However, this stent also causes a negative effect by blocking major branch vessels from the aorta. Based on this problem, the new stent design is used that has uncovered areas through which blood can perfuse into abdominal organs. The challenge is how to match the stent outlet with the area where the splenic artery, hepatic artery and super mesenteric artery are connected. According to the gender and height of individuals, the location of this area can be estimated and located by simple measurement. (Go, 2019) The results suggest that if the location of the outlet of the

stent can be known with respect to bony landmarks in the body, it can be placed for proper blood perfusion and the negative effect can be minimized.

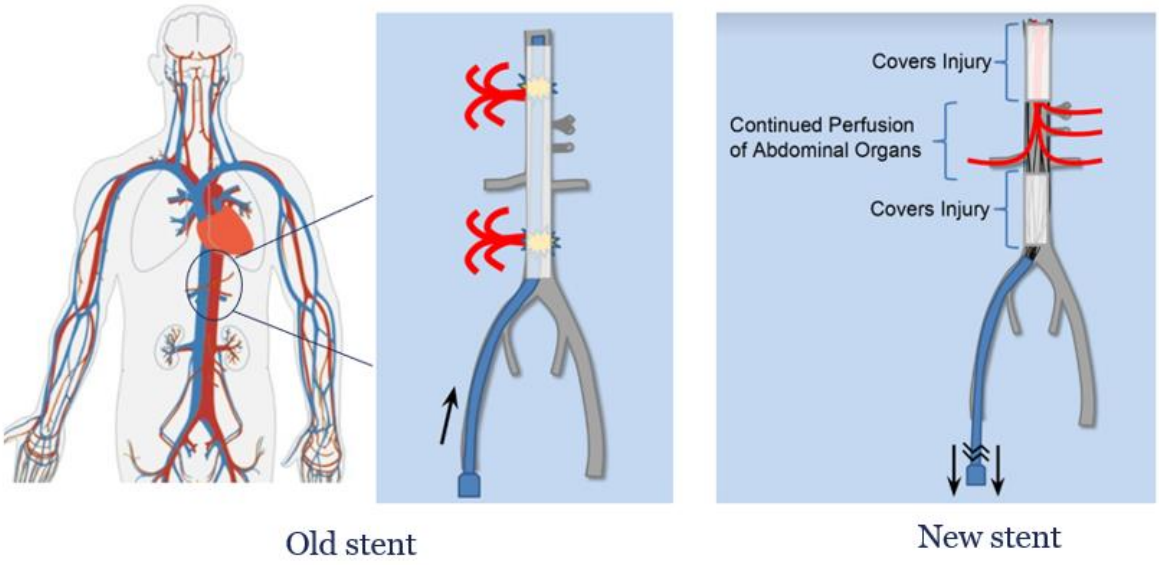

Figure 3 Improved stent with an outlet for blood.

Radio frequency circuits represent one of the potential choices as a means of positioning the stent. Radio frequency circuits are portable and reliable and have been accepted by the public for many applications. For example, chips on smart cards are common. The information stored in the card will be transmitted to the reader when they are in sufficient proximity to each other, and identification of the card can be accomplished within fractions of a second. In this thesis, we utilize radio frequency signals to determine the position of the stent in the body.

The system used in this thesis includes two antennas, a transmitter and a receiver. The transmitter is to be placed within the artery; while the receiver will be fixed outside on the skin, and receives the signal generated by the transmitter. By analyzing the received signal, information of stent's position can be determined.

This thesis is based on the work developed by Yicheng Ding (2018). Radio frequency antenna design and test. University of Pittsburgh. Though the fundamental function of generating and receiving a signal has been achieved, it still far from being applied in the field. To make it practically available, my attempts for improvement include taking into consideration critical factors of antenna performance, optimizing the circuit structure, and applying different materials so that it can be physically embedded within the stent.

Finally, using a reliable antenna, this thesis presents the development of a neural network method for position determination. The neural network contains two separate steps: training and testing. The training for neural network requires a large size of data samples collected under different conditions, which is the discrete distance between the transmitter and receiver in this thesis. With sufficient test data representing known position relationships between transmitting and receiving antennae, the neural network can classify new data into one of the existing classifications so that location information is obtained.

1.2 Literature Review

It was shown from the Centers for Disease Control data in the year of 2000 that trauma-related injuries make up the number one cause of death in people under the age of 44 (Compton, 2005). With a wound that occurs on the surface of the body, hemorrhage control can be achieved with fingers or bandages upon the wound by immediate and direct pressure over it. The bleeding could be stopped with 13.3kPa pressure that directly acts over the wound. This pressure can be easily achieved by an adult whose finger pressure reaches 24kPa in average.

(Astin, 1999). However, hemostasis is much harder to achieve with a deep trauma, which requires the help of specific devices.

One of a basic but effective methods of reducing hemorrhage in a deep wound is to use an occlusive balloon, as the one shown in Figure 4 (Brohi, 2002). The balloon could be advanced in the artery suing the guiding wire, and expanded after reaching the aiming position. With the help of fluoroscopy, the inflated balloon could completely cover the trauma when the location is determined. The blood loss using an occlusive balloon during a successful cesarean hysterectomy has been shown to be limited to 800mL (Jin-Chung, 2005). The balloon is still useful when the trauma cannot be accurately positioned. In this case the balloon should be advanced as deep as possible into the artery. The blood circulation is ceased when the balloon is inflated such that it blocks the passageway within vessel (Kim, 2006). This method is advantageous, because it does not require accurate placement of the balloon with respect to the wound, but because of the blockage of blood flow, the occlusive balloon cannot be left within human body for a long time. To solve this problem, the balloon is replaced with a stent covered by a PTFE film, and the stent is placed such that the wound in the vessel itself is covered by the stent from the inside. In this case, immediate hemostasis can be achieved while the blood can still flow within the affected vessel while simultaneously stopping or greatly reducing hemorrhage at the wound site. Because of this advantage, the PTFE covered stent is called a perfusion stent.

In practical treatment, a patient with progressive dizziness and neck pain caused by hemorrhage from pseudoaneurysm of the right internal carotid artery has been successfully cured with a covered stent. (Scavé, 2001).

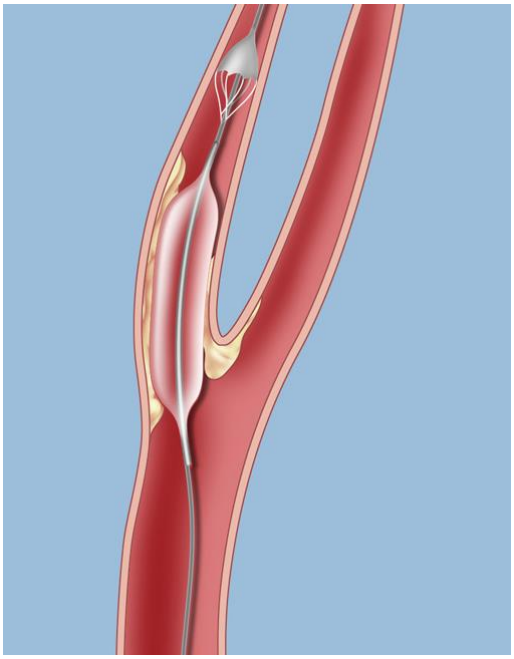

Figure 4 Catheter with balloon on the top (Graves, *2017*)

A retrievable rescue stent has been developed at the University of Pittsburgh, as shown in Figure 5 (Chun, 2017). According to the testing result on pig with aortic injury, this device can stop blood leakage within ten seconds. The stent frame of nickel-titanium allows has flexibility to be used in vessels of various diameters. To test the stent flexibility, a 12mm stent was placed within 13mm and 8mm vessels. For the stent under-size condition, it could reduce 93% of hemorrhage compared with the uncontrolled situation, while for the over-size condition, the blood leakage is completely controlled. (Chun, 2017)

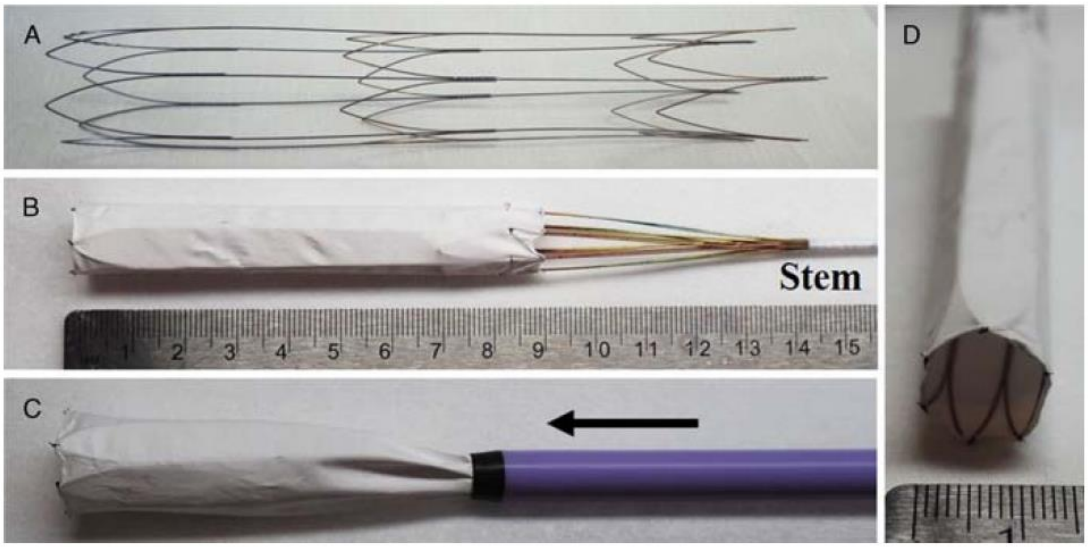

Figure 5 A retrievable rescue stent (a) the nickel-titanium frame of the stent (b) the stent covered with Poly ester-urethane-urea (PEUU) (c) retrieving the stent into a sheath (d) transverse section view of the stent.

The method of the stent deployment is inspired by the schematic of the human circulatory structure. Most organs within human body are connected to the aorta and the main basilic vein by branch vessels. This means that if the supply from the aorta is cut off, then the organs do not get their necessary blood. It also means that stent access to the aorta can be reached by major vessels. In medical practice, Kume developed an angioscope that could successfully reach the coronary artery by entering from femoral artery. (Kume, 1995) Following the same trajectory, if our stent could reach main vessels around the heart and block hemorrhage from what are currently the most fatal traumas, the chance for the patient survival could be increased significantly.

In a hospital setting, the stent could be placed properly with the help of fluoroscopy technique. Using X-rays, it provides a real-time image inside human body. An image of the

deployed perfusion stent of interest in this project is shown in Figure 6(a). However, the size of typical imaging equipment, as shown in Figure 6(b), prevents its use in the field where it would be needed for rapid stent deployment. As a result, our purpose was to develop a portable alternative for the fluoroscopy that can be applied in various conditions.

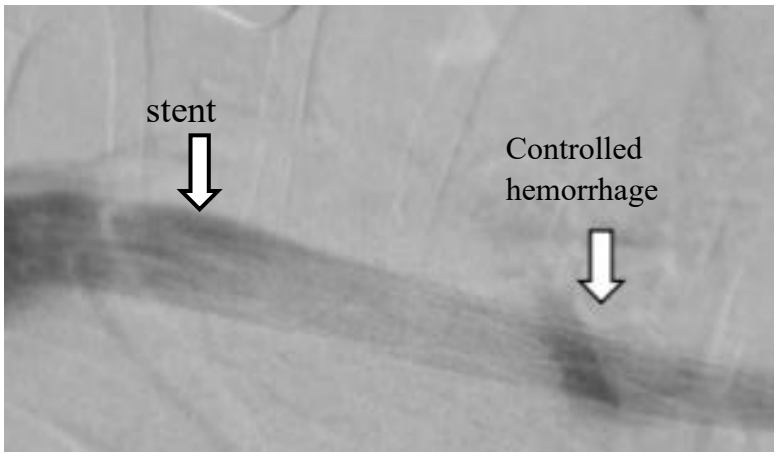

(a)

(b)

Figure 6. Fluoroscopy equipment (Siemens Healthineers)

Though the fluoroscopy technique does not meet the practical requirement for stent deployment in the field, the abundant information carried by electromagnetic field through various tissue is still the basis of developing the new device. In the electromagnetic spectrum, the group with a higher frequency than visible light is classified as ionizing radiation, in which

X-ray for fluoroscopy is included. The groups with lower frequencies are microwaves and radio waves (Lumenistic, 2012). Compared with serious side effects such as vomiting and fainting could be experienced with high doses of X-ray radiation, the harm to human body when exposed to radio waves is slight enough to be ignored. For example, when people are using their cell phone, the effect of radio waves from which is measured by specific absorption rate (SAR), is 1.1W/kg. This value is much lower than the limitation at 1.6W/kg, which would cause no harm to human body. (Brownlee, 2000) (Waight, 1999). This property of radio waves makes it an ideal signal carrier to be applied for medical applications.

Radio frequency identification (RFID) is defined as a technique using short-range radio to communicate digital information between movable objects. (Landt, 2005) Considering examples like contactless smart cards, electronic passports, and ignition keys for vehicles, it is clear that RFID is an irreplaceable part of everyday life. A radio frequency identification (RFID) system is made up with a transponder, which is used to generate a signal from the object, and a reader for receiving and identifying the signal. (Finkenzeller, 2010) For example, one kind of transponder used in the field of animal identification is shown in Figure 7 Available Size for RFID Glass Tag These kinds of tags can be placed under the animal's skin with specific instruments, while not hurting the animal. In practice, the tag is checked against the location, weight, and body temperature of its carrier, so that the amount of feed could be adjusted for the best growth rate. (Floyd, 2015) In one animal tracking experiment carried developed by Oxford University, the receiving system consists of automated radio-telemetry system (ARTS) towers and receiving units as shown in Figure 8 Automated receiving units. With antennas fixed in six azimuth directions separated by 60◦, these automated receiving units (ARUs) could

record the signal strength from each of the six directional antennas. It could also scan over a user-selected radiofrequency that correspond to the tags being worn by the studied animals. (Kays, 2011)

Figure 7 Available Size for RFID Glass Tag

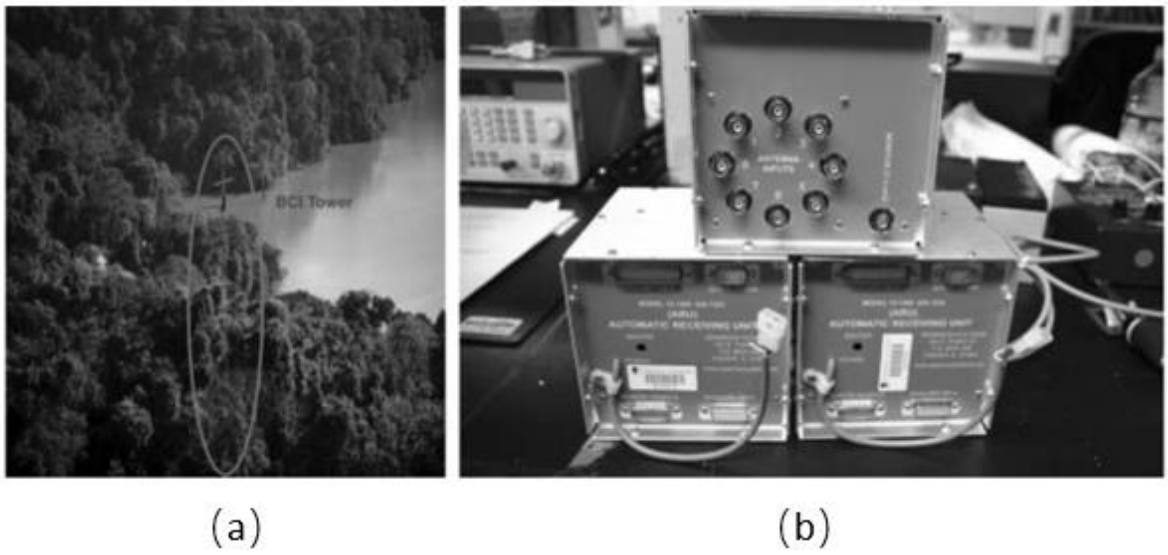

Figure 8 Automated receiving units (a)one automated radio-telemetry system tower near the shore of the Panama Canal (b) an automated receiving unit (Kays et al, 2011)

Radio frequency carrying devices have been proven to be an effective and practical identification tool, which leads to the application for many medical treatments. Based on electromagnetic field principle, the realization of radio frequency devices involves a

transmission line and an antenna. According to the radiation mechanism, the antenna can be classified into single-wire antenna, two-wire antenna, dipole antenna and so on. (Balanis, 2012) Figure 9 shows a dipole antenna implanted in a human head, whose electromagnetic characteristics were then analyzed analytically in dyadic Green's function; while a low-profile antenna went into the human body, then was analyzed numerically in finite-difference time-domain (FDTD) code. (J. Kim, 2004) In another application shown in Figure 10, the stent itself was made in the form of a dipole antenna for cardiac monitoring, while still functioning physically as the support to keep the passageway within vessel opened. (Chow et al, 2009) The focus of improving the performance of radio frequency devices lies mostly on the antenna. How to extend the functioning range, reduce the use of invasive components and maximize the radiation efficiency are some of the main challenges. (Manjulatha et al, 2016)

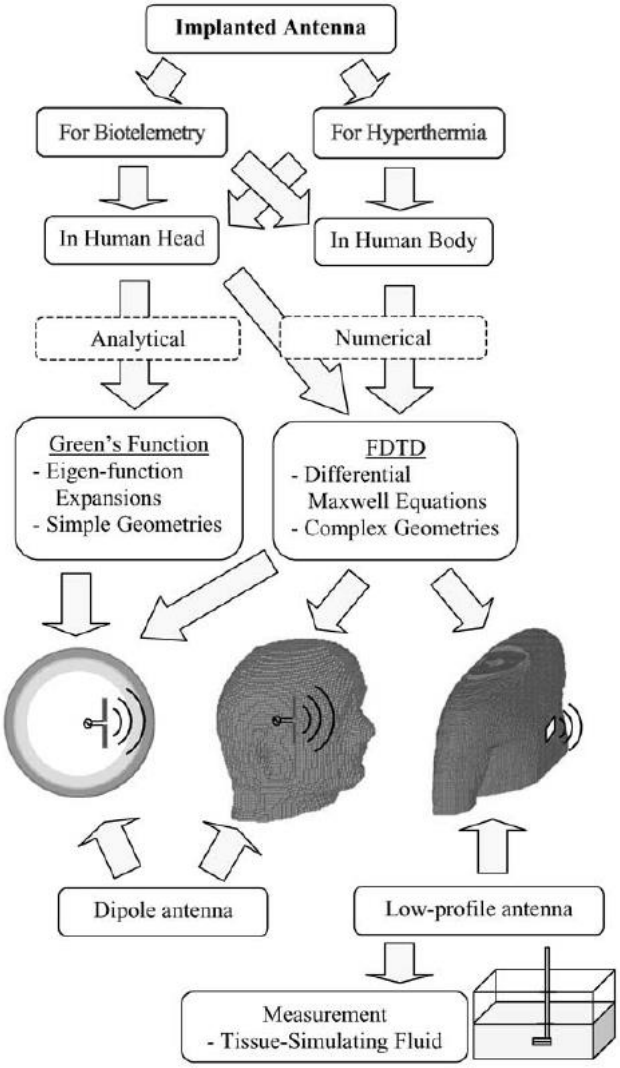

Figure 9 Different types of antenna implanted in human body (J. Kim, 2004)

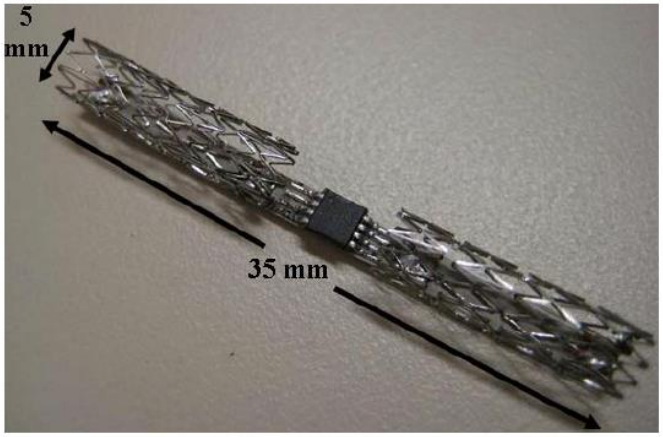

Figure 10 Assembled 2.4 GHz wireless stent-based transmitter(Chow et al, 2009)

This thesis is based on the thesis from Yicheng Ding (2018). *Radio Frequency Antenna Design and Test. The* radio frequency circuit is shown in Figure 11, was constructed on a printed circuit board with hard silicon substrate. The testing result within a certain frequency scope is presented in Figure 11 (c) as a 3-D profile, which suggests there is a relationship between the received frequency-power spectrum and the transmitter position. However, such a vague relationship is too difficult to determine by a mathematical approach. To solve such a complex nonlinear problem, we will introduce a neural network, which is an algorithm that uses features extracted from abundant samples for classification or prediction. (Suykens, 2014).

In addition, though the system worked well when tested in the air, the power amplitude of early models was too weak to be detected when tested inside a body (using a pig model). To solve these two problems, this thesis will introduce improvements made to the transmitter structure to amplify the signal. In addition, the process of analyzing the data for determining location will be presented.

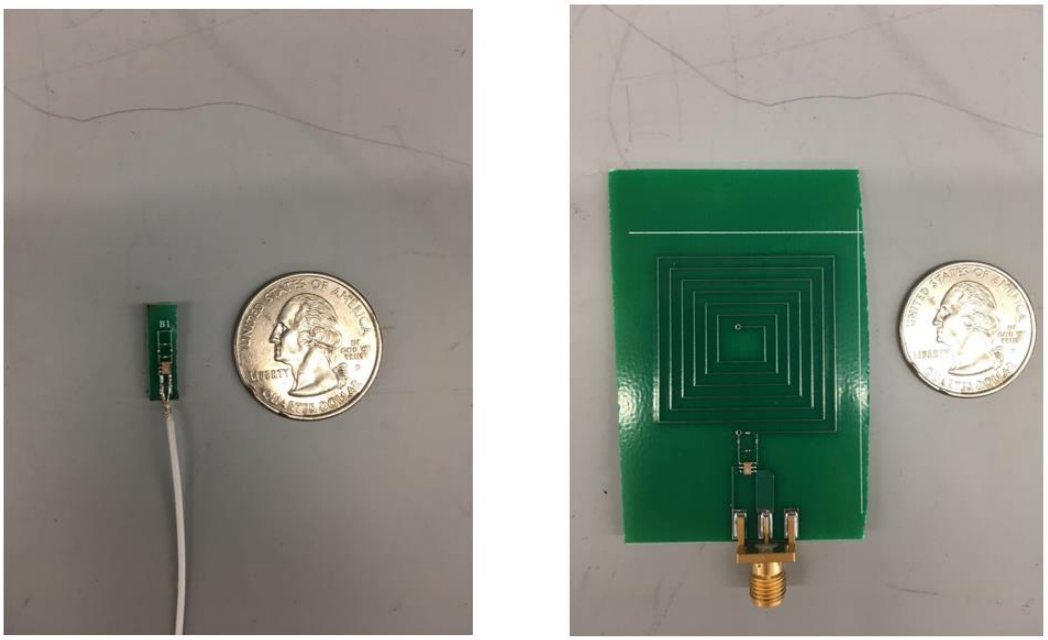

(a) (b)

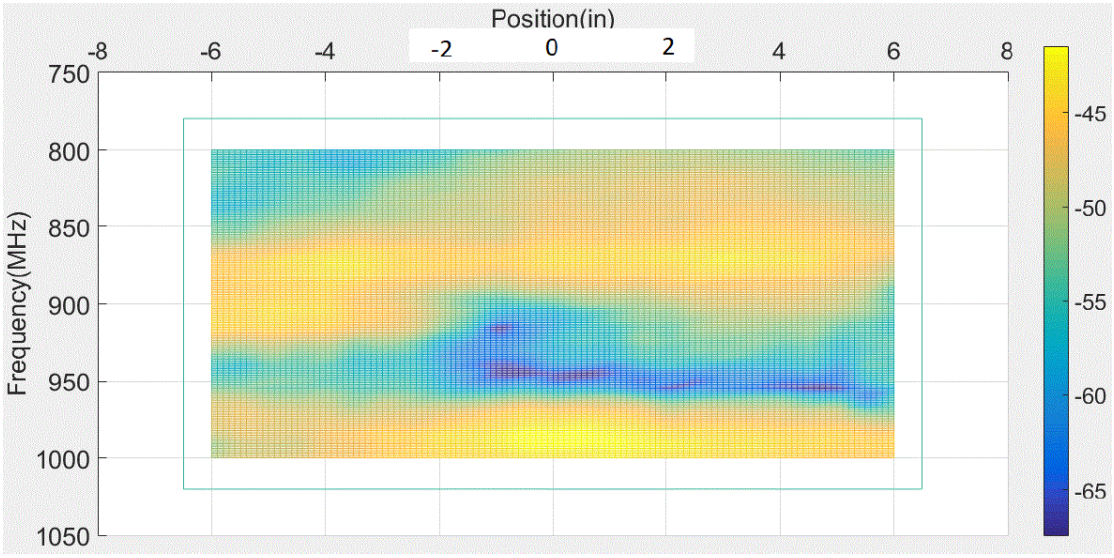

(c)

Figure 11 Developed radio frequency system (a) the transmitter (b) the receiver (c) test result (Ding, 2018)

1.3 Thesis Overview

The following four chapters describe the process of development and the achievements to improve upon the foundation laid by Ding's work. In chapter 2, the main devices in the system will be introduced according to the direction of power flow, including the function generator, transmission lines, transmitter, receiver and data analyzer. To maximize the power that the transmitter could generate, the matching network and a component called balun are added as parts of it. Because of this vital importance, according to antenna theory and former research results, the length, width, relative direction and radiation media of the antenna will be seriously considered.

Chapter 3 focuses on improvements to the transmitter, based on the principle of increasing the effective antenna length. The hard silicon substrate was replaced by flexible film to take full advantage of the limited space in the stent. Practical conditions must be considered, including incorporating the circuit with the catheter and stent to fit the diameter of human artery. By continuous improvements of the system, finally the goal of making the system stable and reliable was achieved so that it can work in a broad range of frequency.

Finally, the testing results for both air test and in-vivo test will be presented in chapter 4. Based on the data, positioning of the transmitter can be achieved with the help of a neural network, which will be introduced in chapter 5. Conclusions and future directions will be stated in chapter 6.

2.0 Structural Components

The testing system is shown in Figure 12. The signal flow is similar to electrical current, starting from the function generator, passing through the transmission lines, then being radiated at the transmitter antenna, which will be perfused into the human body. After penetrating the human body, it will be caught by the receiver and finally delivered to the spectrum analyzer. The arrangement of subsections in this chapter follows this order.

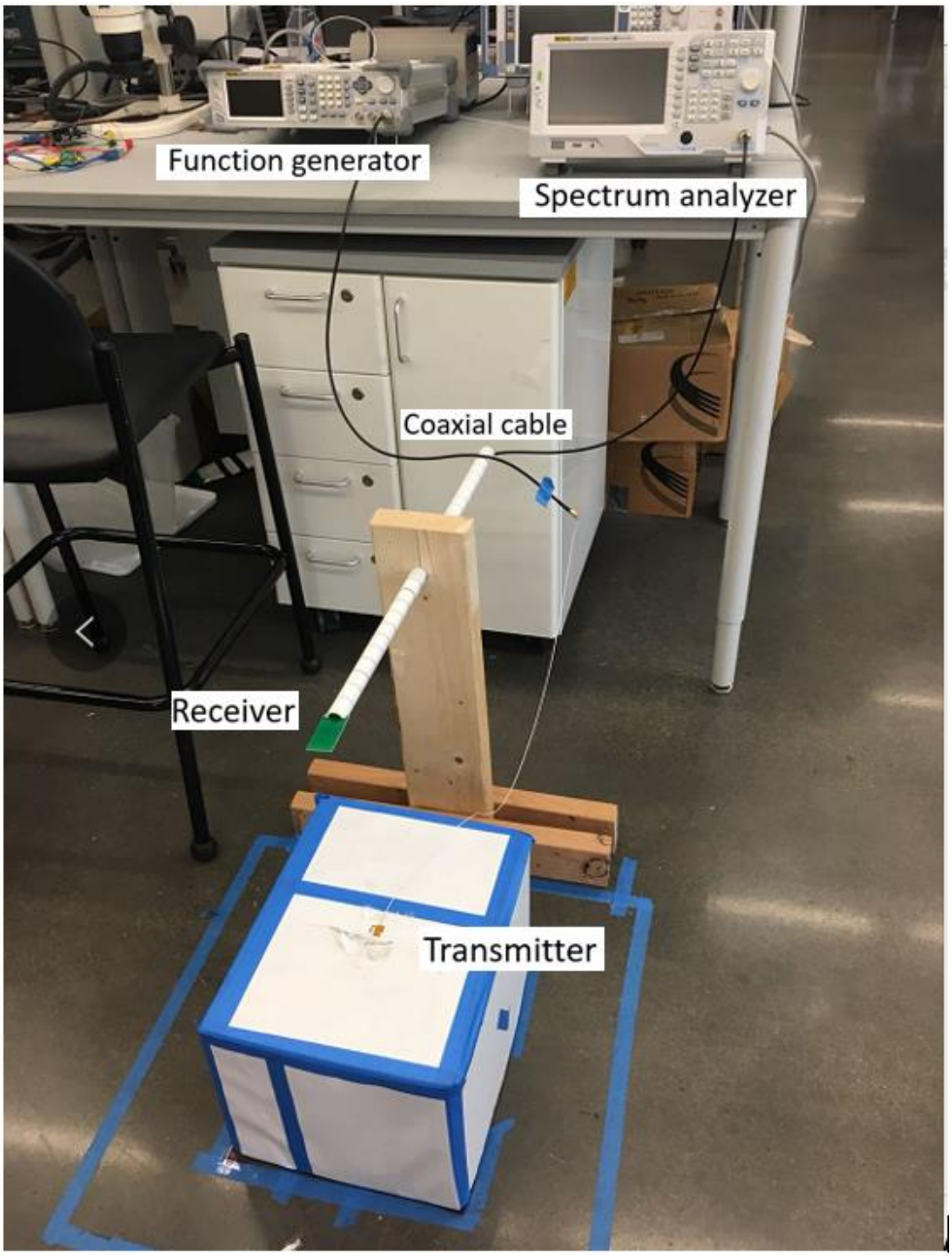

Figure 12 The experiment devices

In practice, the receiver will be fixed on the outside of the human body, and the transmitter will move with the stent in the artery. The translation distance along one direction is the subject we should measure in this set of tests. The setup of devices shown in Figure 12 is designed to simulate this condition in the air. The receiver is fixed at a certain height above the transmitter, while the receiver can only move back and forth along the straight direction. In this thesis, the origin is defined as the position where the center of receiver antenna is right above the center of transmitter antenna. The receiver is fixed at this location with the vertical distance being 30 inches, a curve of the power attenuation, measured in decibels, is obtained This curve would change if the receiver is shifted by a distance, which is the variable we need to determine the relative position between the receiver and the transmitter.

To minimize the error caused by noise and vibration during measurement, each test was repeated for a total of three trials to obtain an average, then a curve was plotted to show the average power gain, as shown in the example in Figure 13(a). If the receiver is moved horizontally over a certain distance increment, with data collected at each position, then a 3-D pattern of radiation can be produced as in Figure 13(b).

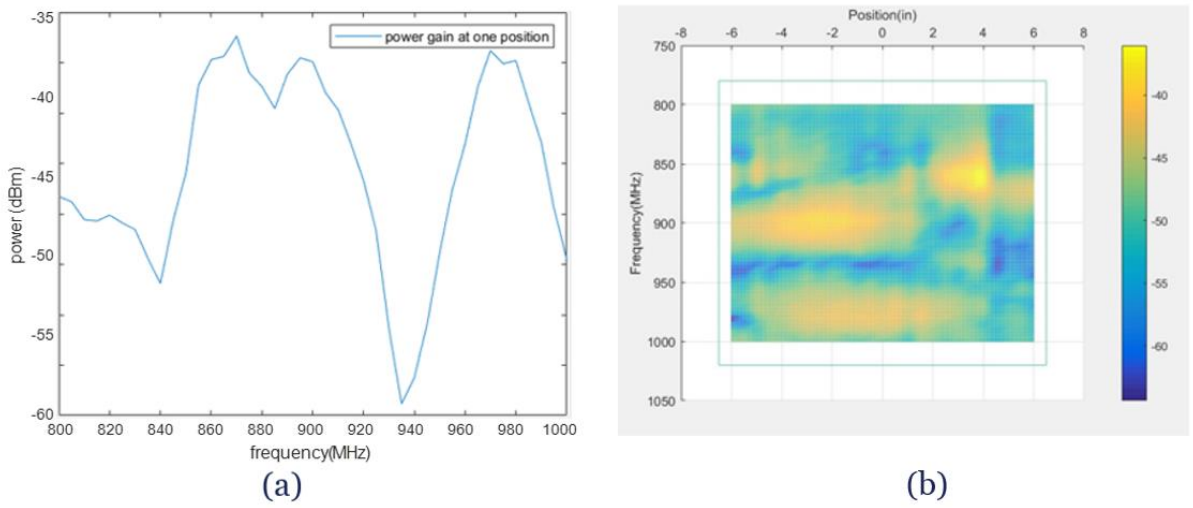

Figure 13 Different forms of testing result (a) a curve from one position (b) 3-D profile from multiple positions

2.1 Function Generator

The radio waves are generated by alternating current, which causes the electromagnetic field to change regularly. A function generator (DSG3030, Rigol), shown in Figure 14 was used as a reliable source of radio waves. It can provide radio frequency within the scope from 9kHz to 3GHz, and the amplitude range of -130dBm to +13dBm, with the output error less than 0.5dB.

Each antenna design has a unique frequency response for high efficiency in power transmission. To measure the antenna performance at different frequencies, the frequency range and increment should be set in advance. Each sweep cycle starts from the lower frequency bound, then increases to the upper bound with the preset step and ends up with going back to the lower bound. The maximum points for one sweep in a certain range of frequency

is 600, however in practice, we can use much less points as long as the frequency increment is small enough, usually chosen as 0.005GHz. For example, in the range of 0.8GHz to 1.0GHz, with a 0.005GHz step, only 41 points are needed. A lot of time can be saved by increasing the frequency step size.

In addition, we can set the output amplitude level, which is measured with decibel-millwatts (dBm). To keep the same pace with the simulation result regarding the power gain expressed in decibel, the level is always set as 0 dBm.

Figure 14 DSG3030 series RF generator

The RF output connector shown in Figure 15 is of great importance because it determines the type of cable that should be coaxial cable. In addition, the output resistance 50 Ohm, is the aiming value for matching network, which will be explained thoroughly in a subsequent chapter.

Figure 15 RF output connector (RIGOL, 2013)

2.2 Spectrum Analyzer

For this work, the Rigol DSA832E spectrum analyzer was used, which is an easy-operating, high-resolution oscilloscope that can transform the received invisible signal into visible plot and discrete data. Its working range is from 10Hz to 3.2GHz, and its displayed noise level less than -161dBm, which satisfies the requirements of this project quite well. (RIGOL, 2011)

Under the 'max hold' model of recording data, the maximum value of received power during the whole process was recorded. Because of transients due to external noise and vibration of the cables, data is collected after a period of three to five sweep cycles so that the peaks reach a relatively stable state. To maintain consistency in this thesis, all data from the spectrum analyzer was collected after three cycles of sweeping.

The advantage of the analyzer is that results are shown visually at each measuring point, which is convenient for the observer to determine if the system is working properly. Also, it is easy to get the results from several desired positions by adjusting the receiver position manually. However, it could be bothersome for the ultimate purpose of determining position in practice with an automated system in which hundreds of groups of data will be needed as

the input. To automate the system, the spectrum analyzer was replaced by a peak detector circuit, which will be introduced in Chapter 5.

Figure 16 RIGOL DSA832E spectrum analyzer

2.3 Transmission Line

2.3.1 Balanced and Unbalanced Circuit

Between the power source and the load, there are always two passageways for the input and output current respectively, which are called the transmission lines in RF engineering. If exact same electrical elements are arranged symmetrically between the two signal lines, which gives them equal impedance, the circuit or transmission lines is defined as balanced. Otherwise it is defined as unbalanced.

In balanced lines, both wires are used to carry signals, which are equal in magnitude and 180 degrees out of phase. The electromagnetic field induced on the two lines cancel each other because they are equal in magnitude while opposite in direction. This property gives balanced lines strong resistance to noise, because the current within the lines induced by external electromagnetic fields can be attenuated significantly. Therefore, most dipole antennae and loop antennae are designed in the balanced form.

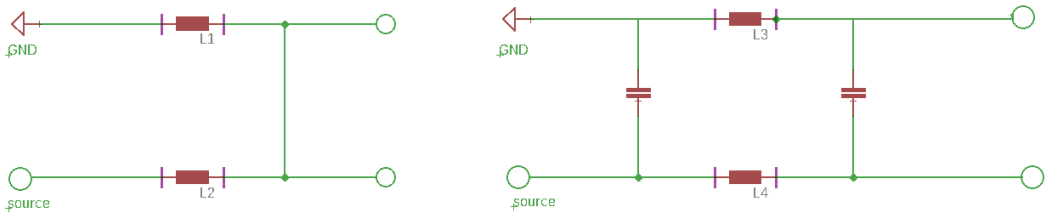

Figure 17 Patterns of balanced circuit

Though a balanced line is advantageous against noise, the coaxial cable we used is a typical kind of unbalanced line. In unbalanced lines, one is used for carrying data, usually the positive line. The other one is used as reference, usually connected to ground. There are four layers contained in a coaxial cable, from outer to inner, are outer protection sheath, woven metal shield, inner insulator, metal core. Figure 18 shows the cable we use, and how we separate the inner conductor from the outer conductor, then respectively connect them to positive and negative ports. It is obvious that the impedance between inner and outer conductor are different because the outer one will be connected to the ground, which is why the coaxial cable is classified as unbalanced line. The multi-layer structure restricts the signal flowing within the inner pass, so the signal attenuation is minimized, and external electromagnetic field

is blocked by the outer woven metal shield (though external RF noise cannot be blocked). (Burgt et al, 2003)

Figure 18 Alpha Wire 9432 WH033 coaxial cable

2.3.2 Length of the Cable

A perfect balanced antenna requires the impedance on both lines to be exactly the same, which only exists in an ideal situation. If a balanced antenna is connected to unbalanced lines, the system can be more vulnerable to noise and electrical interference. We can attenuate the inevitable noise affecting the transmission lines by shortening the length of the coaxial cable.

The effectiveness of shortening the cable is shown in the test, in which two identical transmitter boards were respectively connected to a 40-inch cable and a 20-inch cable. The results are shown in Figure 19. In each experiment, the first group of data was collected when the system reaches steady state after 3 complete cycles of sweep, labeled as ‘without vibration’. To test their steady-state persistence, severe vibration is introduced by manually waving the cable within the next 3 sweeping cycle, after which the data labeled as ‘with vibration’ were collected.

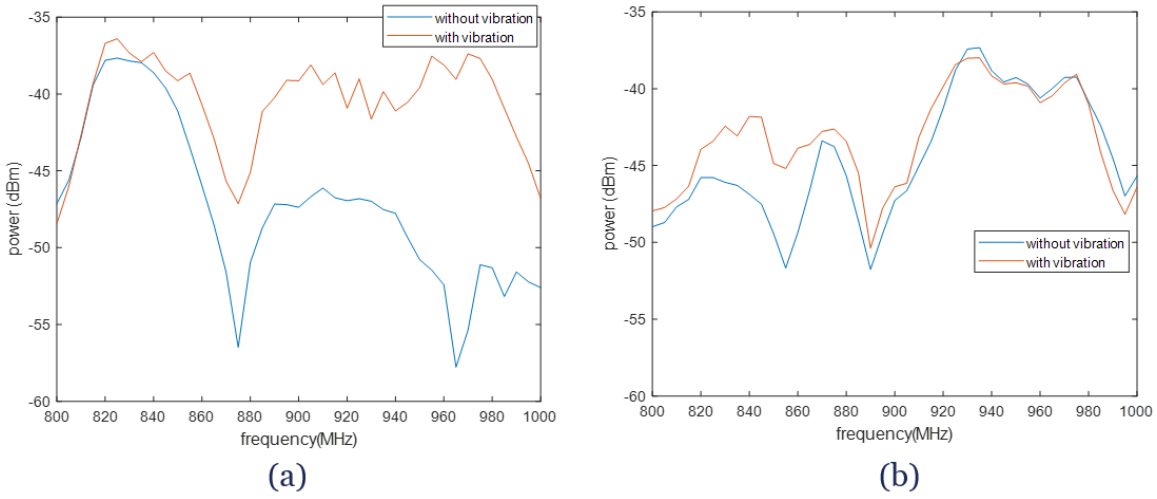

Figure 19 Effect of cable length to maximum radiation power (a) 40-inch cable (b) 20-inch cable

It clear that the two curves in Figure 19(b) are closer to each other than those in Figure 19(a), which suggests the 20-inch cable has a stronger resistance against vibration. Though we need an accurate measurement of divergence between two groups of data. Thus, root mean square error (RMSE) is used through the thesis, which can be calculated in equation (2-1) as:

$$\text{RMSE} = \sqrt{\frac{\sum_{i=1}^{n}(x_{1i} - x_{2i})^2}{n}} \tag{2-1}$$

The RMSE depicts data deviation between two groups, from which x_{1i} is the i^{th} data from the first group, while x_{2i} is from the second group. n is the amount of data in each group. We utilize RMSE in evaluating the system stability by first repeating the test with an antenna for a total of five trials under the exact same conditions. Then we calculate the RMSE between each two groups among the five trials. For example, for 5 groups of data, all different

combination can be listed as 1-2, 1-3, 1-4, 1-5, 2-3, 2-4, 2-5, 3-4, 3-5, 4-5, which are 10 groups in total. Finally, all these ten RMSE are averaged, which is 1.34 for this repeated test. In this thesis, we regard this value as the standard tolerance of noise. In evaluation of a certain variable, if the RMSE is smaller than 1.34, we can say this test object has insignificant impacts.

In Figure 19(a), the RMSE is 5.44, while it is 1.83 in Figure 19(b). This gives us enough evidence to say the shorter cable has stronger resistance against physical vibration on the cable. We also calculated the average power gain under vibration for the 40-inch line is -40.53dB, and -43.21dB for the 20-inch line. This can also be explained by the antenna theory because the cable also acts as radiation source in the unbalanced situation, so that a longer cable contributes to a stronger power radiation.

2.4 Transmitter Circuit

In this thesis, the transmitter specifically indicates the printed circuit board (PCB) connected to the function generator, where the waves are propagating into the environment. Figure 20 is the prototype of the transmitter in the form of loop antenna designed by Yicheng Ding.

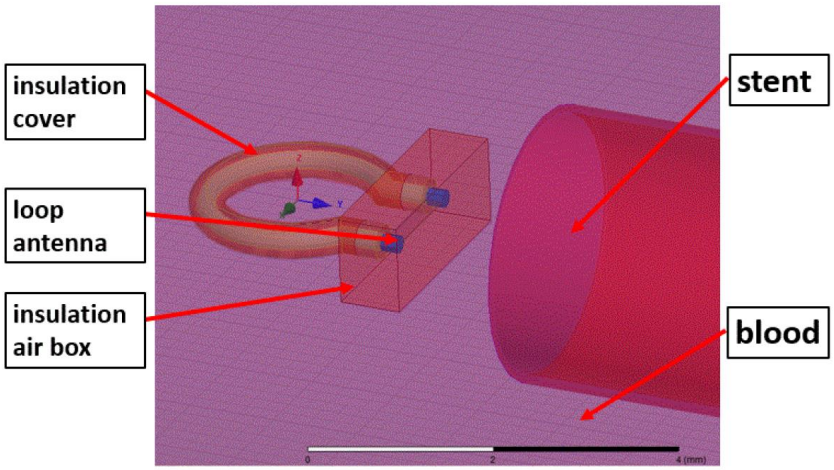

Figure 20 Prototype of the transmitter loop antenna within artery (Ding, 2018)

All the simulation models used in this thesis were developed in HFSS, which is a finite element method solver, especially for RF electronic circuits design in ANSYS Electronics. From the simulation we can get the input impedance, the output impedance, the power gain on certain ports, which are all critical references for design and improvement for the circuit.

The simulation result is shown in Figure 21. In this plot R represents the radius of the antenna loop, and r represents the radius of its cross section. The highest power gain with this model is lower than -70dB. This magnitude is unrecognizable for the spectrum analyzer in practice because the noise level is around -70dB, which can be measured on the spectrum analyzer with the power source cut off. To increase the level of power radiation, the construction of a matching network, and the effect of the antenna structure will be introduced in the following sections.

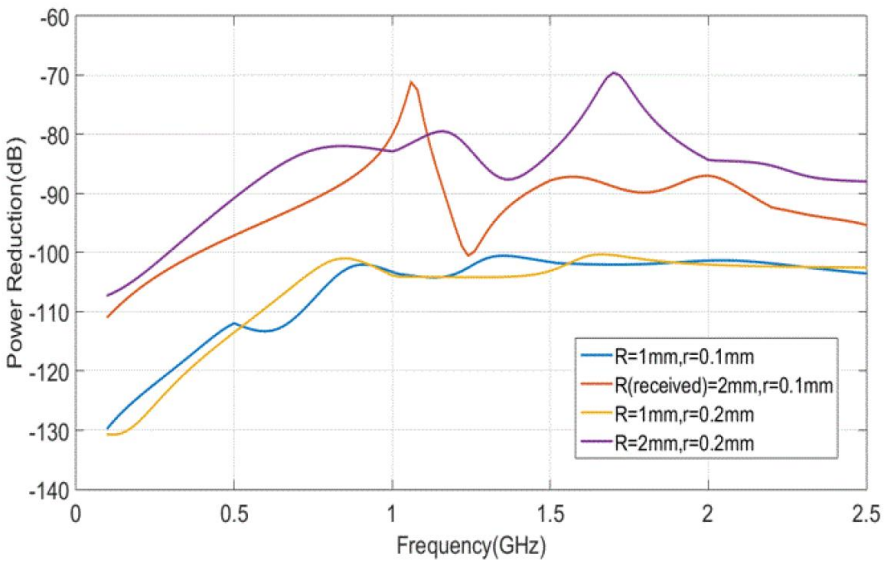

Figure 21 Effect of loop radius and wire radius on power gain(Ding, 2018)

2.4.1 Balun

According to antenna theory, when the system is not balanced, the difference between inner core and outer shield on the cable will induce a new electrical field, which makes the coaxial cable a part of the radiation source. If the desired signal from the antenna, which is no longer than several centimeters, is mixed with the signal from a long cable, the reliability of the data in determining position of the antenna is not guaranteed.

Limited by the diameter of human artery, which dictates the diameter of the sheath in which the stent and antenna are delivered, the width of the circuit board cannot exceed 3 millimeters (90 French). While there is no strict limit on the circuit length, it could reach several centimeters. The circuit route with such small size leads to a subtle value of impedance, which requires high accuracy of elements to keep the balance between the circuit and transmission lines. In addition, the symmetry of the circuit layout could be easily broken by errors introduced

in every step when constructing the devices. From the side of manufacturers, the common error for ceramic elements is 5%, which grows more significant as the value of elements decreases. For example, the error for a 0.3pF capacitor is ± 0.1 (Figure 22), which equals to 33.3%. In addition, various errors could be introduced during the soldering work. For example, the impedance of the soldering joints can neither be calculated nor measured. Unpredictable change of impedance is also unavoidable because the circuit expands along with the substrate when enduring the soldering heat. To eliminate the effect from the error, a component called balun is introduced on the interface to match the two parts.

Figure 22 The kit for standard capacitors and their error

Balun is short for balanced-to-unbalanced. As the name suggests, it reversibly converts the two sides from balanced circuit to unbalanced circuit. The most widely used kind is a

transformer balun, which receives signal from the primary winding, then induces current in a secondary winding. To choose a proper balun, we need to consider the size, the operation frequency range, and the impedance on the balanced and unbalanced sides. These can be found on the product's datasheet (Figure 23). In this project, the balanced/unbalanced impedance is chosen to be 50/50 Ohms according to the transmission line impedance. According to the terminal configuration, the balanced port 3 and 4 should be connected to the antenna side, while the unbalanced port 1 and ground port 5 should be respectively connected to the positive and negative lines. Inserting the balun would result in power loss. The insertion loss for an electrical element can be calculated by $20\log_{10}\frac{P_1}{P_2}$, from which P_1 is the power without this element, and P_2 is the power after insertion. It is similar with the power attenuation and measured with decibel.

General Specifications	
Part Number	1850BL15B050
Unbalanced Impedance (single ended)	50 Ω
Differential Balanced Imp.	50 Ω
Operating Frequency 1 (MHz)	1700 ~ 2000

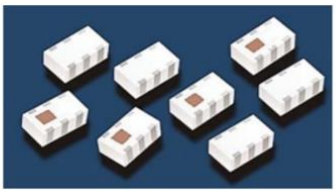

Mechanical Dimensions	In	mm
L	0.079 ± 0.004	2.00 ± 0.10
W	0.049 ± 0.004	1.25 ± 0.10
T	0.033 ± 0.004	0.85 ± 0.10
a	0.012 ± 0.004	0.30 ± 0.10
b	0.008 ± 0.004	0.20 ± 0.10
c	0.012 +0.004/0.008	0.30 +0.1/-0.2
g	0.014 ± 0.004	0.35 ± 0.10
p	0.026 ± 0.002	0.65 ± 0.05

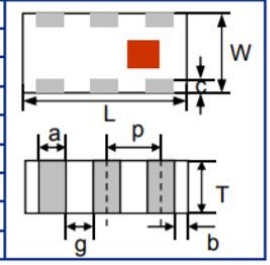

Terminal Configuration			
1	Unbalanced Port	4	Balanced Port
2	GND or DC Feed+RF GND	5	GND
3	Balanced Port	6	NC

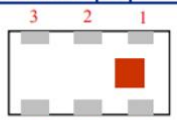

Figure 23 Basic information for 1850BL15B050 balun (Johanson Tech, 2008)

2.4.2 Matching Network

In AC or time-varying circuits, the maximum power will be transferred from a source to its load when the load impedance is equal to the complex conjugate of the source impedance. (Bowick et al, 2018) Usually the impedance of the source is settled to be 50Ω, thus the principle of constructing matching network is to make up the transmitter circuit with capacitors and inductors to attain 50+j0Ω for impedance. The schematic of the transmitter and the receiver are identical as shown in Figure 24, with the two ports on the left to be connected to the coaxial cable, capacitors and inductors should be placed on X1-X4, and signals to be radiated from the antenna on the other end.

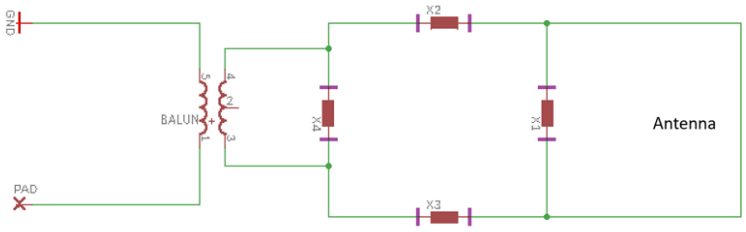

Figure 24 Schematic of transmitter circuit

The advantage of the square structure layout is that it is easy to keep the balance of the circuit by always placing same elements at X2 and X3. However, this layout is different from a standard matching network (Figure 25), in which all parallel elements are connected to ground. For a standard circuit, many easy-operation methods are available to determine the type and value of each element, including Smith chart and built-up impedance matching network designer. (Leivre, 2016)

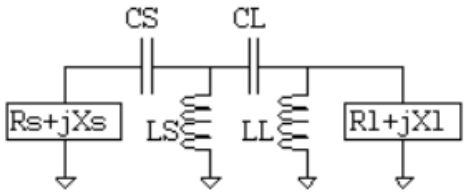

Figure 25 standard matching network (Leivre, 2016)

Unlike a common circuit in which all elements are connected by wires, the impedance of the transmitter-receiver system cannot be calculated from any formula, thus the principle of series and parallel impedance is not available here. Without a theoretical basis, our attempt was to replace one element for each time while keep the others unchanged, until the load and the source are matched. The simulation was operated in ANSYS HFSS model (Figure 26), in which

we can gradually change the value of all elements. There can be countless element combinations. Instead of arbitrarily changing the value of elements, we concluded that the matching process can be simplified to the following four steps, which are synthesized from circuit theory and test experience:

1. Before placing any elements, keep the parallel branch opened and the series elements shorted. Then analyze the output impedance. Regard it as the source impedance.
2. Choose a proper balun according to the frequency range, then import and connect the balun sample file into the circuit model. Beware of the balanced ports and unbalanced ports.
3. Treat the source impedance as the terminal for a fictitious receiver circuit. Fictitious means it only exists in simulation, while is not needed in practice. Using an online designer significantly simplifies the designing process. (Leivre, 2016) Set the middle point within the frequency range to be the reference, then analyze to check if the output impedance is 50+j0Ω at this frequency. Record the input impedance.
4. The impedance of the antenna has direct but undetermined relation with its structure. However, in most of the antenna layouts the imaginary part of the input impedance is positive (inductive). In this case inductors with the same value should be placed in the parallel branches, and capacitors with same value should be placed in series ports.

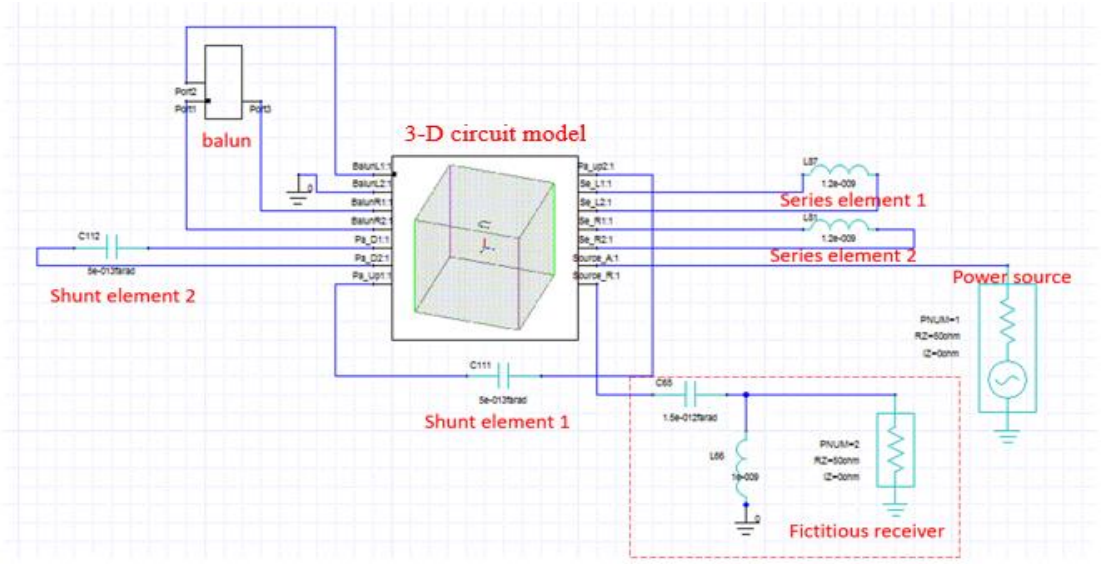

Figure 26 The transmitter circuit model in ANSYS

In our PCB, the load consists of the antenna route and the connection route between other elements. Since the antenna route and connection route are same in material, width and thickness, the load impedance is evenly distributed along the circuit. However, to simplify the calculation of impedance for matching network, we integrate the load impedance into one separated element. Because of this difference between simulation and the real case, it's hard to make the load impedance at exact 50+j0Ω.

To solve this problem, the power gain curve is used alternatively as an indication—which is more direct than the impedance value. In a two-port system shown in Figure 27, G_p is defined in equation (2-2) as:

$$G_p = \frac{P_{avo}}{P_{avs}} \tag{2-2}$$

In which P_{avs} being the input power, P_{avo} being the power transferred to the load. (Well, 1966)

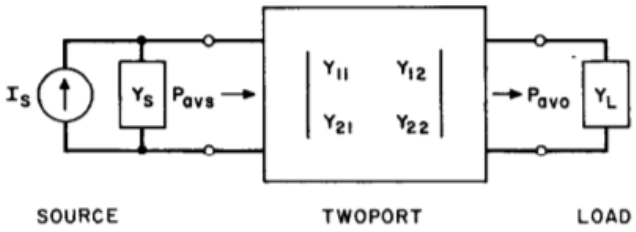

Figure 27 A two ports system (Well, 1966)

An example of constructing a matching network following these principles is shown in Figure 28, whose antenna is a square with the side length to be 8mm. Inductors are put in parallel ports, and capacitors are put in series ports. Within the frequency range of 1.7GHz—2.0GHz (the reason for choosing this range will be discussed in next chapter), by regularly and discretely changing the elements with available value in the kit, we found the power gain reaches maximum when the capacitor is in the range of 0.2-0.3pF.

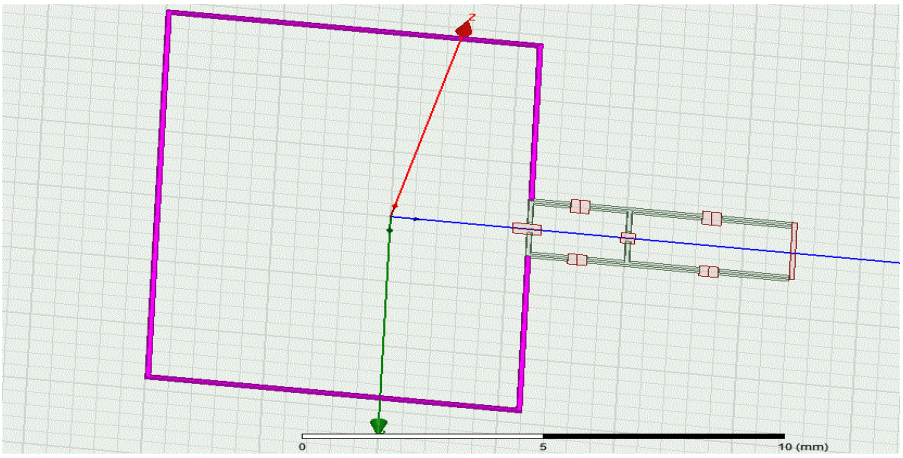

Figure 28 Matching network simulation model

After fixing the capacitors, we found the power gain keeps increasing as the value of inductor increases, but the increasing rate drastically slows down after the value of the

capacitors reaches a certain threshold though the value of capacitance threshold varies according to the circuit layout and cannot be accurately determined, after testing on different layouts, it is set at 0.3pF. With the capacitors fixed to be 0.3pF, using the largest value of inductor available from the kit which is 39nH, the result of power gain is shown in Figure 29(a). The peak occurs perfectly occurs at 1.85GHz, the center of the frequency range, with the value being -28.0dB. Then we simulated an inductor of $10^6 nH$, which can be regarded as infinitely large. The performance shown in Figure 29(b) was improved but only with a subtle degree, with the peak value of -24.5dB occurring at 1.85GHz. This simulation result suggests that the 39nH inductor in the feasible range is an acceptable choice.

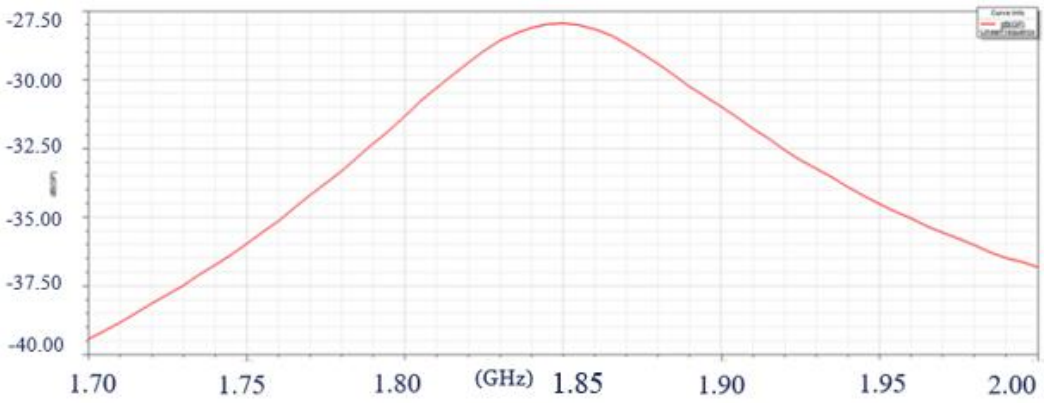

(a)

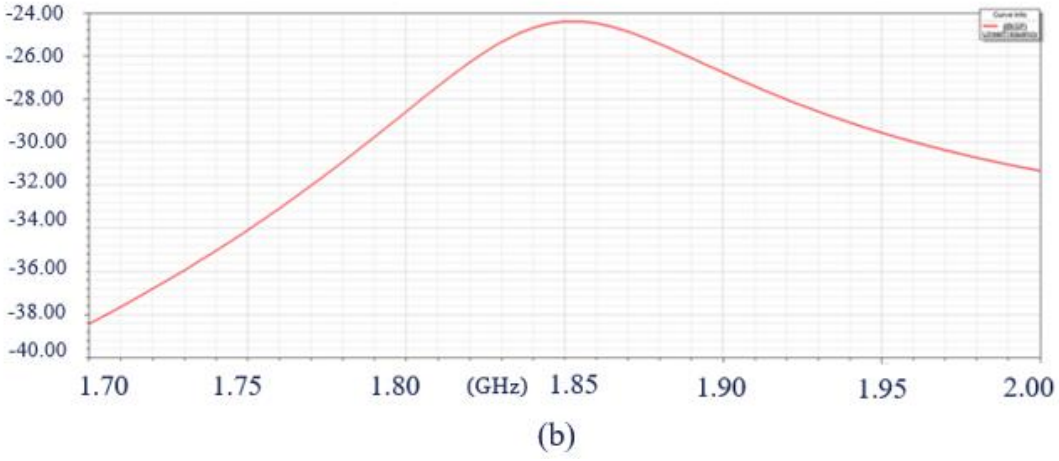

Figure 29 The power gain with different value of elements (a)with available inductors in the kit (b)with infinite large conductor

2.5 Influence Factors on Antenna Performance

For the first version of antenna (Figure 30) developed by Yicheng Ding, whose antenna loop is a 2mm×2mm square. Though it has good performance in simulation and tests in the air, when it was tested in a pig body to simulate use in a human body, the power radiation was too weak to be recognized because the body tissue significantly attenuated the radio signal. (Ding, 2018) There are various factors that could potentially influence the antenna performance. While some are critical to the level of power radiation, others are proved to be insignificant, as it will be discussed in this section.

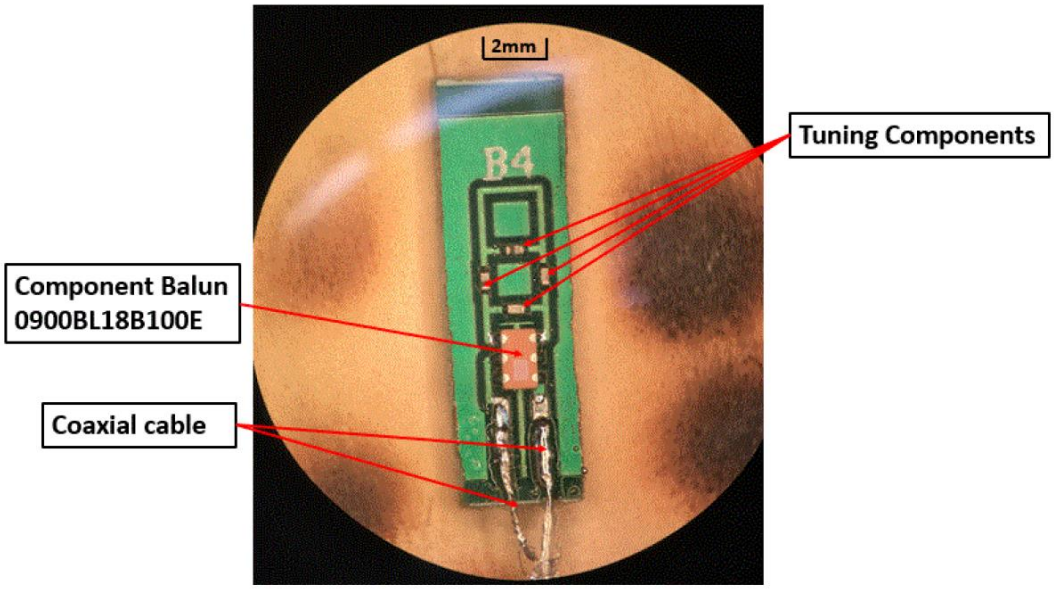

Figure 30 The first version antenna developed by Yicheng Ding (Ding, 2018)

2.5.1 Antenna Surface Area

To improve the power radiation in magnitude, increasing the antenna surface area could be the most effective method in our assumption. This has been proved by Yicheng with a simple loop antenna model shown in Figure 20, whose result shown in Figure 31 depicts the positive relation between the antenna length and the power radiation. In addition, increasing the route width for the antenna is another effective aspect of expanding radiation surface area.

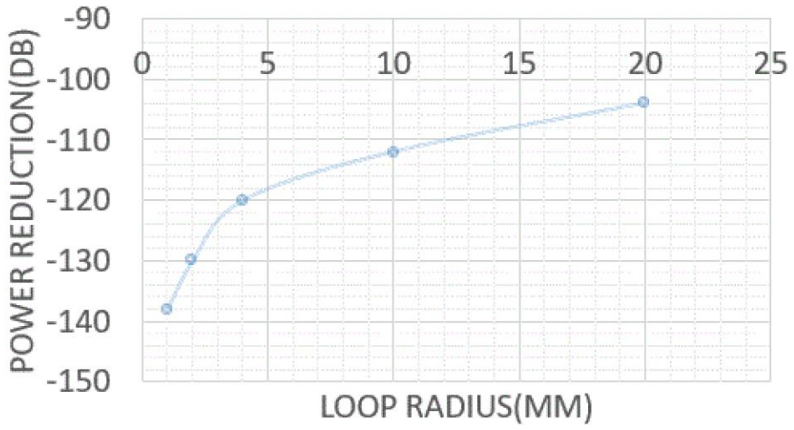

Figure 31 Effect of loop radius to power radiation on the receiver (Ding, 2018)

However, the expansion of antenna size must be strictly limited by the diameter of the sheath that holds the antenna and stent, which is 3mm. To utilize the space within the sheath more effectively, we replace the PCB with hard silicon substrate by flexible-substrate PCB, which could be curled and inserted into a cylindrical shell, so that a circuit with much larger size is achievable. The second version of PCBs, on flexible substrate, are shown in Figure 32.

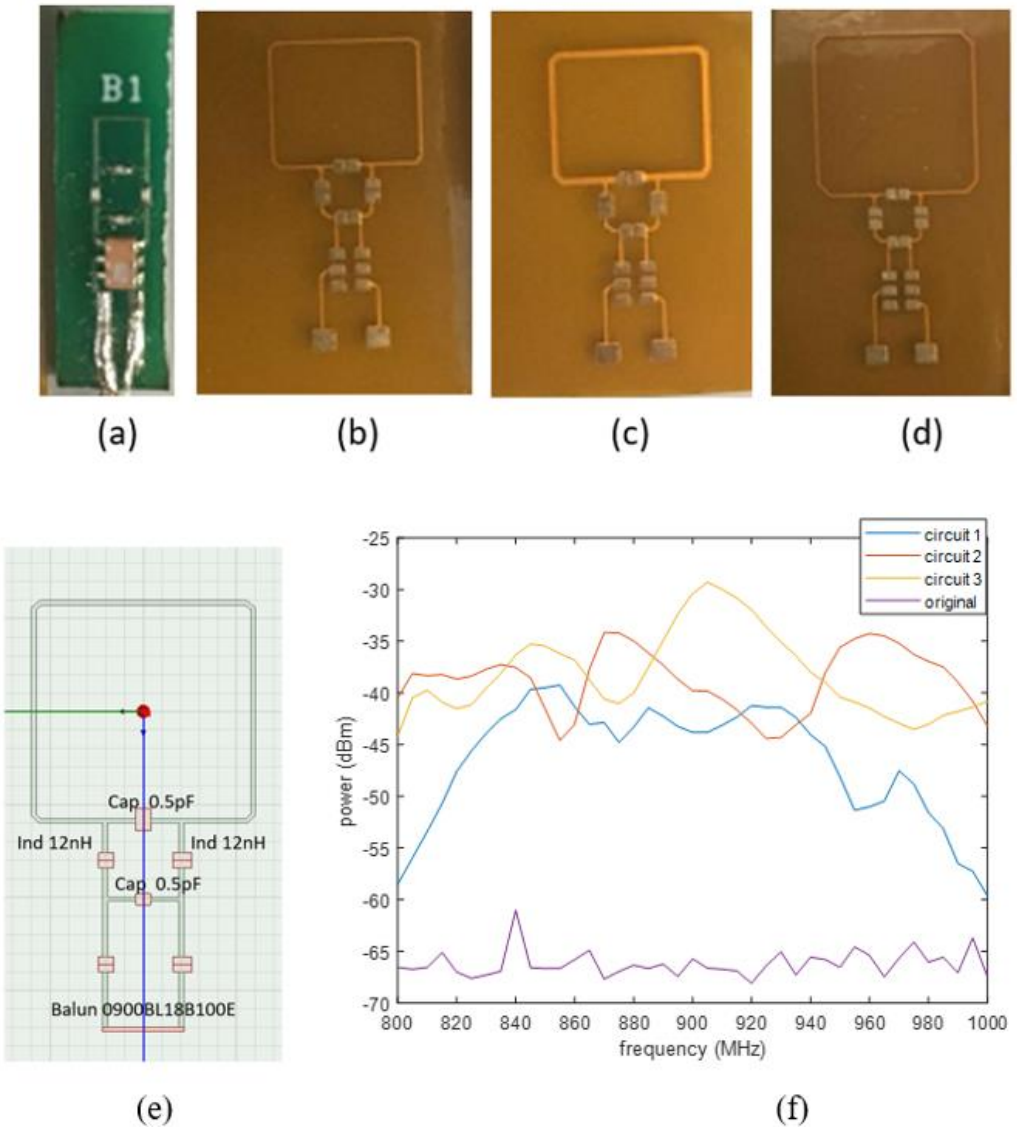

Figure 32 Transmitter on printed circuit board (a) original antenna on a silicon substrate (b) (c) (d) improved antenna on a flexible substrate (e) the elements for matching network (f) the power attenuation for the three antennas

Table 1 Parameters of the flexible circuit board

Board / Parameter	a	b	c	d
Sides length(mm)	2	6	6	8
Route width(mm)	0.15	0.15	0.30	0.15

Two types of receiver developed by Yicheng Ding are shown in Figure 33, which are called single turn receiver and multiple-turn receiver. Theoretically, the ability of receiving radio waves with an antenna should be positively related to its length, which should be the same as that of the transmitter. However, besides the receiver layout, we found that the ability to receive the signal also depends on the frequency range. For example, the power gain from the single turn receiver is slightly higher within 0.8—1.0 GHz (Figure 34). After re-matching both receiver in 1.7—2.0 GHz, the multiple-turn receiver could have a much higher power gain. Without a perfect theory to explain the abnormal results in practice, it is necessary to repeat the receiver performance test regarding various conditions.

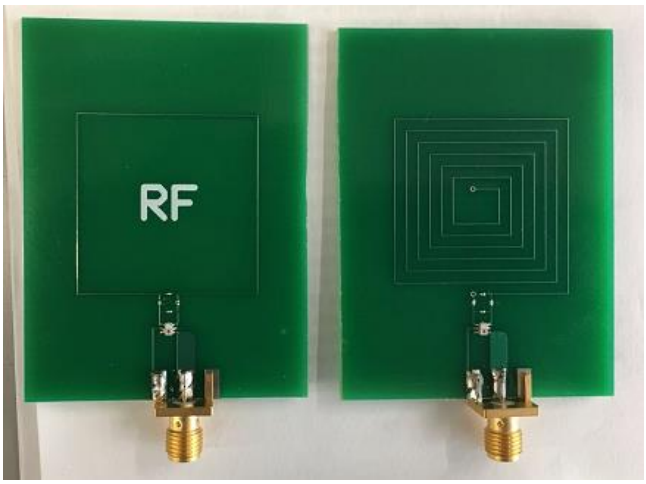

Figure 33 Left: single turn receiver Right: multiple-turn receiver

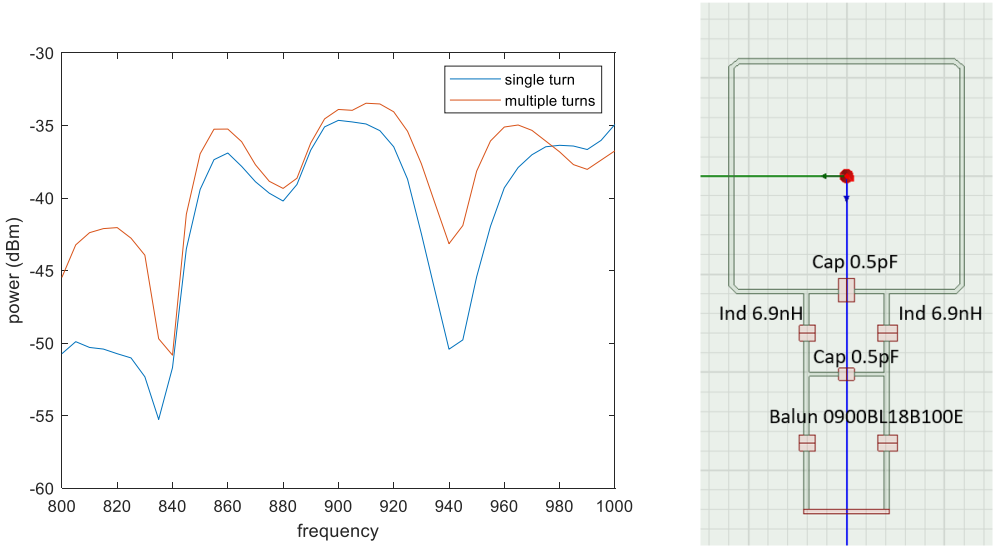

(a) (b)

Figure 34 Receiver performance in 0.8-1.0GHz (a) power attenuation for the two receivers (b) the elements for matching network

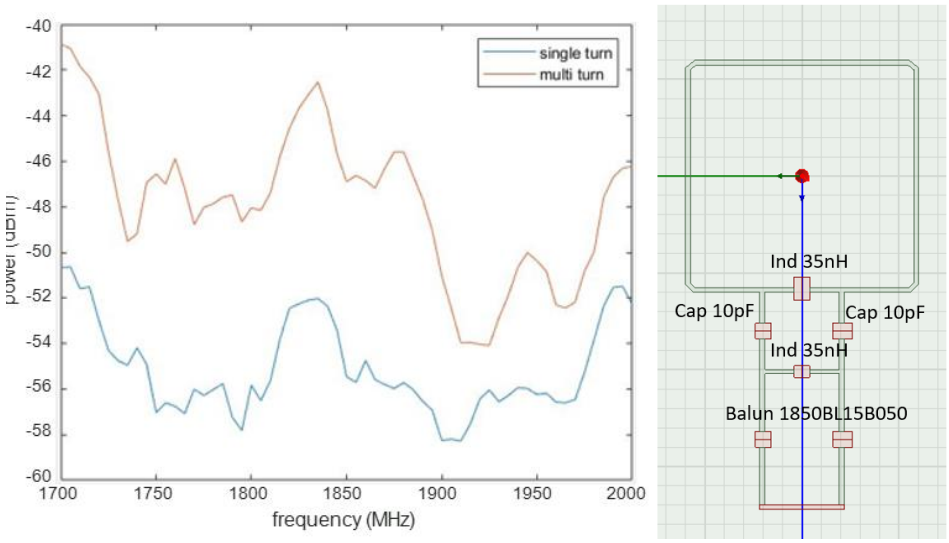

(a) (b)

Figure 35 Receiver performance in 1.7-2.0GHz (a) power attenuation for the two receivers (b) elements for matching network

2.5.2 Directionality of Antennae

An isotropic radiator that can generate and receive radiation equally from all directions is not physically achievable. Instead, actual antennae always radiate and receive electrical waves more effectively in some directions than the others. (Balanis, 2012) For example, when our transmitter is placed as shown in Figure 36(a), it has a radiation pattern shown in Figure 36(b). The major lobes represent the direction with highest power radiation, while the minor lobes represent the other directions with lower power.

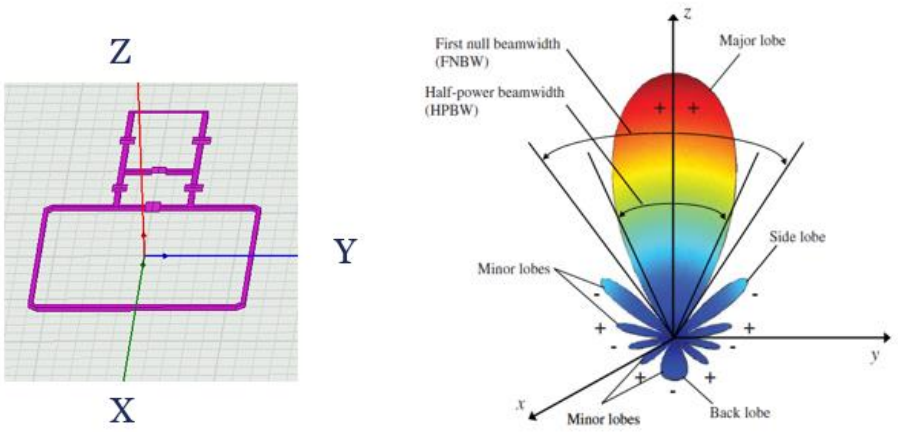

(a) (b)

Figure 36 The radiation amplitude lobe of a loop antenna (Balanis, 2012)

We prefer to have the receiver located in the major lobe so as to see the highest power gain. In addition, the power amplitude change is the only reference to determine the transmitter position shift as it is moved along a straight path. If the amplitude also varies with the receiver shift from the major lobe into a side lobe, we cannot accurately track the transmitter movement in the desired direction, so symmetry is important. In this section, if not mentioned, all tests will be operated within 0.8—1.0 GHz, with the transmitter in Figure 32(b) and accordingly the single-turn receiver. For the convenience of expression, regarding all the circuit boards, we call the side with all elements soldered on as side A, and the other one as side B. As it shown in Figure 37.

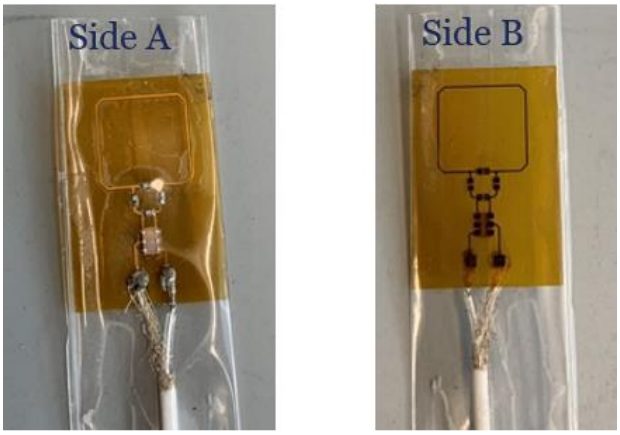

Figure 37 Two sides of the flexible pcb

After the transmitter is delivered into the artery by the catheter, there are two possible working states: to keep it wrapped around the catheter or unfold it. In conclusion, we have to determine the optimal working condition for the transmitter. In practice, one of the possible methods of attaching the circuit board to the stent shown in Figure 38, by wrapping the board outside the sheath. However, the coaxial cable or any kinds of leading wire is too soft to restrict the sheath in axial direction during deployment.

Figure 38 Flexible circuit board attached outside the catheter

First, tests were operated by assuming the antenna would have better performance when unfolded because of the increased radiation area. For tests in this section, the receiver is fixed 30 centimeters right above the transmitter. The 0° direction is defined as the receiver and transmitting antenna planes being parallel with another, and with the transmitter side A facing up, as shown in Figure 39. Then the transmitter board is rotated around the X axis for 45° in each following test, until the side B is facing up, which is called 180°. Then a sponge with little impact to radiation is used to support the board at one end, to create the rotation angle respectively at $0°, 45°, 90°, 135°$ and $180°$.

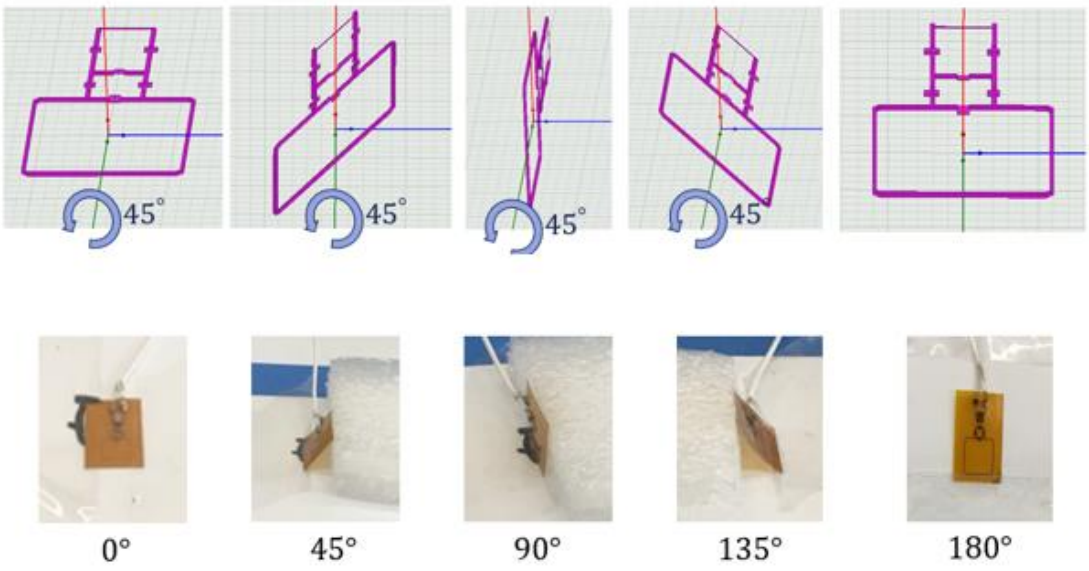

Figure 39 Performance test with different relative angles

The result of power gain in each direction is shown in Figure 40, which shows an obvious trend of decreasing in power gain with the transmitter rotation angle increases. To evaluate the maximum divergence between various directions, we only need the top curve and the bottom curve, which are labeled as 0° and 180°. For a more accurate evaluation, *average* is used to measure the overall magnitude performance, and *RMSE* is used for measuring the divergence between two results. The average for the 0° and 180° curves is -48.4dB and -57.3dB respectively, and the RMSE between them is 8.80. This suggest the significance of the antenna facing direction.

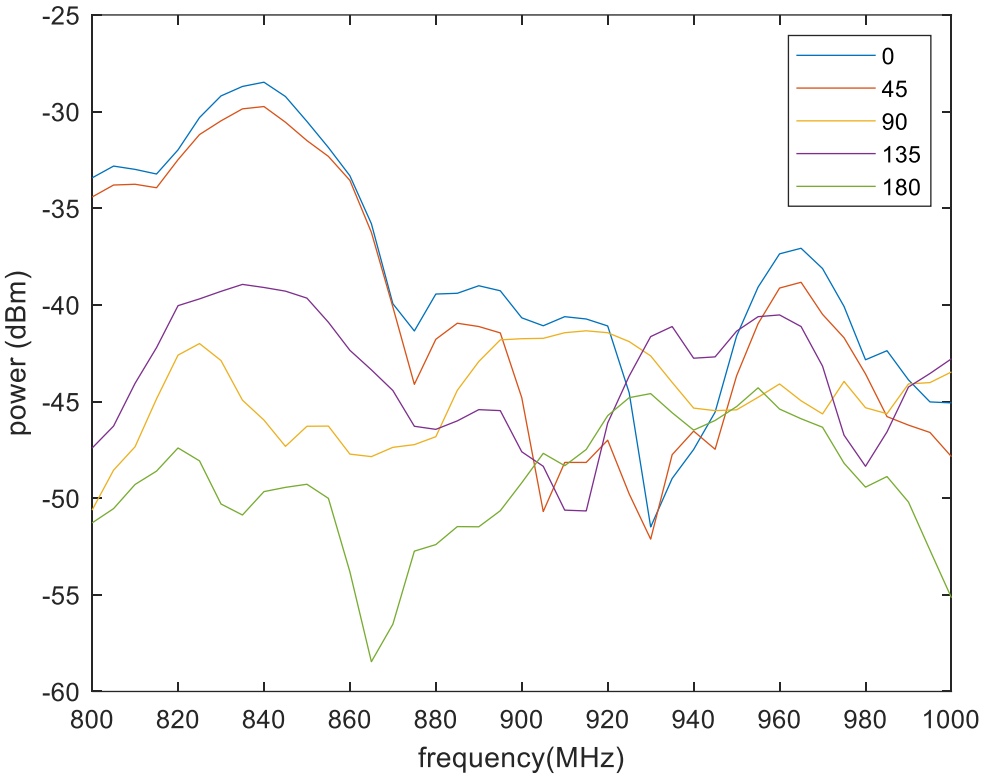

Figure 40 The result for a flat transmitter in different directionality

Then we are testing the transmitter in the folded state. Instead of gluing the board to the catheter, which could damage the transmitter when separated from the catheter, the transmitter is loosely inserted into a cylindrical shell with 3.5mm diameter. As we did in the last test, to test the effect of directionality, the folded transmitter is rotated along with the cylindrical shell by 180°. (Figure 41).

Flat Direct Opposite

Figure 41 The transmitter inserted loosely in a shell

The result is shown in Figure 42, in which the ‘flat’ curve indicates the flat transmitter as the comparison group; the curve ‘in the shell’ indicates second condition in Figure 42, and the ‘opposite’ curve indicates the third condition, where the circuit board is rotated along with the shell with 180°. From the test result we could tell the ‘flat’ condition leads to the highest power amplitude, and the ‘direct’ takes second place, the ‘opposite’ being the lowest. However, the difference between the three groups are trivial. The evaluation in average and RMSE is shown in Table 2.

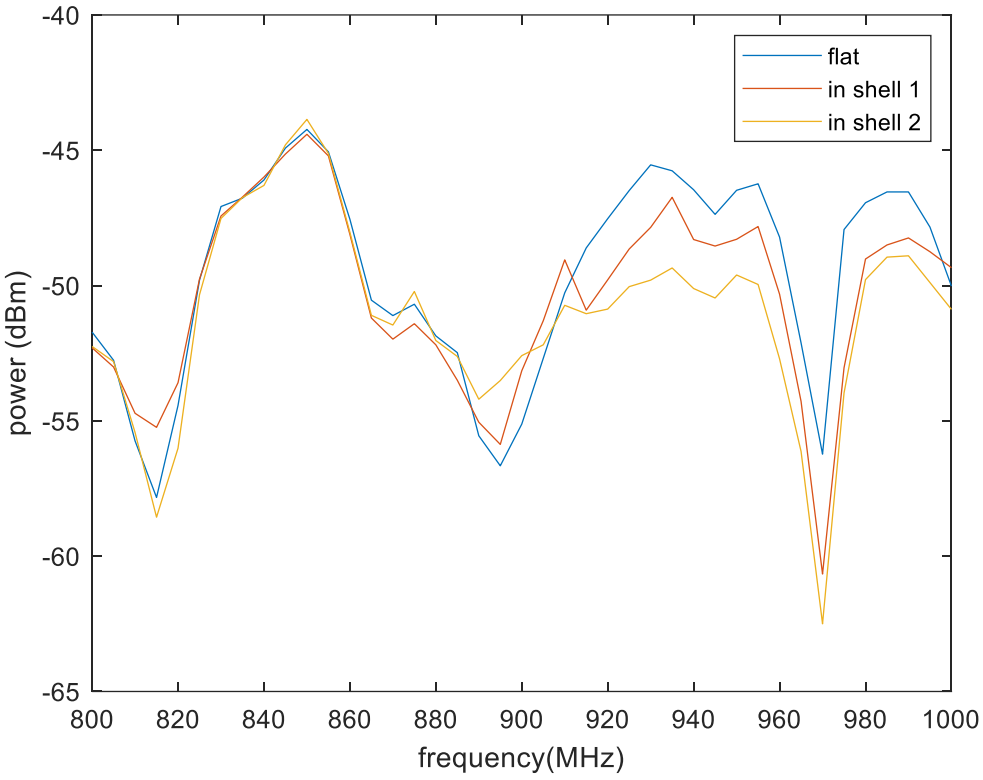

Figure 42 Performance for the flat and folded transmitter

Table 2 Use RMSE to evaluate deviation between each two groups

Measurement / Test	Average(dBm)	RMSE to Flat	RMSE to Direct	RMSE to Opposite
Flat	-49.60	(--)	1.71	2.55
Direct	-50.32	1.71	(--)	1.36
Opposite	-51.06	2.55	1.36	(--)

Now it can be concluded from the test results that the antenna direction is a much more important factor to a flat board than to a rolled-up board. For the flat pattern, the highest gain occurs when the side A on the transmitter is directly facing the side A on the receiver. The power gain drops obviously as the transmitter plane rotates with respect to the receiver plane, and the lowest gain occurs with the transmitter is oriented at 180°. On the contrary, the rolled-

up board has much lower sensitivity against axial rotation, though the average power gain is slightly lower than the highest condition in the flat pattern.

With the conditions mentioned above, we can estimate a better performance from a curled board. However, we cannot extrapolate this conclusion to other boards with various antenna structures and working conditions. It is an assumption that the effect of folding and overlapping the board will grow stronger as the antenna size increases. Thus, the best choice of fixation shape depends on the negotiation between the flat form, which provides the highest power level, and the curled form, which generates similar radiation pattern in all directions.

2.5.3 Insignificant Influence Factors

There are many other factors that can affect antenna performance besides those mentioned above. Though they may have been proved effective in textbooks or papers, in our test system some show little effect practically.

2.5.3.1 The Surroundings of the Antenna

Unlike the mechanical wave, which must propagate within a media, the electromagnetic wave does not require a media for propagation. However, it still can be reflected or absorbed by surrounding materials, which would potentially lead to changes in direction and magnitude of the wave.

We used two kinds of materials, wood and aluminum, with which to build the frame holding the test devices. It is hard to find a specific measurement results regarding the characteristics of absorbing and reflecting radio waves for different materials. However, based on the application of electrostatic shielding, we assume that a metal frame could have a stronger impact for internal electromagnetic waves. To illustrate this, first we made a wooden frame, shown in Figure 43(a), which only stands on one side of the transmitter to minimize its impact. Then we built an aluminum frame that contains all components inside, as shown in Figure 43(b). Finally, to further strengthen the impact of a metal frame, four aluminum bars are piled around the transmitter antenna, as shown in Figure 43(c).

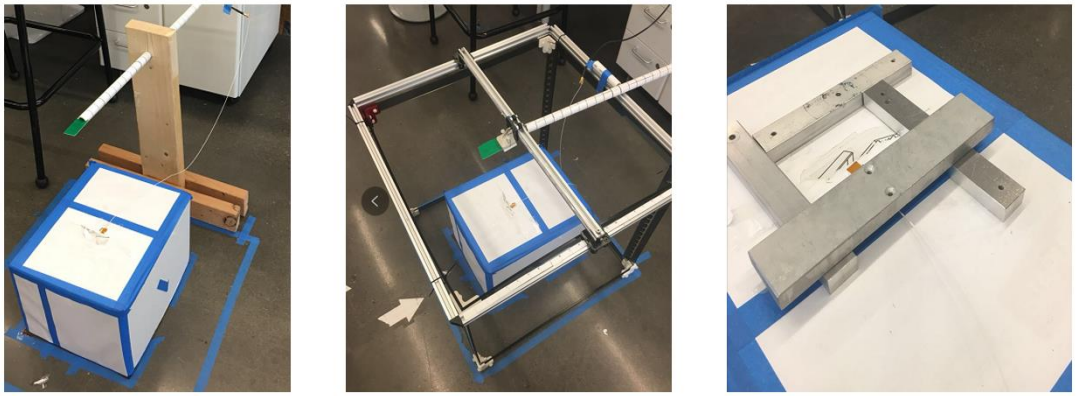

(a) (b) (c)

Figure 43 Test for impact of the antenna surroundings (a) receiver fixed on wooden frame (b) the system contained inside a metal frame (c) the transmitter surrounded by steel bars

The result shown in Figure 44 is a little surprising. The three curves have similar trends and have close average power gain, which are respectively -43.28dB, -43.67dB and -45.18dB.

Because there is no fixed relation in amplitude within the whole scope, we can say the antenna surroundings has little impact for its performance.

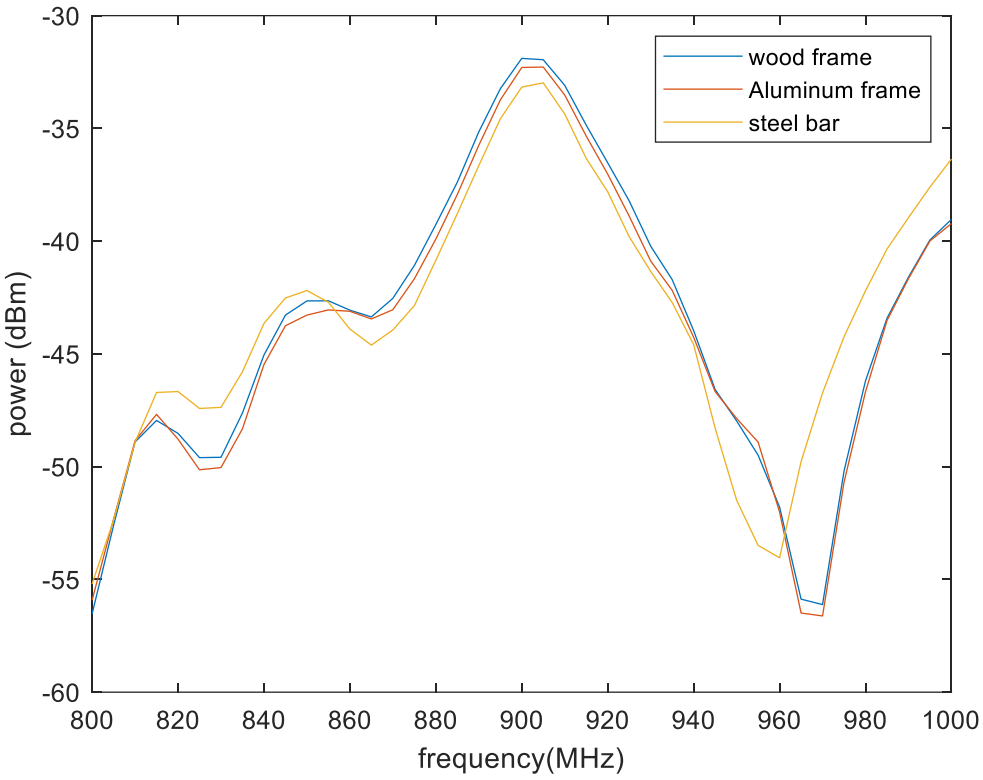

Figure 44 The test result for antenna frame and surroundings

It must be mentioned that if the steel bar touches the coaxial cable, the situation would be different, as the result shown in Figure 45 (b). This variation might be the result of changed impedance along the transmission lines. The average of the curve labeled with ‘press on wire’ is -43.56dB. Compared with -43.67dB, though they are still close in magnitude, the results are quite different because the shape of the sweep results. There is an abrupt valley at around 845MHz, and in the range of 860MHz--1000MHz the curve has little variation in magnitude,

unlike the reference curve. These changes could cause great inaccuracy when used for locating the position of the antenna.

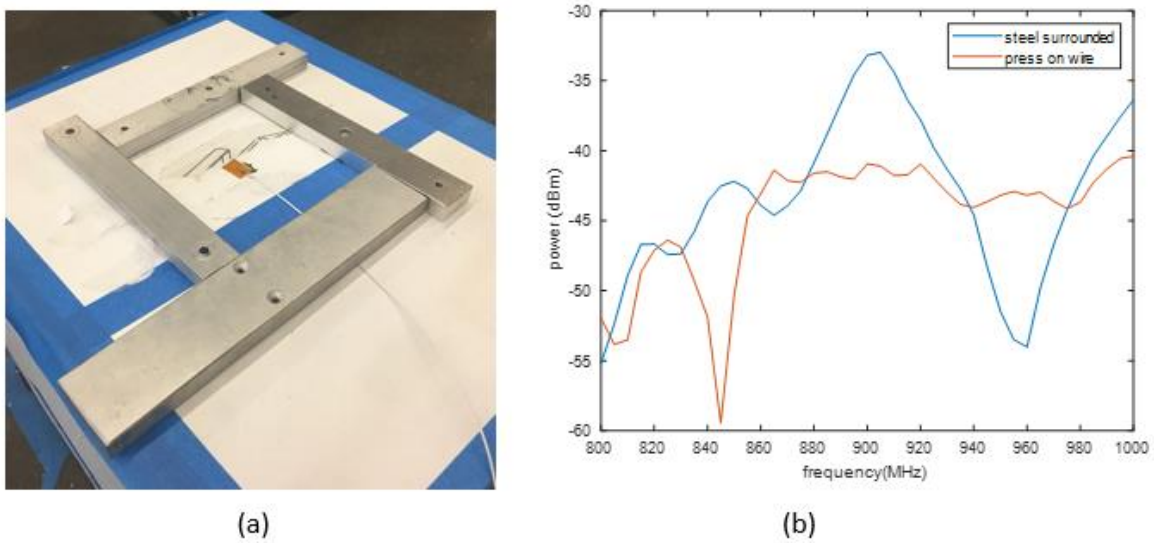

Figure 45 One steel bar cover on the transmission line (a) the test device (b) the test result

2.5.3.2 The Dwell Time and Impedance Discontinuities

In practice, we can set the ‘dwell time’ on the function generator, which is the time it stays at each frequency increment, to different values to allow the received signal to reach steady-state. We tested three dwell times, which are respectively 50ms, 250ms, 500ms. And the result is shown in Figure 46. It is obvious that these curves are close to each other. The largest RMSE is 1.16, the one between 50ms and 500ms, which is even smaller than the noise tolerance (1.34).

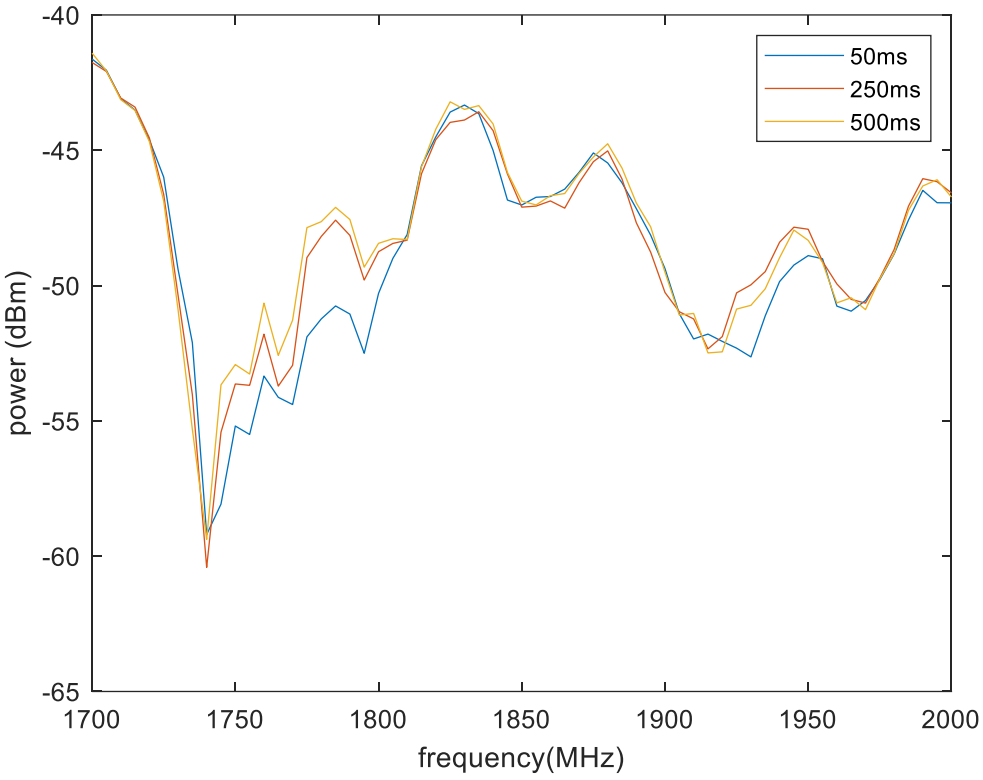

Figure 46 Result of dwell time impact

Radiated power can be affected by impedance discontinuities, which can be physically achieved when the antenna is curved, bent, truncated and so forth. (Balanis, 2012) Such circuit irregularities were constructed for testing by adding solder joints on the antenna route. In our test, it is easier to manipulate the circuit on the receiver board because of its large space and pcb substrate. For the first test, three joints were added, and four more joints were added in the second test, as shown in Figure 47. Since the receiver has the same circuit structure as the transmitter, in this case, it could work as the transmitter by connecting it to the function generator.

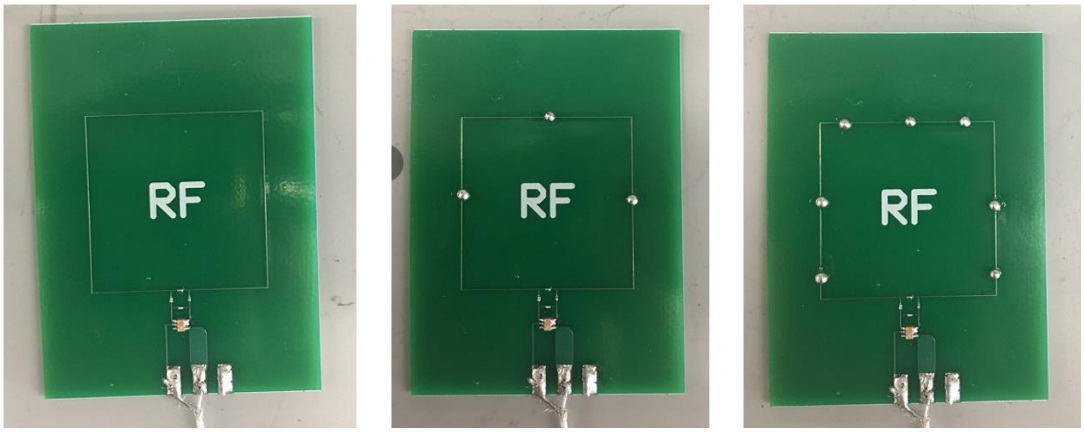

Figure 47 Soldering joints on the receiver board

The result is shown in Figure 48. Though there is significant variation in the transmitted power at individual frequencies, the general trend across the band from 800 – 1,000 MHz follows a similar trend.

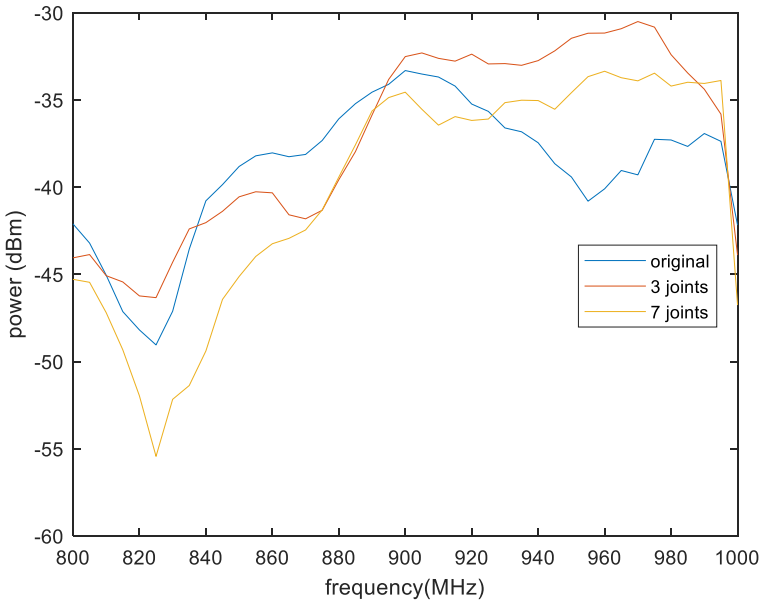

Figure 48 Result of introducing impedance discontinuity

3.0 Transmitter Improvement

Based on the theoretical conclusions about the factors that affect the RF signal performance, we made improvements on the transmitter accordingly to reach more powerful and stable transmission. In this chapter, we will introduce the improvements including new antenna layouts, structure of matching network, and potential choice of new materials for the circuit substrate.

3.1 New Antenna Layouts

We already knew the radiation amplitude has direct relation with the antenna size and shape, therefore new antenna layouts are designed and simulated in this section. There are several consistent conditions for all the simulations. First, to determine the best frequency range, the scope was expanded to 0.8GHz--2.5GHz, which is the maximum scope the function generator could provide. Second, the circuit route width was increased to 0.3mm from 0.15mm because the effectiveness has been proved. Third, to fit the antenna within the sheath whose diameter is 2.1mm, the width of a rectangular circuit board cannot exceed $2.1 \times 3.14 = 6.594\ mm$. Given the necessary free space between the route and the board ridge, the antenna width is settled as 6mm. Since there is no strict limitation regarding the antenna length, we extended the antenna length in one direction.

For expression convenience, the direction that is parallel to the long side of the rectangular board is called the X direction, while the direction parallel to the short side is called the Y direction. Since the length in Y direction has been settled as 6mm (under the 6.594 limit), the antenna length will only be extended in the X direction. As the square antenna becomes rectangular, to take full advantage of the expanded board space, right-angle turns are added to the antenna route along the X direction, as the one shown in Figure 49 (b) and (d). To find out a proper antenna length instead of unbounded expansion, the simulation starts with the 6mm-square antenna, then one square turn is added for each sample. The performance will be compared with the rectangular antenna as the contrast group. Some layouts are shown in Figure 49. The detailed simulation results are shown in Table 3.

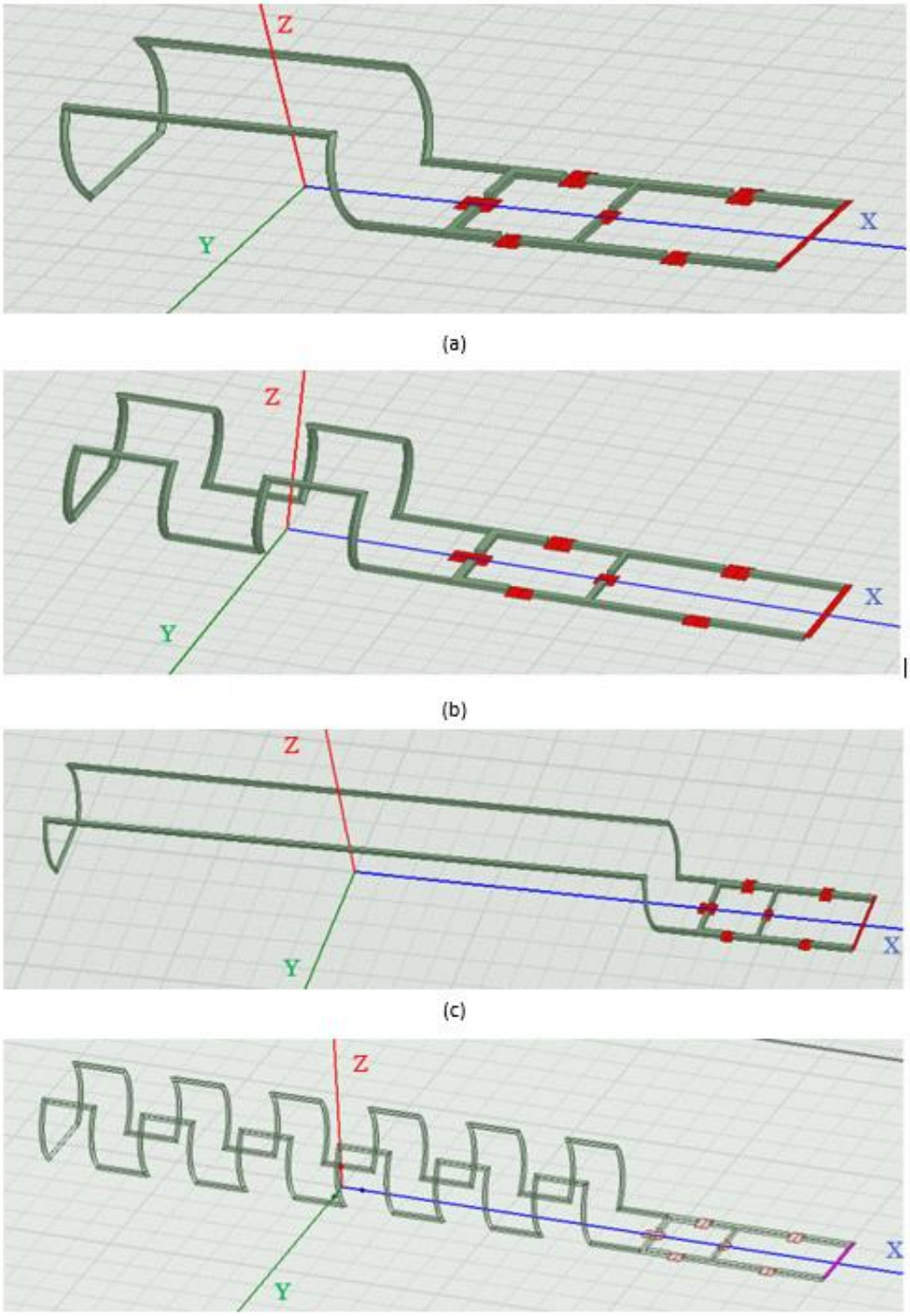

Figure 49 Simulation models for rolled-up antenna (a) 8mm*6mm, no turn added (b) 8mm*6mm, one turn added (c) 20mm*6mm, no turn added (d) 20mm, 5 turns added

Table 3 Test for rectangular antenna and square-wave antenna in different length

Test Number	Length in X direction (mm)	Number of square turn(s)	Increased length (%)	Highest power gain (dB)	Frequency for the highest point (GHz)	Average power gain(dB)
1	8	0	(--)	-31	1.25	-38.25
2	8	1	23.1	-31.5	1.2	-39.37
3	11	0	(--)	-29.5	1.25	-35.27
4	11	2	37.5	-29	1.25	-34.76
5	14	0	(--)	-27.5	1.25	-33.68
6	14	3	47.3	-28	1.25	-32.13
7	17	0	(--)	-25.5	1.25	-30.28
8	17	4	54.5	-22	2.2	-27.78
9	20	0	(--)	-20.5	2.25	-25.18
10	20	5	60.0	-22	2.1	-26.64
11	23	0	(--)	-21	2.15	-25.41
12	23	6	64.3	-22.5	1.9	-25.23
13	26	0	(--)	-21	2.0	-25.61
14	26	7	67.7	-22.5	1.85	-27.14

First, all circuits are matched following the steps introduced in section 2.4.2. To evaluate the antenna performance, here we attach more importance to the point of the highest power gain instead of the average. The samples were simulated within expanded frequency range, whose power gains are shown in Figure 50. We can identify several peaks separated by an abrupt valley, which could be introduced with the combination of inductors and capacitors. One capacitor-inductor pair could function as a filter, which allows the signal within a certain frequency band to pass, as it shown in Figure 50(c). When multiple pairs with different frequency passbands are combined, typically, we can get the response curve with a central valley shown in Figure 50(d) , which is similar to our simulation result. (Bowick et al, 2008)

To avoid these valleys, we restrict the actual working range to be a narrow scope centered with the peak. The balun also benefits from a narrow scope because its accuracy would decrease if the frequency scope is wide. (Doug Jorgesen, 2014) In addition, it takes more time for wider frequency sweep with a fixed resolution, which would put the patients in a great risk.

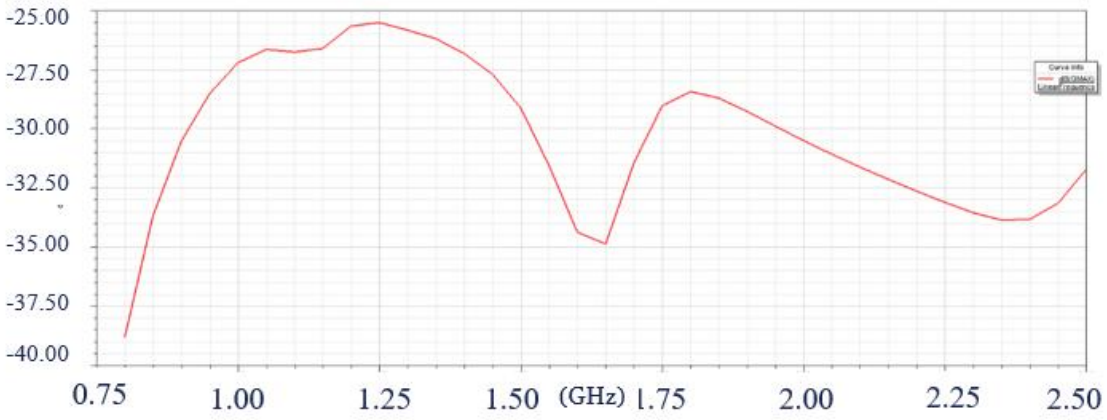

(a)

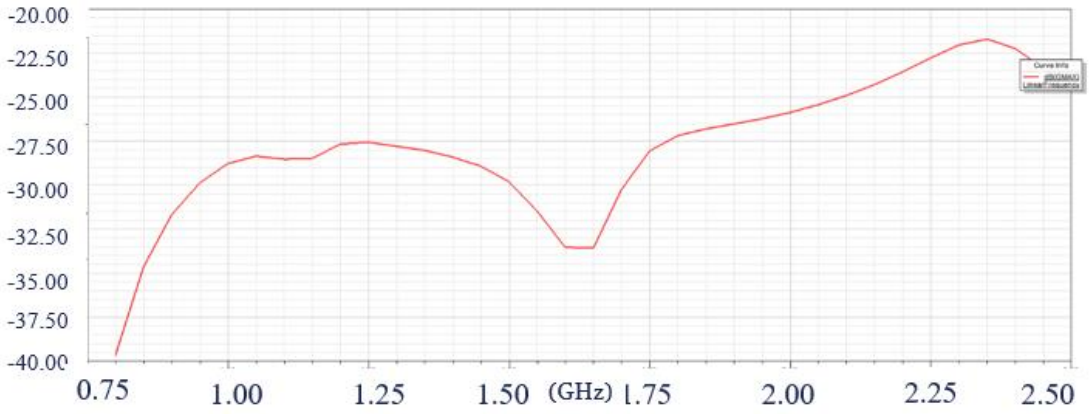

(b)

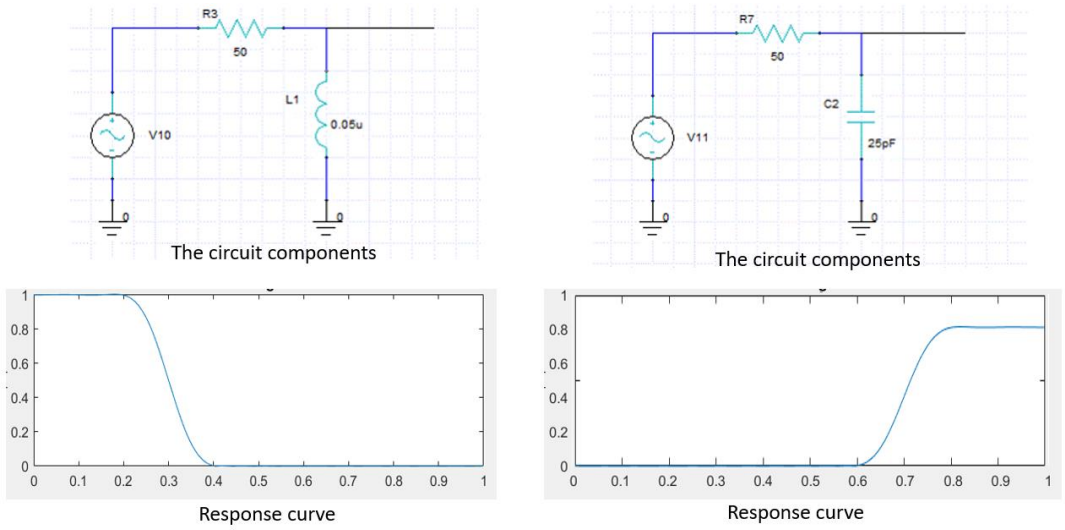

(c)

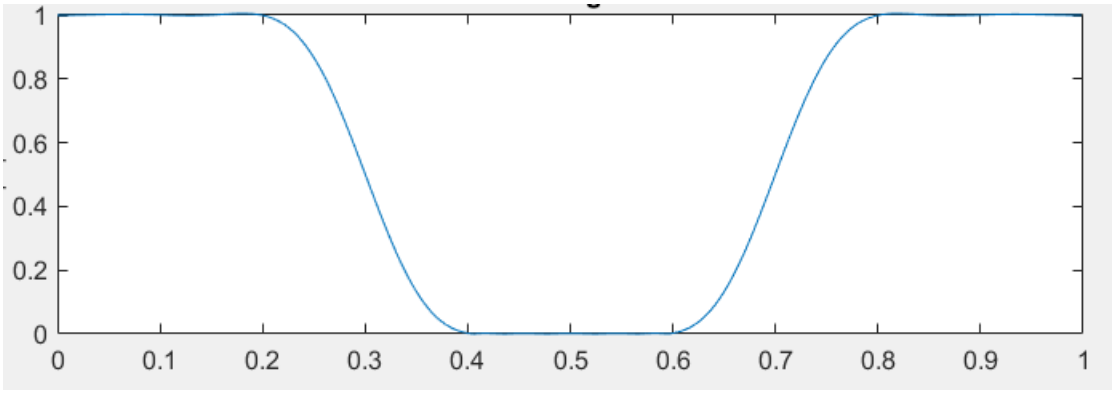

(d)

Figure 50 (a) the power gain for test NO.7 (b) the power gain for test NO.8 (c) response with one pair of capacitor/inductor (d) response with multiple elements combined (Bowick et al, 2008)

First, by analyzing the power amplitude regarding the length in X direction, we find the highest power occurs in both form with the length to be 20mm, after which there is no evident increase in power even as the length continues to increase. We assumed it is caused by the increased impedance from the circuit itself with its growing length. Therefore, instead of expanding the antenna size unboundedly, a 20mm antenna is a practical choice.

Second, we compare the power amplitude between two layouts with the same length. The term ‘increased length’ is the percentage of increased route length by transforming the

rectangular antenna into the square-wave like antenna. For example, the total route length for the rectangular antenna No.1 contains two sides in X (2×8mm), one side in Y (6mm) and one side in Y connected with the matching network (4mm), which adds to 26mm. The side length for each square turn is settled as 1.5mm, which means the total length increases by 6mm with two turns added symmetrically on both sides. With one turn added, the route length increases to 32mm, and the increased percentage can be calculated by $\frac{32-26}{26} \times 100\% = 23.1\%$.

However, as the increased part becomes more significant for longer antenna, we see subtle difference in power between the two layouts. One of the potential explanations is based on the power pattern, which was shown in Figure 36. By adding square turns, we only increased the antenna length in the Y direction, while the length in X direction was unchanged. If the major radiation lobe for the vertical part does not occur in the same direction with the horizontal part, the radio waves reaching the receiver will not increase significantly. To deal with this problem, we developed another layout, in which the added paths align in the vertical direction, as the one shown in Figure 51. We call this new layout a fence antenna. From the result shown in Figure 52, we can tell the power gain is significantly improved. However, compared to the rectangular layout with the same horizontal length, the antenna length has increased 4 times in the fence antenna. With more than one variable introduced, we cannot identify which is the major factor in effect.

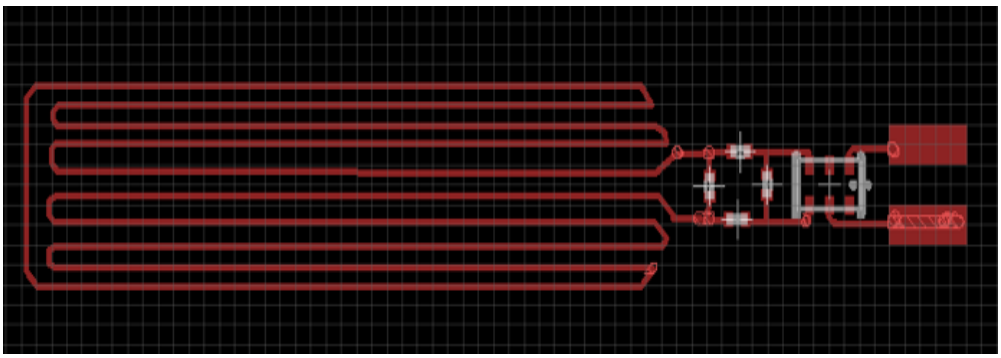

(a)

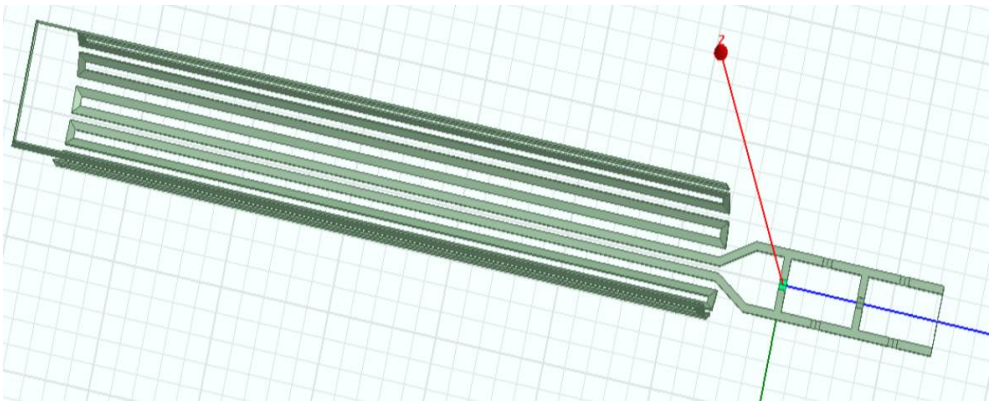

(b)

Figure 51 The fence antenna (a) The flat layout (b) The simulation model

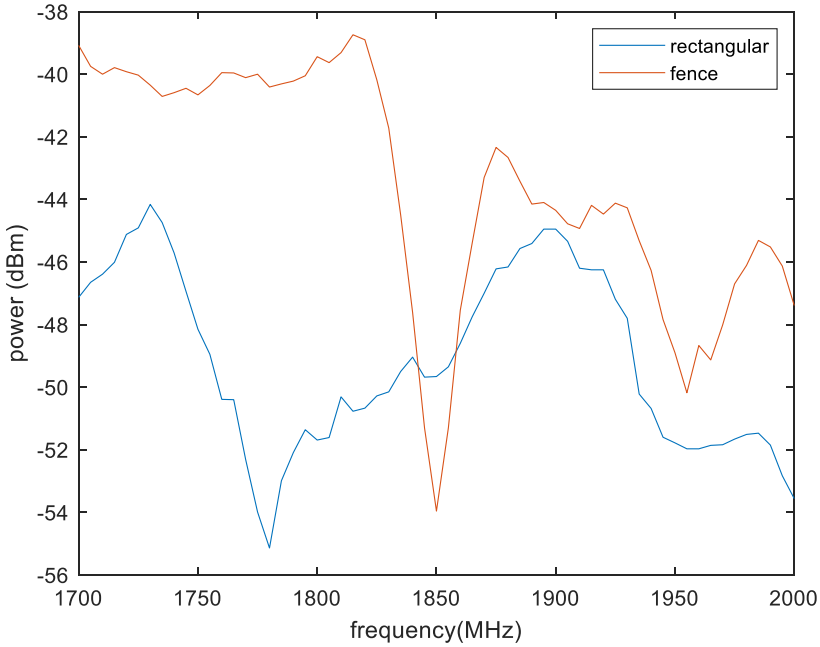

Figure 52 The result for rectangular antenna and fence antenna

Based on the result shown in Table 3, we can reduce the frequency scope from 0.8 – 2.5GHz down to a narrow band centered at the frequency where the peak occurs. For the 20mm antenna labeled as test 9 and test 10, the peak frequencies are respectively 2.25GHz and 2.1GHz. Unfortunately, we could not find a standard balun which could fit in every aspect, including size, frequency range, and balance ratio. From the list provided by the balun supplier, three appropriate choices are listed in Figure 53. Finally, 1805BL15B050 is regarded as the best choice because higher accuracy can be achieved in exchange for narrower frequency scope. In addition, it has the lowest insertion loss. For example, the insertion loss of 1.0 means the power is attenuated by coefficient of 0.793, and the insertion loss of 1.5 accords with attenuation coefficient of 0.631. Thus, we chose 6mm*20mm as the antenna size, and the working frequency fixed within 1700-2000MHz.

Part number	Frequency (MHz)	Balanced (Ohms)	Insertion Loss (max)	Return Loss (min)	Phase Difference	Amplitude Difference (max)	Product Life Cycle Status
1720BL15B0050	625-2815	50 (1:1)	1.5	9.5	180°±10°	1	PROD
1850BL15B050	1700-2000	50 (1:1)	1.0	9.5	180°±10°	2	PROD
2450BL14C050	2400-2500	50 (1:1)	1.2	9.5	180°±10°	2	PROD

Figure 53 Standard high frequency baluns *(*Johanson Technology)

3.2 Matching Network Improvement

The impedance matching network has the effect of maximizing the efficiency during power transmission. However, since the impedance of inductor and capacitor varies with frequency, the matching network can only match the impedance perfectly at one frequency point. For example, Figure 54 shows the impedance of a circuit matched at 0.85GHz. The resistance (real part of impedance) is 38.7, and the reactance (imaginary part) is 11.37, which is increased from -4.89. It is not perfect 50+j0Ω because of the unavoidable errors introduced in section 2.4. Generally, we regard the condition is matched when the resistance is close to 50, and the reactance passes through 0.

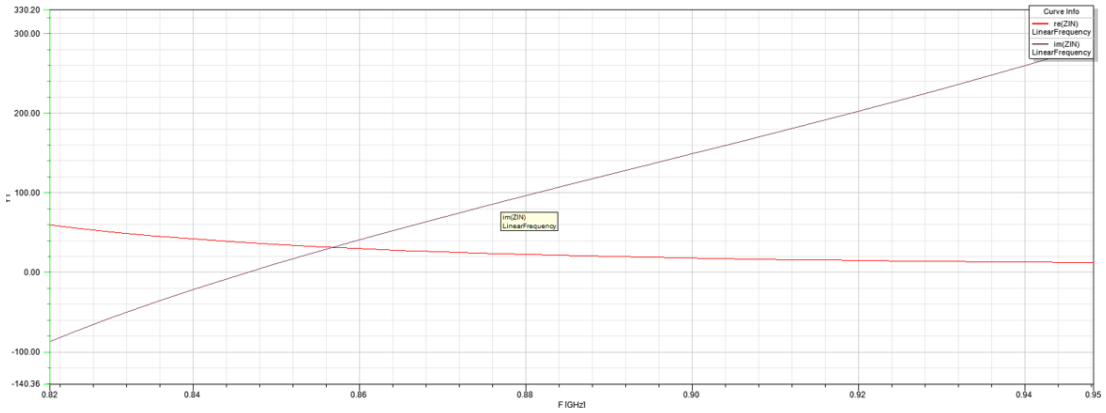

Figure 54 Impedance with matching network for a 6mm*6mm square antenna

Around the peak in the curve of power attenuation, Q is defined as the ratio of the peak frequency to the bandwidth at certain decibel. (Bowick et al, 2008) We need to broaden the bandwidth so that the power is kept strong in a wider range. This can be achieved by a cascading L-network in series. (Breed, 2008) The L-network (Figure 55) is the smallest unit for a standard matching network. In each unit, there should be one capacitor and one inductor, and no elements placed on the ground line. The order of series port and parallel port in each unit should not change when being cascaded. The relationship between the number of added L-networks and the value of Q is not identified in any reference. Generally, two L-networks can significantly improve the bandwidth.

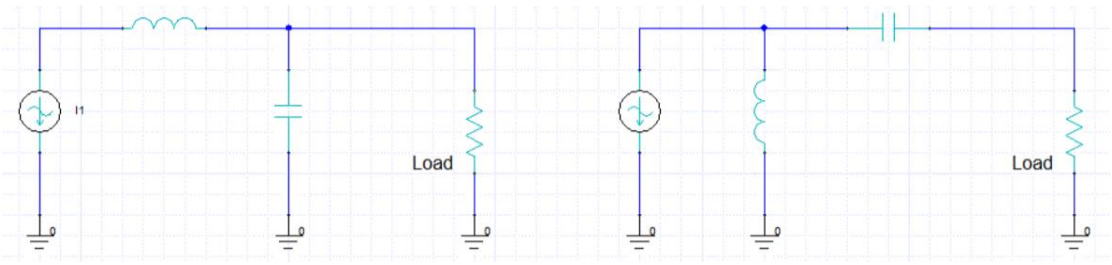

Figure 55 The structure of L-network

The second generation of the transmitter schematic with two L-networks added is shown in Figure 56. Compared to the first version shown in Figure 24, there are two advantages of this form. First, the square-network is removed, which leaves the antenna directly connected with the balun. As a result, the antenna will always stay balanced regardless of the impedance matching structure and transmission lines. Second, the cascaded L-network has no elements placed on the ground line, which transforms the circuit into the standard form shown in Figure 25. It is much easier to solve the impedance matching problem in the standard form because there are handy methods including mathematical, Smith Chart, and well-developed programs that provide multiple layouts by entering required conditions. (Leivre, 2016)

There is an extra requirement for the L-network cascaded circuit, which is that the load reactance must be cancelled before the matching network. Two methods could achieve this: according to the sign of load reactance, an element with the opposite sign and same value can be placed in series; or an element with the same sign can be placed in parallel to resonate with the load. The parallel method is more complicated than the series method because the value of the resonating element is harder to calculate. However, the parallel arrangement would result in a wider bandwidth. (Breed, 2008) Therefore, here we set the parallel port X1 to cancel the reactance.

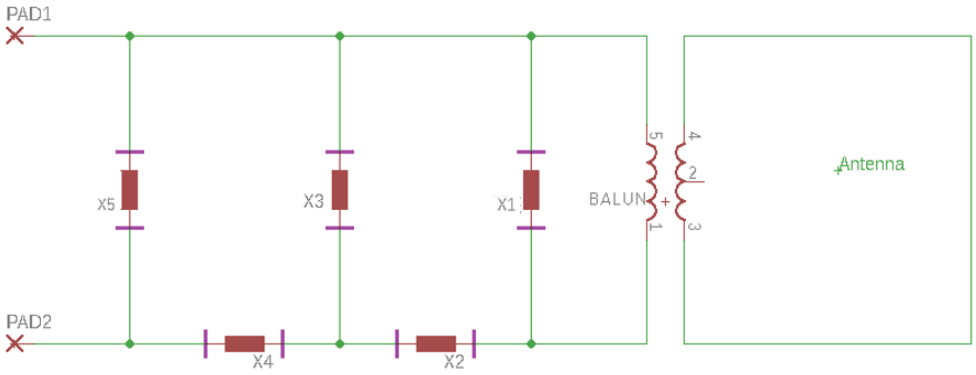

Figure 56 Improved schematic of transmitter

As we introduced in section 2.5.1, the mathematical methods of impedance matching are based on the ideal situation where the transmission lines do not contribute impedance to the circuit. However, the effect of circuit route between elements cannot be neglected, especially in such small scale. Therefore, instead of the value of impedance, we directly use the power gain curve to show the antenna performance. For example, the improvement of replacing the square-network with cascaded L-network was operated on the 6mm*20mm square-wave like antenna. From Figure 57(b), the improvement of a wider bandwidth can be identified. In addition, the peak value increases from -45.5dB to -35.0dB, which suggests a better matching result is achieved.

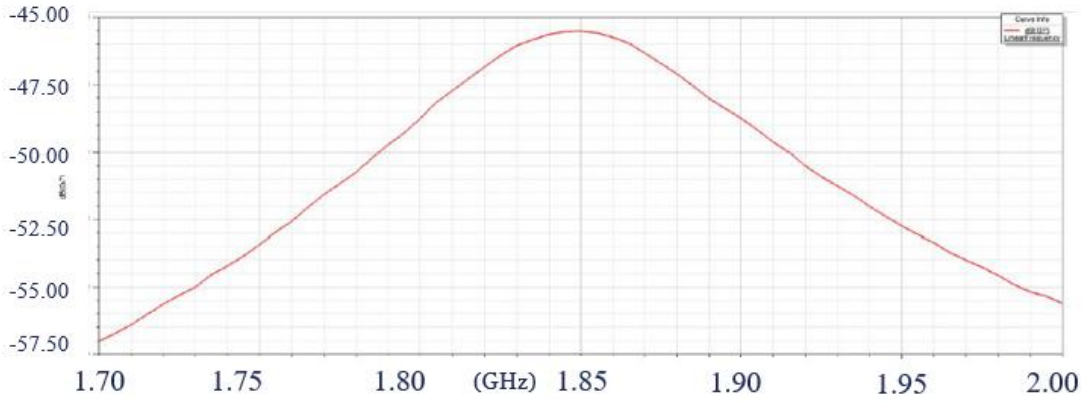

(a)

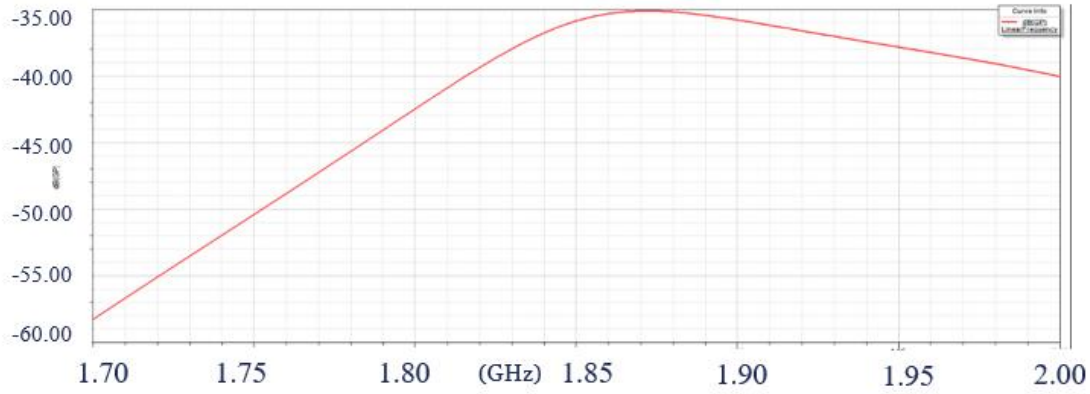

(b)

Figure 57 Simulation result of power gain (a) with square matching network (b) with two L-network

3.3 Construction of New PCBs and Test Results

After synthesizing all the aspects introduced before, four typical layouts as shown in Figure 58 (a) were manufactured. For actual test, each board is connected to a 15-inch coaxial cable. Components were soldered on the board according to the schematic shown in Figure 58 (b).

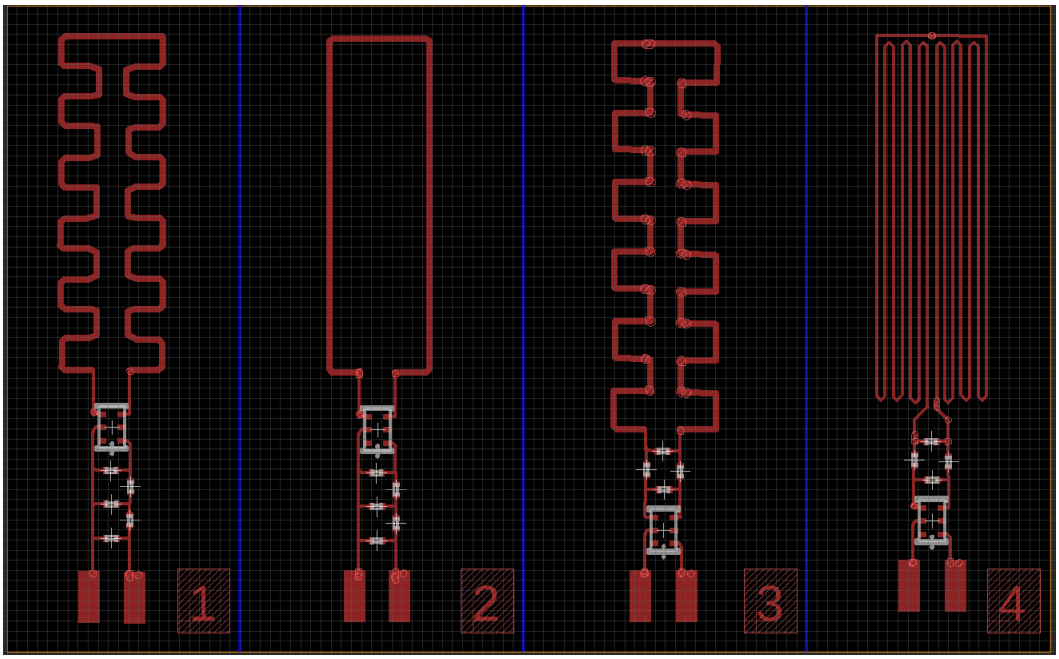
1
2
3
4

(a)

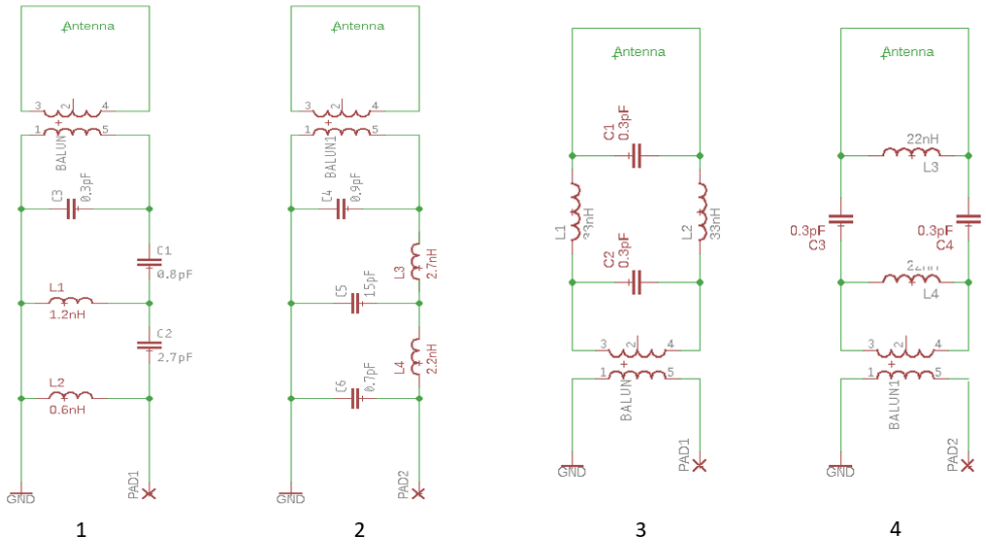
Antenna
BALUN
C3
0.3pF
C1
0.8pF
L1
1.2nH
C2
2.7pF
L2
0.6nH
GND
PAD1
Antenna
BALUN
C4
0.9pF
C5
1.5pF
L3
2.7nH
C6
0.7pF
L4
2.2nH
GND
PAD2
Antenna
C1
0.3pF
L1
33nH
L2
33nH
C2
0.3pF
BALUN
GND
PAD1
Antenna
22nH
L3
0.3pF
C3
0.3pF
C4
L4
BALUN
GND
PAD2

1 2 3 4

(b)

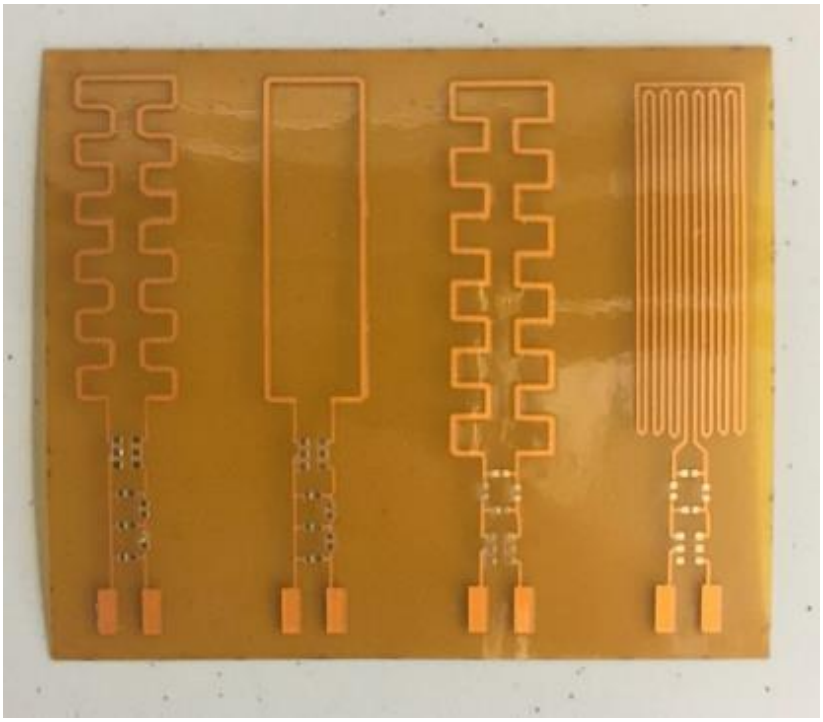

(c)

Figure 58 (a) The layout for new PCBs (b) The according matching network within 1.7-2.0 GHz (c) The manufactured PCB

The test results are overlayered in Figure 59, from which we can validate the simulation conclusions:

1. Comparing the curve ‘circuit 1’ with ‘circuit 2’, we can find they are similar with each other in both shape and amplitude, though ‘circuit 2’ is slightly higher than ‘circuit 1’. This demonstrated that increasing the route length by adding square corners has little or even negative effect on its performance.
2. Comparing the curve ‘circuit 1’ with ‘circuit 3’, we can see ‘circuit 1’ is much higher than ‘circuit 3’, which suggests the performance is significantly improved by replacing the square impedance matching network with cascaded L.

3. Comparing the curve ‘circuit 3’ and ‘circuit 4’, we can see the great advantage of keeping increasing the antenna length.

In conclusion, it could generate the highest level of power if we combine the fence antenna with cascaded L-network. However, because of the limit on time, it was not manufactured and will not be included in this thesis.

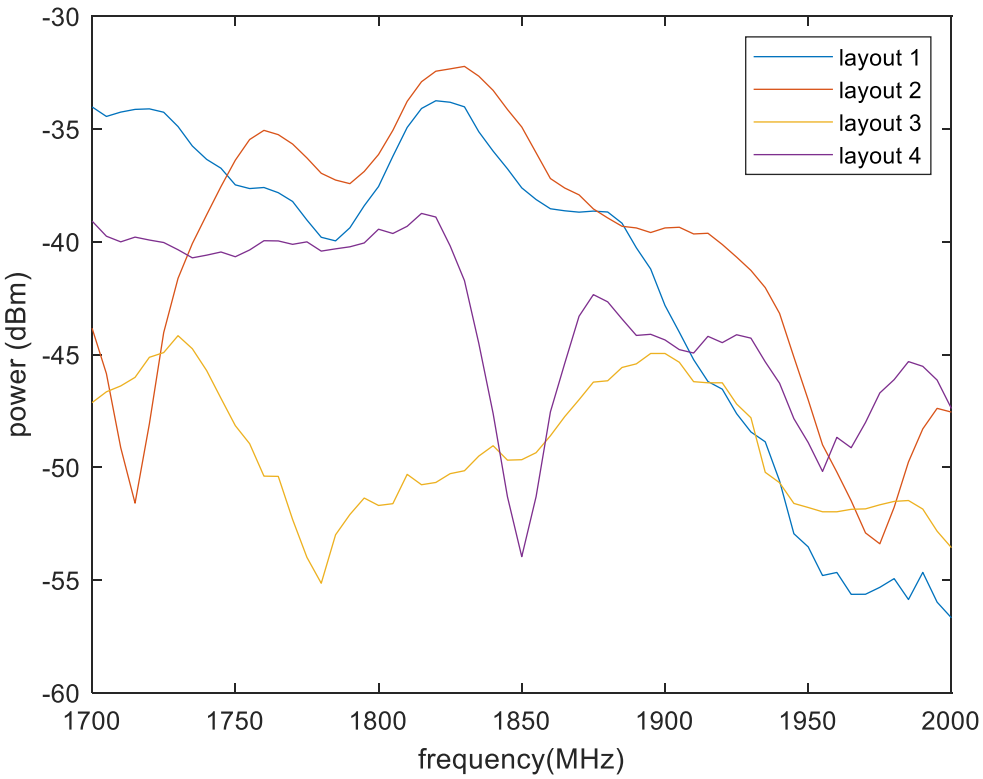

Figure 59 The result for the second-generation PCBs

3.4 New Choice of Substrate for the PCB

For most flexible PCB manufacturers, the most common choice for the board is Polyamide, which has high resistance to repeated bending stress and high temperature.

However, problems occurred when we tried to insert the antenna into the catheter with 2.1mm diameter. The flexibility of the board is seriously restricted with elements soldered on. This motivates us to find other materials with better physical properties.

The first alternative we sought is Nitinol, which is the material for our stent. It is widely applied for medical treatment because it is harmless to the human body. Short for nickel and titanium, the metals it is made from, Nitinol has two unique properties, which are super elasticity and shape memory effect. (Wikipedia, 2015) The super elasticity permits maximizing the uncurled surface area of the antenna while enabling the curled diameter to be small. In addition, the shape memory effect can help the antenna maintain the best working shape. More specifically, the shape of Nitinol board should be fixed according to its best performance condition. During deployment, the board can be folded or curled to the sheath. If the board reaches the desired position, it can be released from restriction and recover to the original shape within human body.

Before practically developing the PCB on Nitinol substrate, we need to make sure the radio wave will not be blocked by an alloy substrate. We experimented with a thin Nitinol foil shown in Figure 60(a). To identify the effect of Nitinol foil, first we needed a reference group without the interference of Nitinol, as shown in Figure 60(b). The next test had the Nitinol foil tightly wrapped around the antenna. Lastly, the antenna was rolled up and inserted into the shell shown in Figure 41, then the Nitinol foil was wrapped outside.

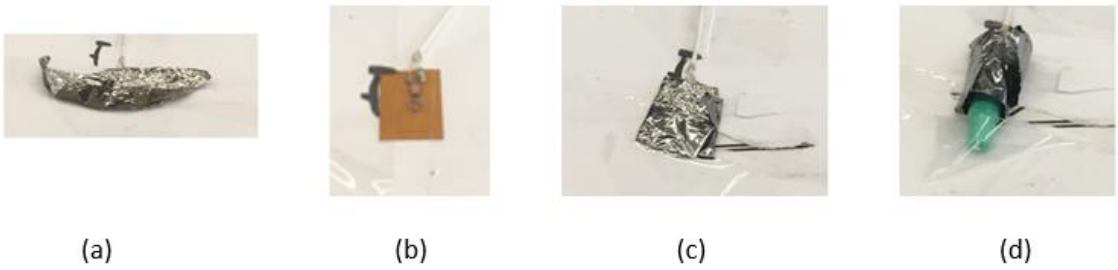

Figure 60 The test for Nitinol effect (a)The Nitinol foil (b)The reference test without Nitinol (c) Nitinol foil wrapped on the flat antenna (d) Nitinol foil wrapped out the shell holding the antenna

The result is shown in Figure 61. The two groups with the Nitinol foil attached are close to each other, and surprisingly, their power gain is much higher than the reference test without the Nitinol foil. A possible explanation for the growth in power is due to the ground effect. The efficiency for the antenna when it is put on perfect conductor is different from that when it is put on lossy earth. (Balanis, 2012) In our test, the antenna is fixed on an empty carton, which would cause the input resistance to increase and the antenna efficiency to decrease accordingly. One of the effective improvements to increase the efficiency is to place radial wires or metallic disks under the antenna, (Balanis, 2012) which could be a similar situation to the Nitinol foil wrapped around the antenna in our test.

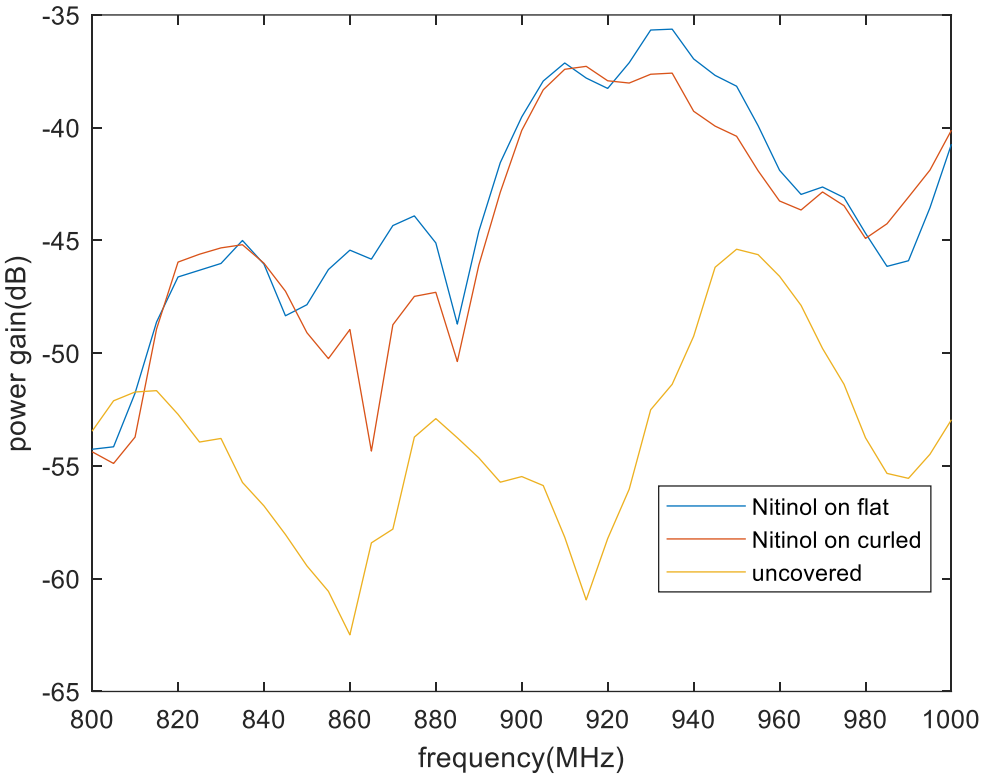

Figure 61 The effect of Nitinol foil

Based on the results above, we expect to see advantages from a Nitinol substrate, but the idea is hard to be realized because of the obstacle of how to construct the circuit on it. In addition, notice that Nitinol is a good conductor with electrical resistivity of $82 \times 10^{-6}\ \Omega \cdot cm$. To avoid causing short circuits, insulating layers will be necessary, which will unpredictably change its physical property. In conclusion, enabling Nitinol to be feasible as the PCB substrate, or continuing to search for other alternative material will be the potential directions in developing a more flexible and effective antenna.

4.0 Test the System in Pig Necropsy

We have proved the effectiveness of improvements on the RF system with the tests operated in the lab setting, a situation with low level of noise and vibration. However, the practical application for the antenna is under more severe and noisy conditions. In addition, the destination of the stent is deep within a human artery, surrounded by various body tissue including skin, fat, muscle, skeleton, and blood. Generally, the multiple tissue layers and surrounding blood will attenuate the radio waves by reflection and absorption up to 15dB. (Vychytil et al, 1999) Thus, tests for the transmitter resistance under practical conditions are necessary. Since human testing is not feasible at this stage of research, testing was carried on pigs during necropsy. It is widely accepted that the anatomy of a pig heart is almost identical to human, which makes it an ideal model for cardiovascular research. (Simon et al, 2018)

Figure 62 shows all the transmitters we have introduced. For the convenience of expression, these transmitters are labeled as No.1 to No.7. All these antennae were tested within pig body, so that the body's attenuation effect can be learned with each test object.

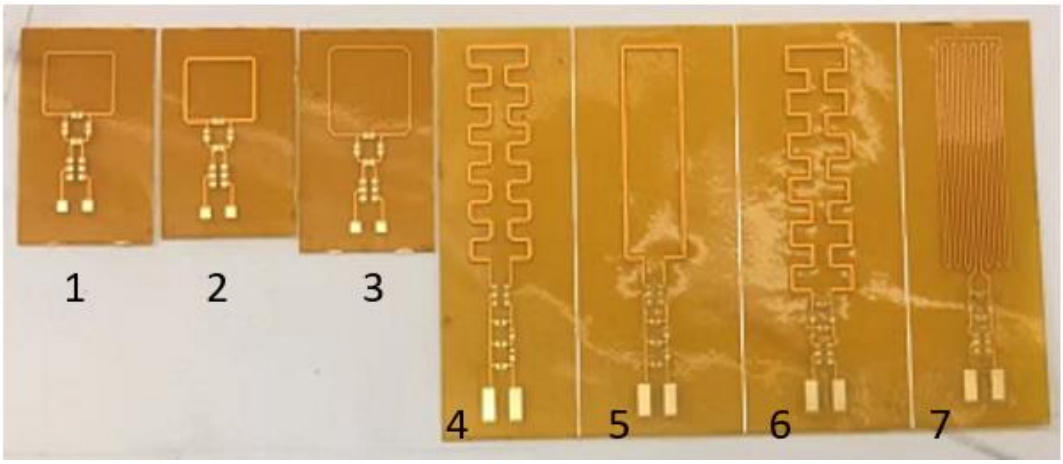

Figure 62 All the transmitters

For the pig necropsy, an auxiliary PVC frame was used to deploy the antenna. The frame is shown in Figure 63(a). Similar to the tests in the lab, the origin is defined as the location vertically under the receiver. The receiver is left outside the body in a fixed location on the upper branch, while the transmitter will move back and forth in one direction inside the lower branch. The transmitter is attached to a guiding rod, marked with scale of distance, from which we can tell how far the transmitter is advanced. During the operation, the lower branch will be buried in the pig body as it shown Figure 63(b). Considering the actual length of human body, we set five positions with an increment of 2 inches and centered at the origin. In another words, the transmitter stops at -4, -2, 0, 2, 4 for each test.

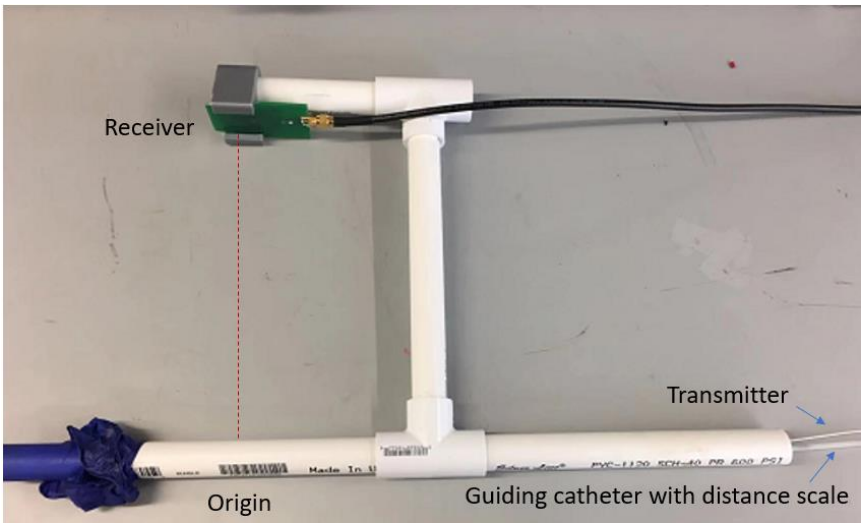

(a)

(b)

Figure 63 The auxiliary PVC frame (a)the components arrangement (b)the deployment within pig

The power patterns for transmitters 1-7 are shown in Figure 64. As the receiver is fixed, the vertical profile represents the amplitude variation at each desired location. According to our design, the first three square antennae were tested within 800--1000GHz, while the rest were tested within 1700--2000GHz. These 3-D profiles suggest the flexible antenna we

developed is powerful enough to penetrate the human body and deliver abundant valuable information regarding its position.

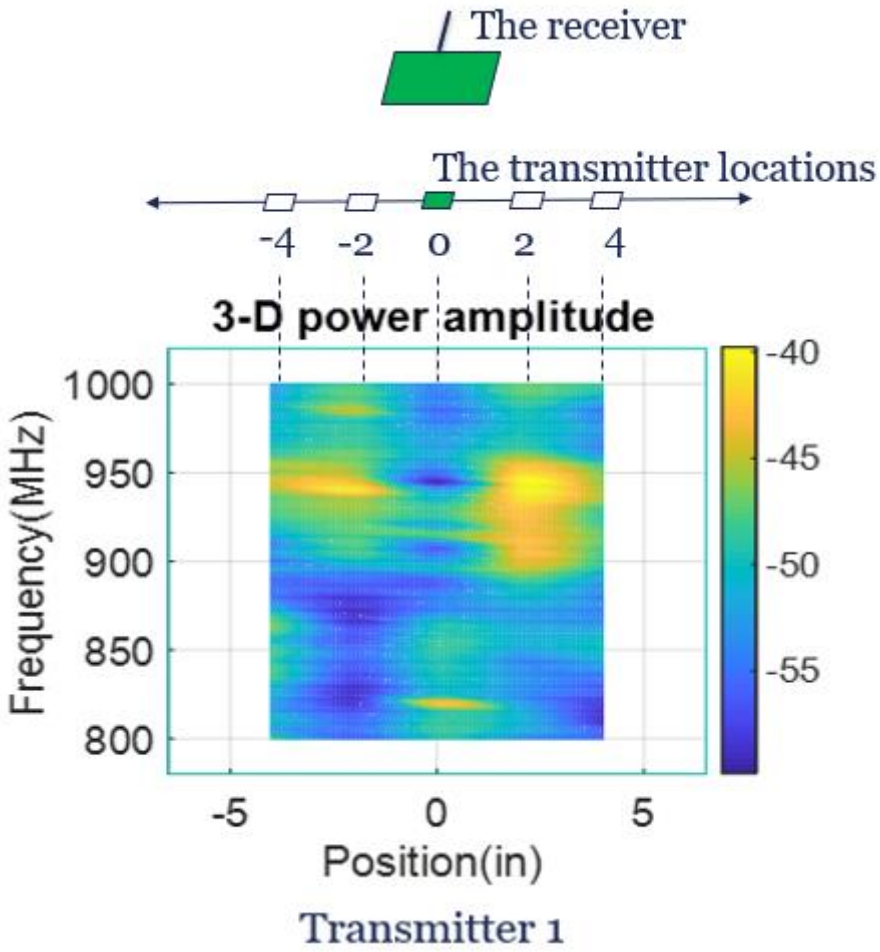

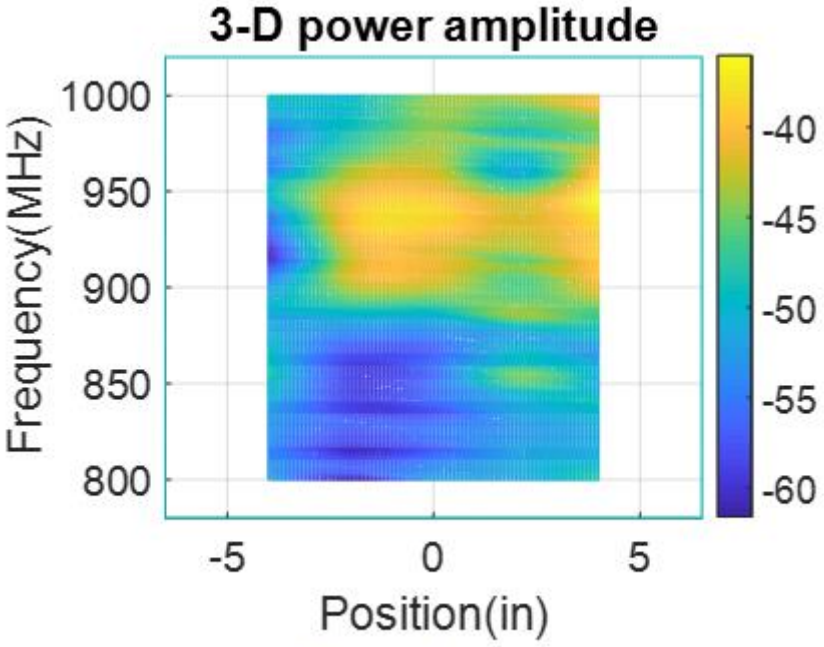

Transmitter 2

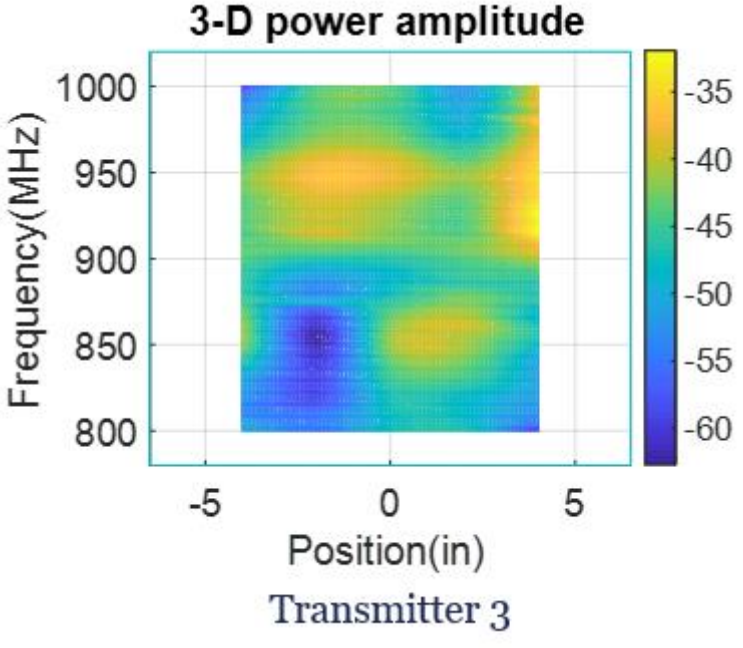

Transmitter 3

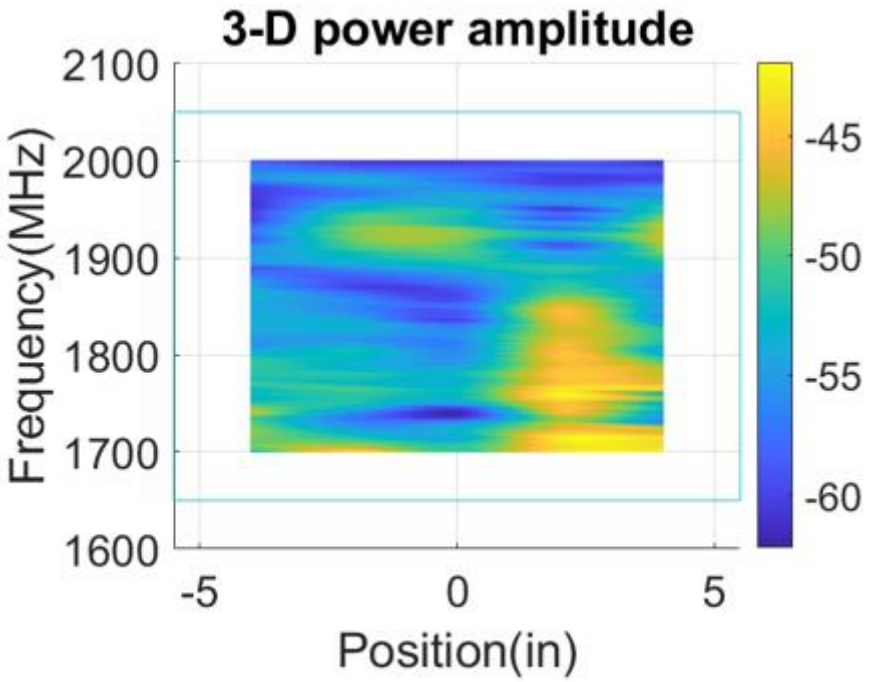

Transmitter 4

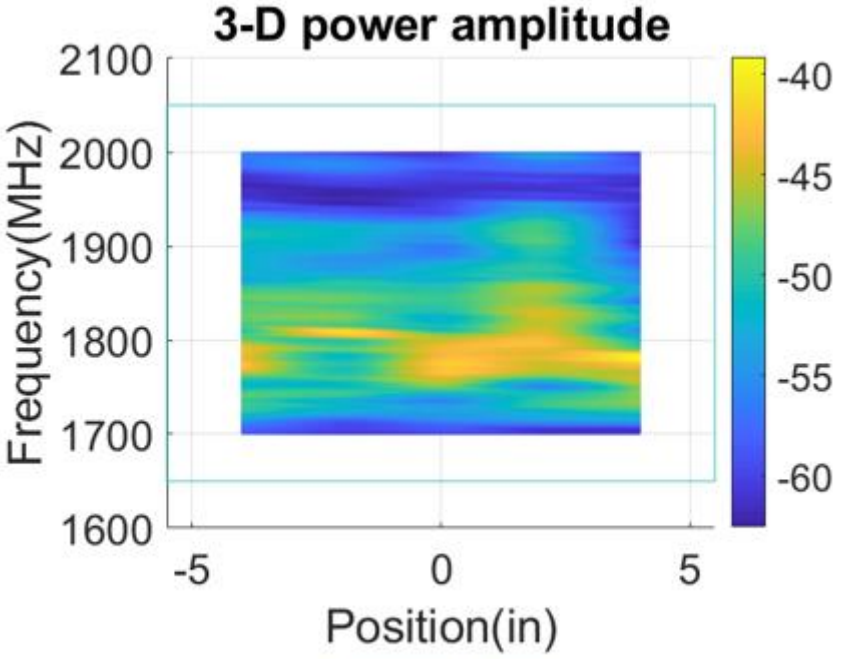

Transmitter 5

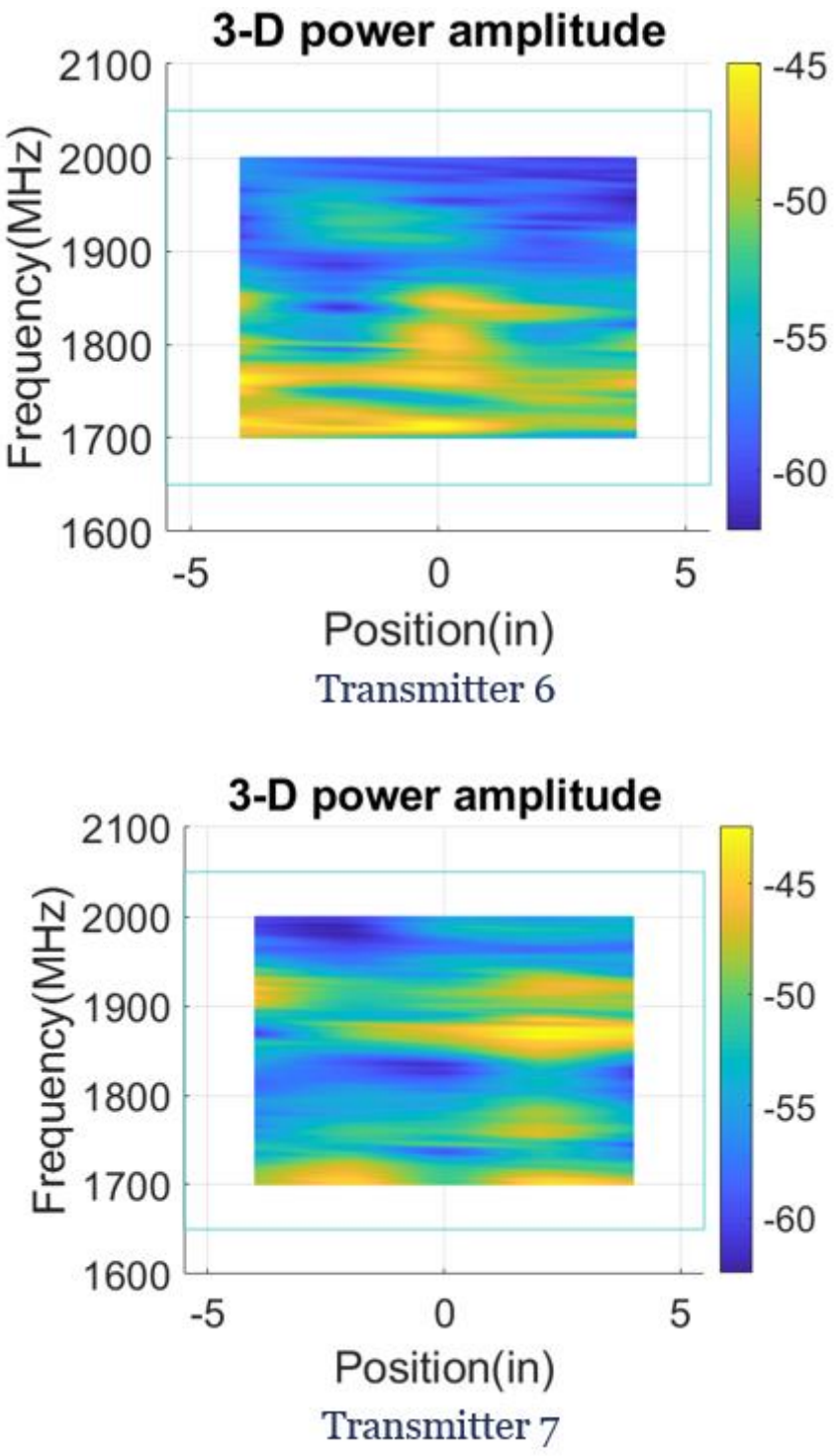

Figure 64 the radiation pattern for all the antenna (from No.1 to No.7) with pig necropsy

5.0 Determining the Position with Neural Network

In previous chapters, we simply evaluated the antenna performance by the amplitude of its radiation power. However, when applied for determining position, more factors except the power should be considered. In this chapter, we will introduce how we predict the position with neural network, and how we choose the antenna with highest accuracy.

Neural network is a branch of machine learning, which is used for data classification or prediction by processing the existing data with a mathematical algorithm. Because of the ability of learning complex nonlinear functions, neural networks are widely applied for pattern recognition. (Suykens, 2014) In this thesis, we will not introduce how to develop a neural network algorithm. Instead, we took advantage of the MATLAB built-in neural network toolbox, so that we could focus on how to improve the process for data collection and selection, which are essential to the prediction accuracy.

5.1 Automate the Data Collection Process

5.1.1 The Disadvantages of Manual Work

All the data applied in previous chapters were collected manually, which is inefficient and arduous work when a large amount of data is needed. Using the spectrum analyzer

introduced in section 2.2, we must adjust the transmitter to the desired position after each frequency sweep. Depending on the number of set-up positions and the frequency range, it takes 5-7 minutes for each trial. In the machine learning theory, it is understood that a large size of training data could help in improving the prediction accuracy. Especially for neural network, the algorithm can keep improving itself given more training data. (Brownlee, 2017) Here we applied a popular heuristic approach which set 50 random samples for each class. (Foody, 2009)

Besides inefficiency, the manual work inevitably introduces unpredictable variables. Ideally, we want the variables that affect the radiation to only include frequency and position. However, we identified many factors whose effects should be eliminated but that occur with manual operation. For example, with our testing devices shown in Figure 12, where the receiver is fixed on a tube, every time we move the scaled tube back and forth to change the relative position, a small error could be introduced. Figure 65 shows the significant difference for two trials in which the origin of the second trial was set to 0.5 inch deviated from the origin for first trial. In addition, the placement of cable and the rotation of the transmitter also have significant effect on the result.

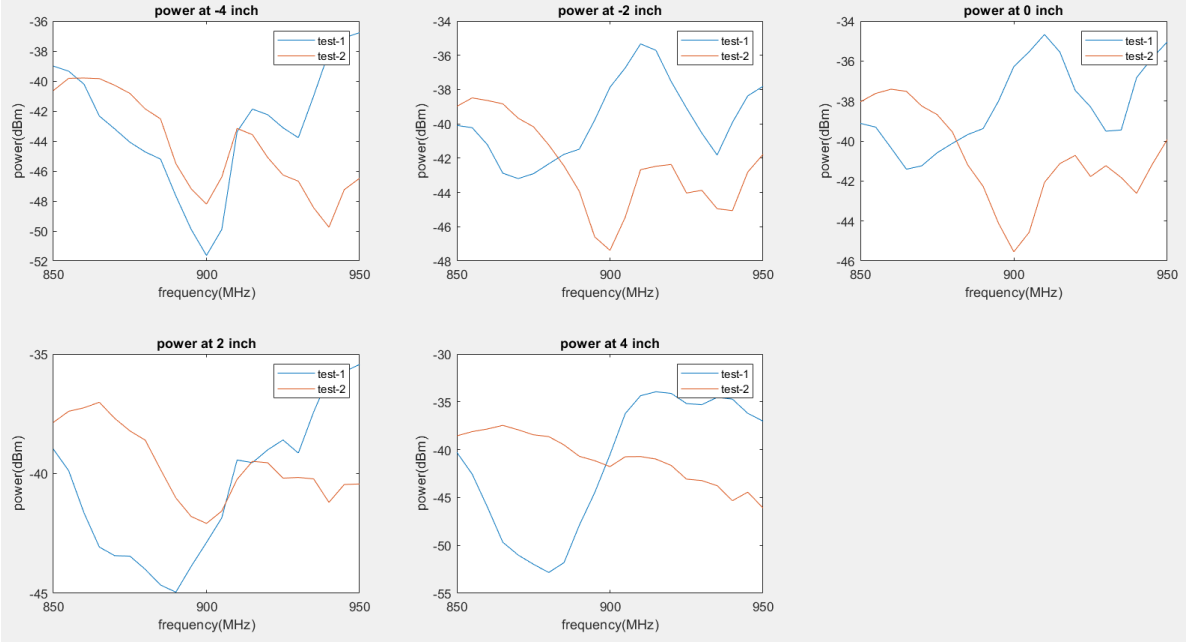

Figure 65 The error with a deviation of origin

5.2 The Automated System

5.2.1 The Basic Capabilities

To facilitate collection of large data sets for assessing the various antennae performance and for training the neural network, an automated data collecting system was developed, as shown in Figure 66. The main program is built in MATLAB, from which we can set the frequency scope, frequency increment, desired positions and number of trials. Then these commands are realized with the help of several microcontrollers. Given all required inputs, the cart departs from the origin, and drives the transmitter to each prescribed position, at which point the function generator sweeps frequency by the prescribed scope and increment.

Simultaneously, the received signal is recorded. After repeating the process for the required number of trials, the cart returns to the origin and is ready for the next test.

This system perfectly solved the problems introduced in the last section. First, people can be freed from the test bench as the system keeps running repeatedly. In addition, the system has a high resolution in distance, so that the uncontrollable errors that existed in manual operation are minimized.

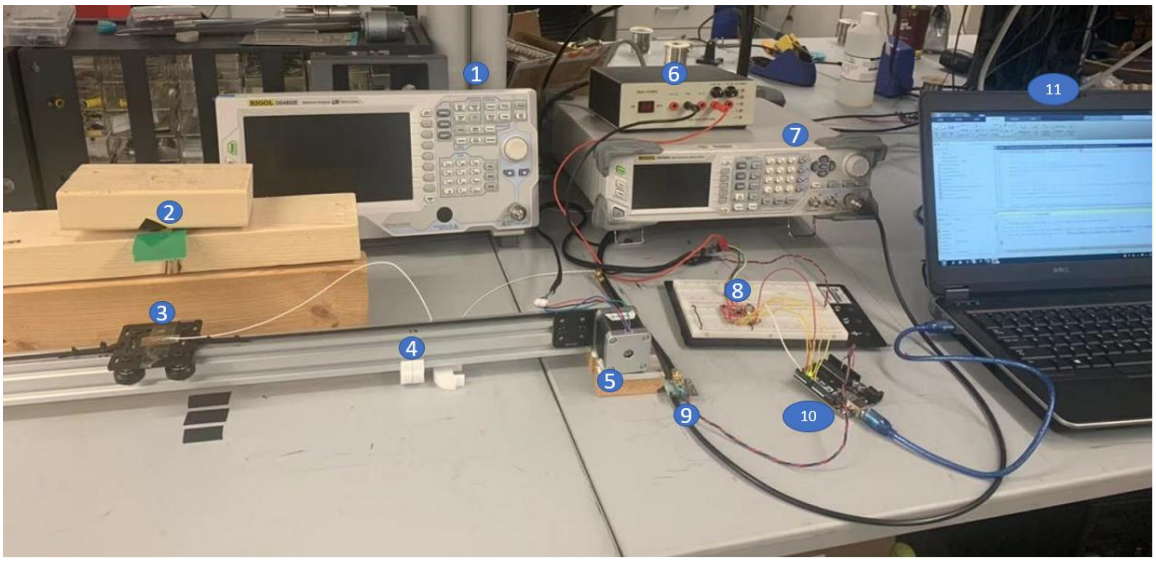

Figure 66 Automated data collecting system ①Spectrum analyzer ②Receiver ③Transmitter ④Rail ⑤Stepper motor ⑥Power supply ⑦Function generator ⑧Motor driver ⑨Peak detector ⑩Arduino ⑪Controlling laptop

5.2.2 Control Boards

The receiver is placed in a fixed location, as shown in Figure 65, and the transmitter is mounted to a stage that moves along a rail by a belt drive. A MT-1704HS168A stepper motor

(Openbuilds Partstore) is used to drive the stage. The motor is controlled by an Arduino microcontroller by way of an H-bridge stepper motor driver (Sparkfun Easy Driver V4.5).

The Easy Driver provides the stepper motor with the resolution of 3.75×10^{-2} mm for each step signal, which provides accurate control over the cart's position.

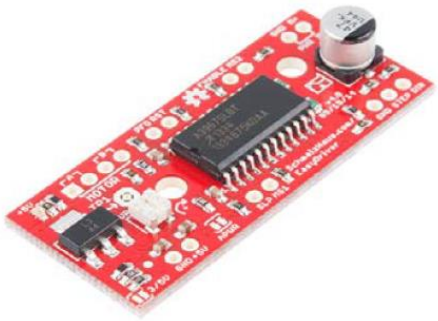

Figure 67 The Easy Driver (Sparkfun, 2016)

The power detector LTC5582IDD (Analog Devices), is capable of measuring the power on the receiver in a wide range of frequency, and precisely converts the decibel-scaled AC power into DC voltage on a linear scale. (Analog devices, 2010) The relation between the RF input power and the output voltage is shown in Figure 68(b), from which we apply the curve under 880MHz to represent most conditions. The approximated relation is:

$$output\ Voltage(V) = 0.02875 * RF\ input\ power(dBm) + 0.75 \qquad (5\text{-}1)$$

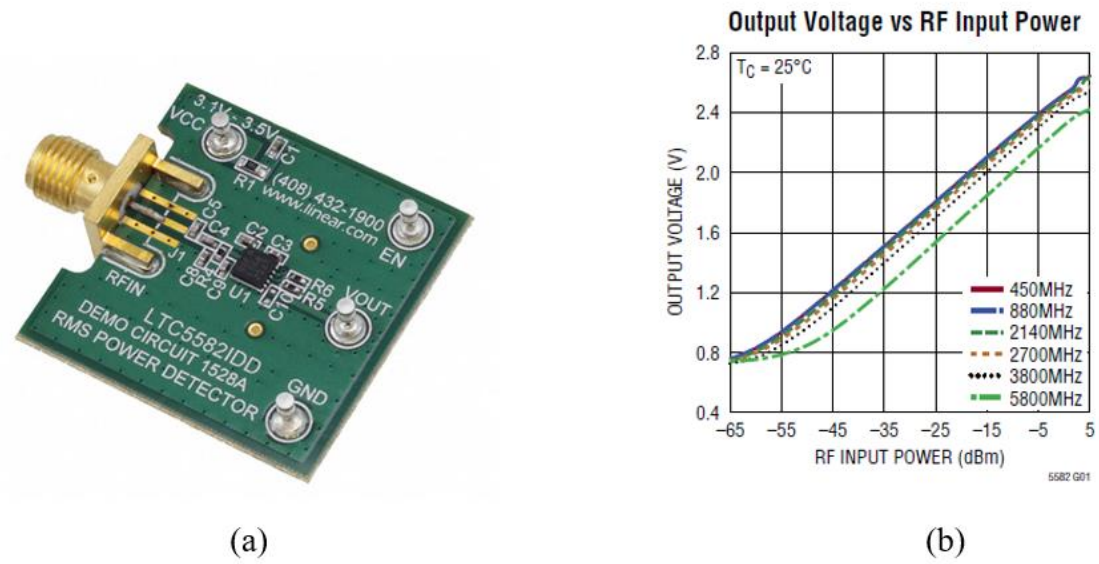

Figure 68 (a)power detector LTC5582IDD (Analog Devices, 2013) (b)convert from dBm to Voltage

The schematic of the system shown in Figure 66 can be expressed as Figure 69. The data collection process starts with entering the commands on the computer to set the frequency scope and frequency increment to the function generator, while sending the desired positions and number of trials to the Arduino (Figure 70). The Arduino makes the commands recognizable for the Easy Driver, so that the transmitter is moved to certain positions where the frequency sweep occurs. The radio frequency signal is caught by the receiver and transformed into voltage by the power detector. Finally, each analog voltage is transferred by the Arduino and then stored in the computer. When the whole process is finished, the data can be manipulated, and plots can be drawn in MATLAB.

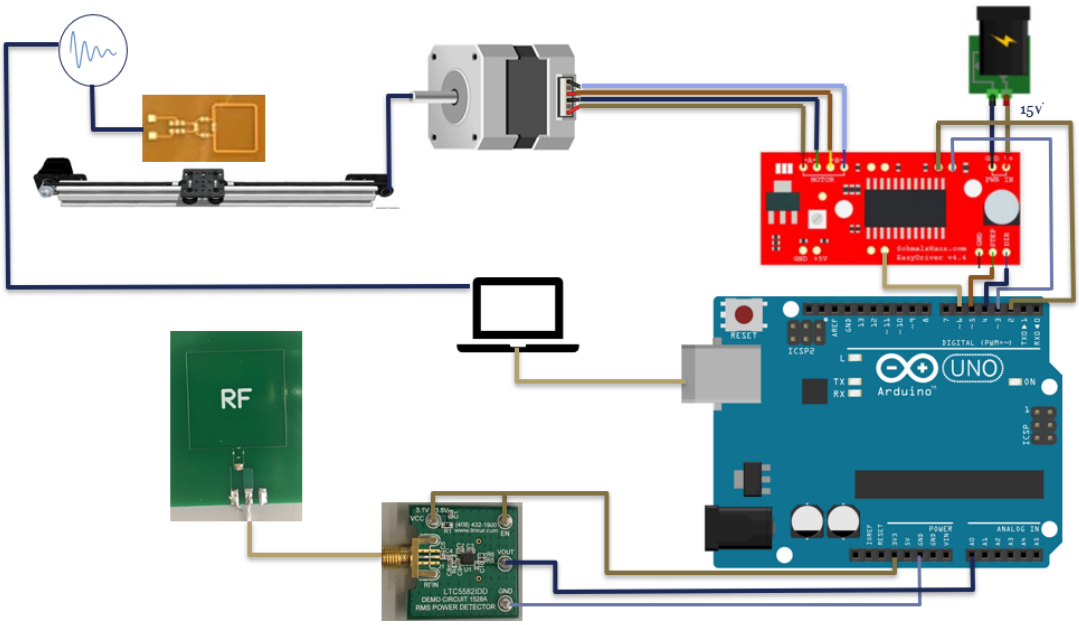

Figure 69 Schematic of the position test system

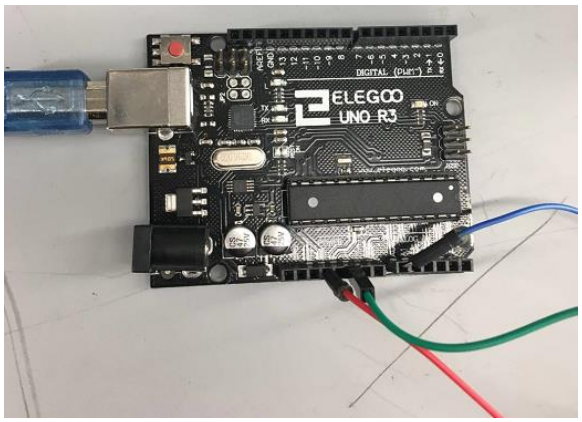

Figure 70 Arduino UNO R3

5.2.3 Analysis Based on Large Size Sample

Now a comprehensive analysis can be made based on a large size sample, which can help us evaluate the performance of certain antenna and for reliably determining position when it is applied with a neural network. For the convenience of illustration, we define a trial as the process of the transmitter being driven by the cart from the first position to the last. At each stop among the desired positions, the frequency sweeps five times, then is averaged as one sample.

To learn the relation between the transmitted power and the transmitting antenna's position, the test results are separated into several subplots. Each subplot is a synthesis of all trials. As it was introduced in Figure 64, the result for each trial could be represented in a 3-D profile. Imagine each profile is evenly divided along the axis of position. Then for all the trials, the profile belt at each position is extracted and compiled into a new plot, which is shown in Figure 71. For each subplot, each row presents a frequency sweep trial, and the column represents all trials at a certain frequency. This plot gives us a direct overview for the antenna performance,

Figure 71(a) shows a set of 20 trials, with frequency sweep in the range of 0.8GHz—1.0GHz. From the 3-D profile, we can identify if there is any abnormal situation included. Some of the abnormal spots which have distinct amplitude against the surrounding are circled in Figure 71(a). These spots might be caused by external noise or vibration, which is inevitable for a long-time test. Thus, we still regard this antenna as feasible because there is no abrupt change in the vertical direction, which indicates the antenna performance under a certain

position and frequency is stable and repeatable during all the trials. However, sometimes serious problem can happen unnoticed. For example, Figure 71(b) shows a test when the cable-antenna joint was broken during the test. With a glance of the 3-D profile, we could tell the data from this set should not be applied and there are problems that must be figured out.

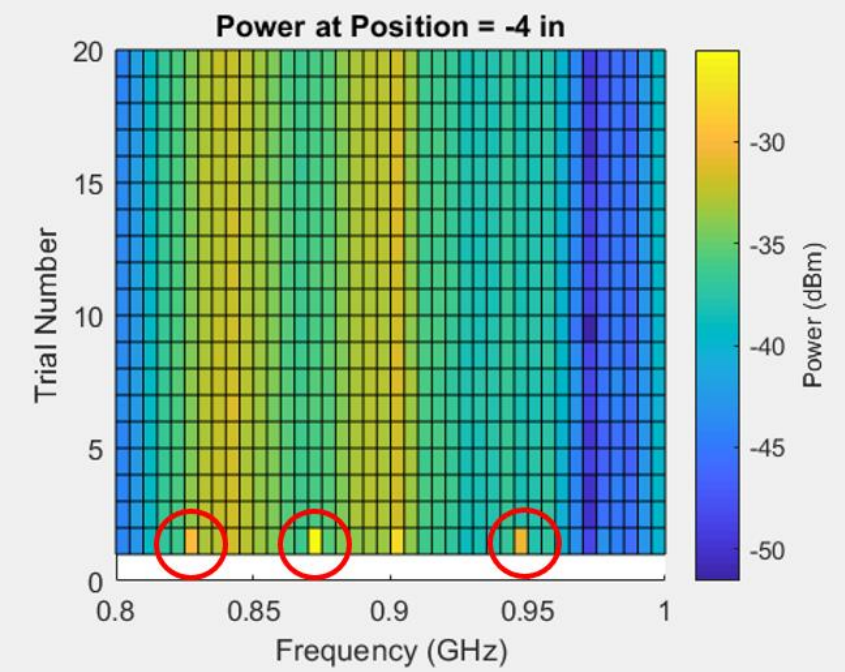
Power at Position = -4 in
Trial Number
Frequency (GHz)
Power (dBm)
20
15
10
5
0
0.8
0.85
0.9
0.95
1
-30
-35
-40
-45
-50

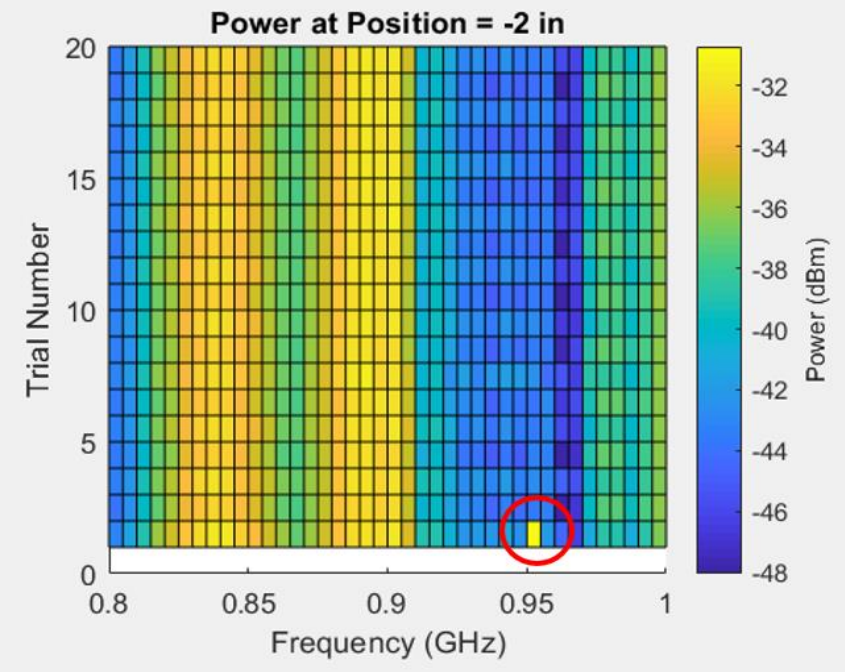
Power at Position = -2 in
Trial Number
Frequency (GHz)
Power (dBm)
20
15
10
5
0
0.8
0.85
0.9
0.95
1
-32
-34
-36
-38
-40
-42
-44
-46
-48

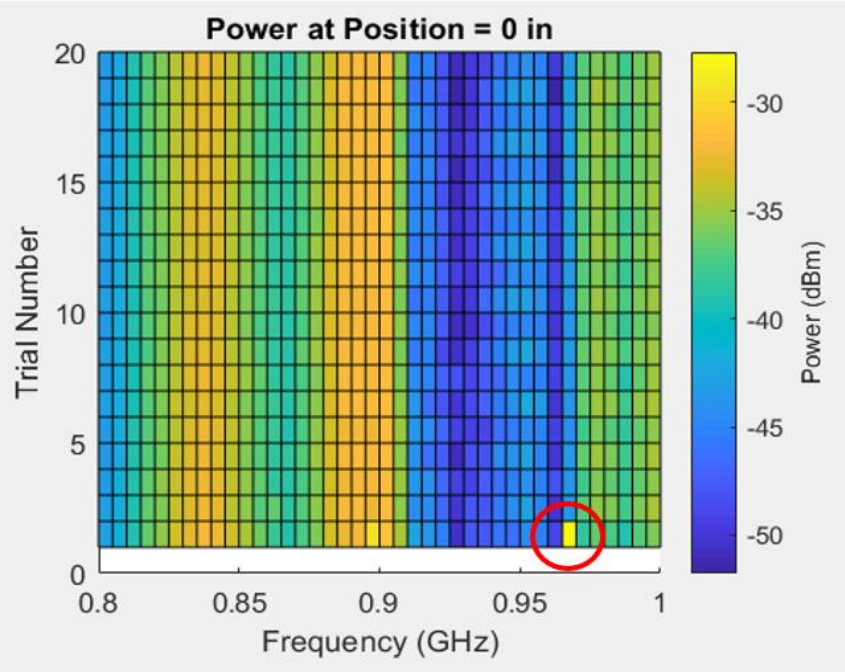
Power at Position = 0 in
Trial Number
Frequency (GHz)
Power (dBm)
20
15
10
5
0
0.8
0.85
0.9
0.95
1
-30
-35
-40
-45
-50

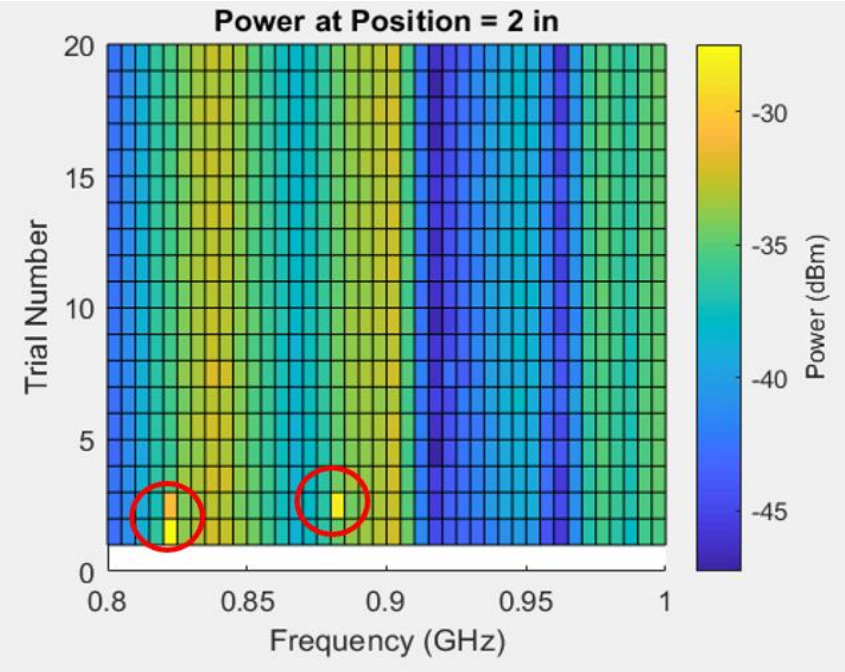
Power at Position = 2 in
Trial Number
Frequency (GHz)
Power (dBm)
20
15
10
5
0
0.8
0.85
0.9
0.95
1
-30
-35
-40
-45

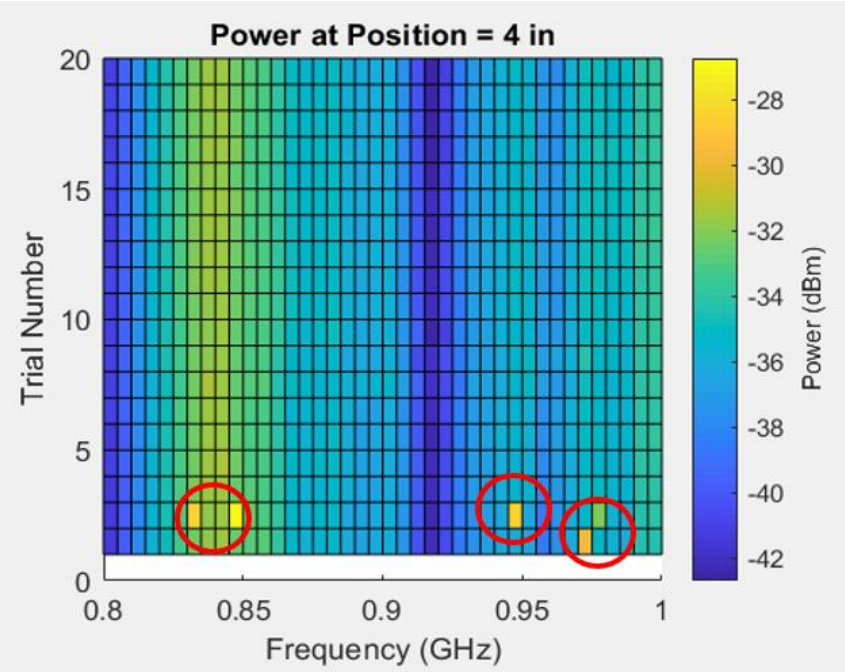
Power at Position = 4 in
Trial Number
Frequency (GHz)
Power (dBm)
20
15
10
5
0
0.8
0.85
0.9
0.95
1
-28
-30
-32
-34
-36
-38
-40
-42

(a)

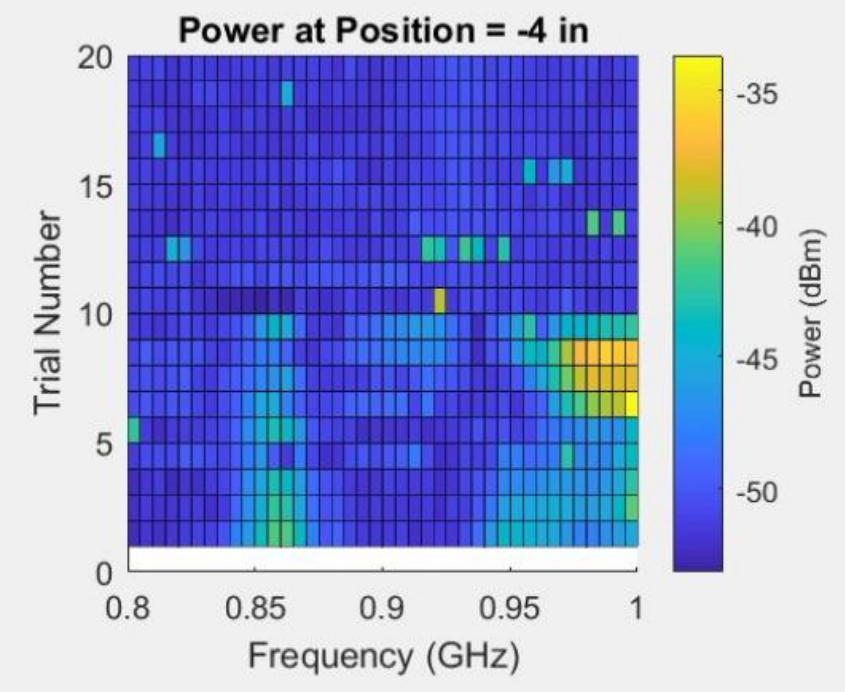
Power at Position = -4 in
Trial Number
Frequency (GHz)
Power (dBm)
20
15
10
5
0
0.8
0.85
0.9
0.95
1
-35
-40
-45
-50

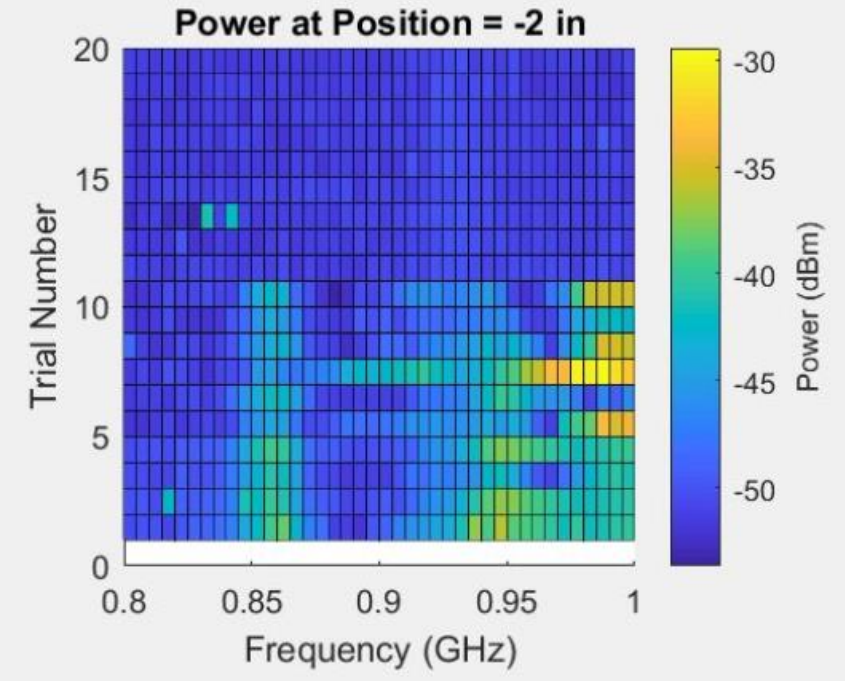
Power at Position = -2 in
Trial Number
Frequency (GHz)
Power (dBm)
20
15
10
5
0
0.8
0.85
0.9
0.95
1
-30
-35
-40
-45
-50

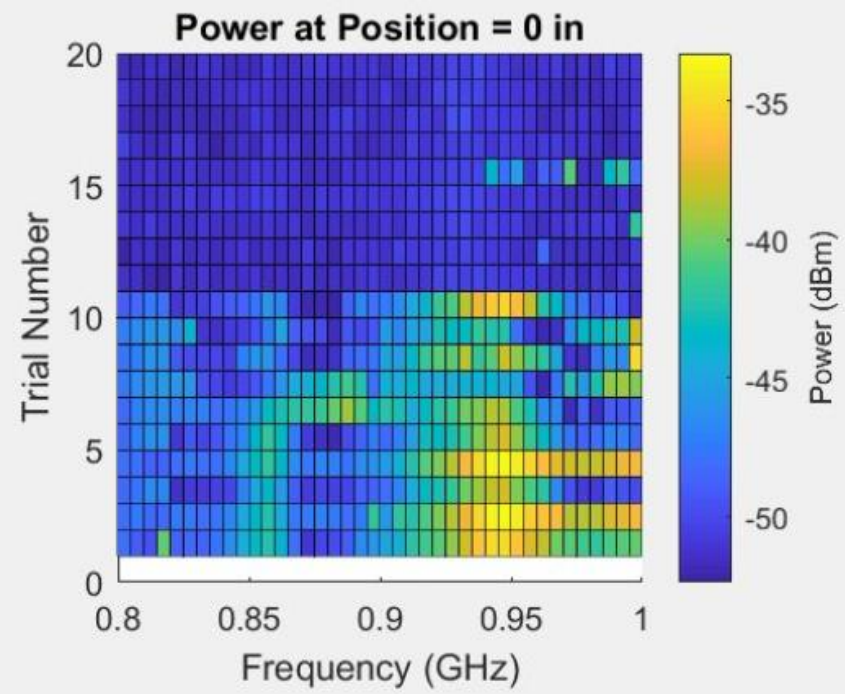
Power at Position = 0 in
Trial Number
Frequency (GHz)
Power (dBm)
20
15
10
5
0
0.8
0.85
0.9
0.95
1
-35
-40
-45
-50

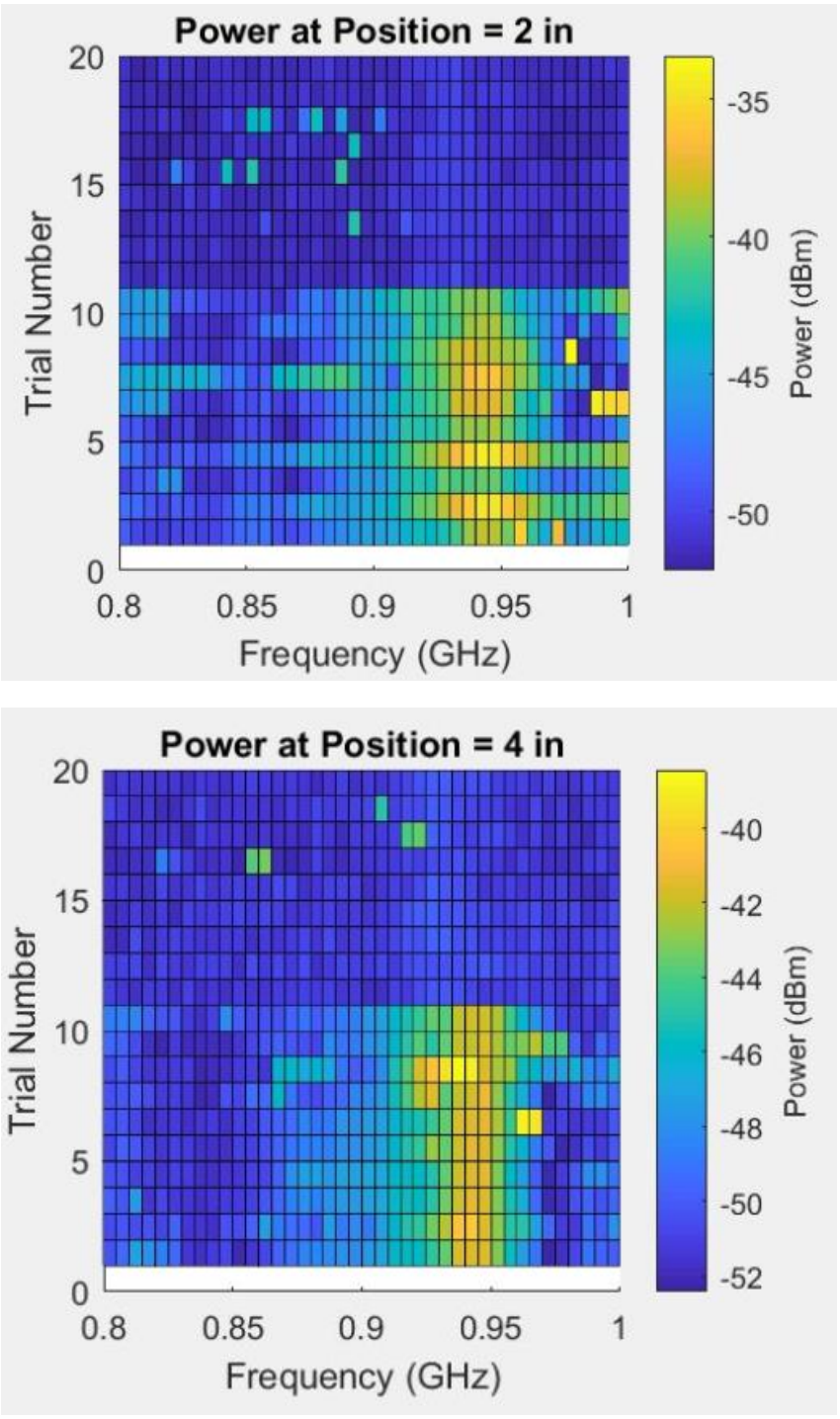

(b)

Figure 71 (a)normal 3-D profile (b)abnormal 3-D profile

Once the data from all position trials is collected, we average the values of each column to convert the 3-D profile into the 2-D plot, so that we can make more accurate evaluation for the test sample. For the 2-D plots shown in Figure 72, the blue line is the averaged power among 20 trials. In addition, when the sample size becomes large, it is more comprehensive to evaluate the range of sample expectation rather than the averaged line. Thus, we introduce the dash line envelope representing the 95% confidence level, which are calculated by:

$$confidence\ level = average\ \pm 2 \times standard\ deviation \tag{5-2}$$

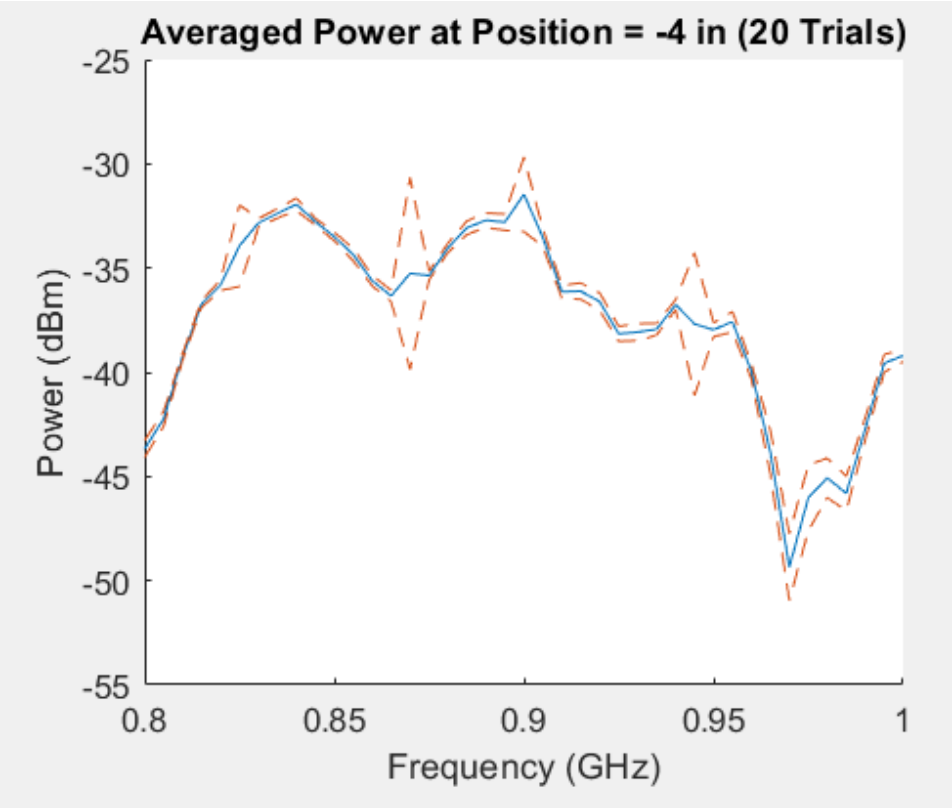

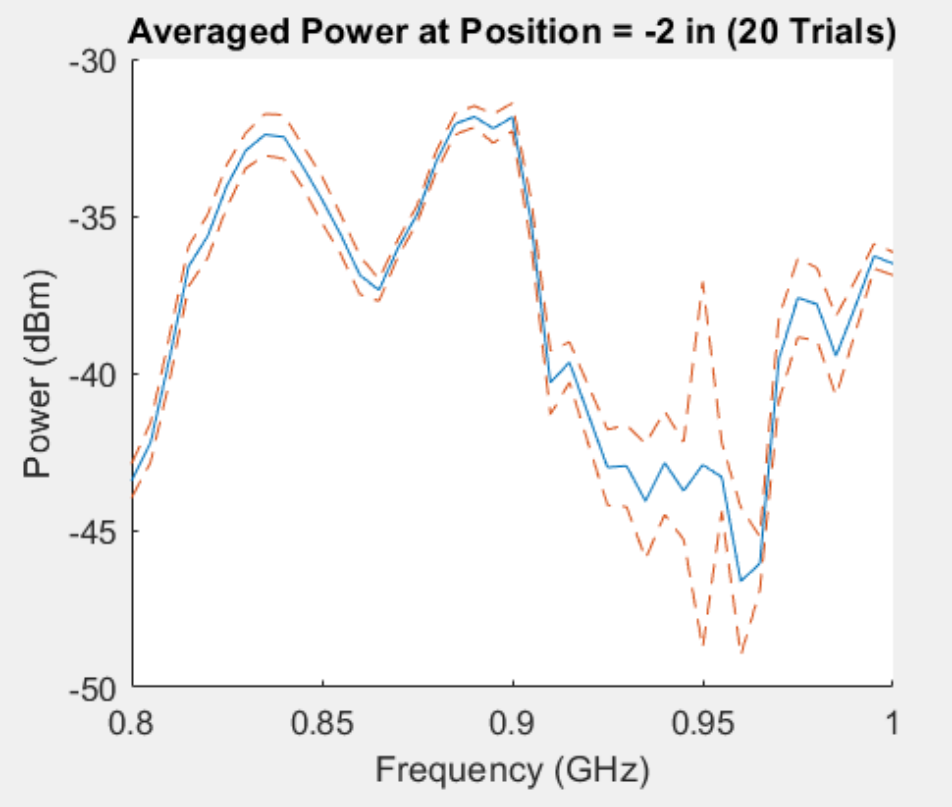
Averaged Power at Position = -2 in (20 Trials)
-30
-35
-40
-45
-50
Power (dBm)
0.8
0.85
0.9
0.95
1
Frequency (GHz)

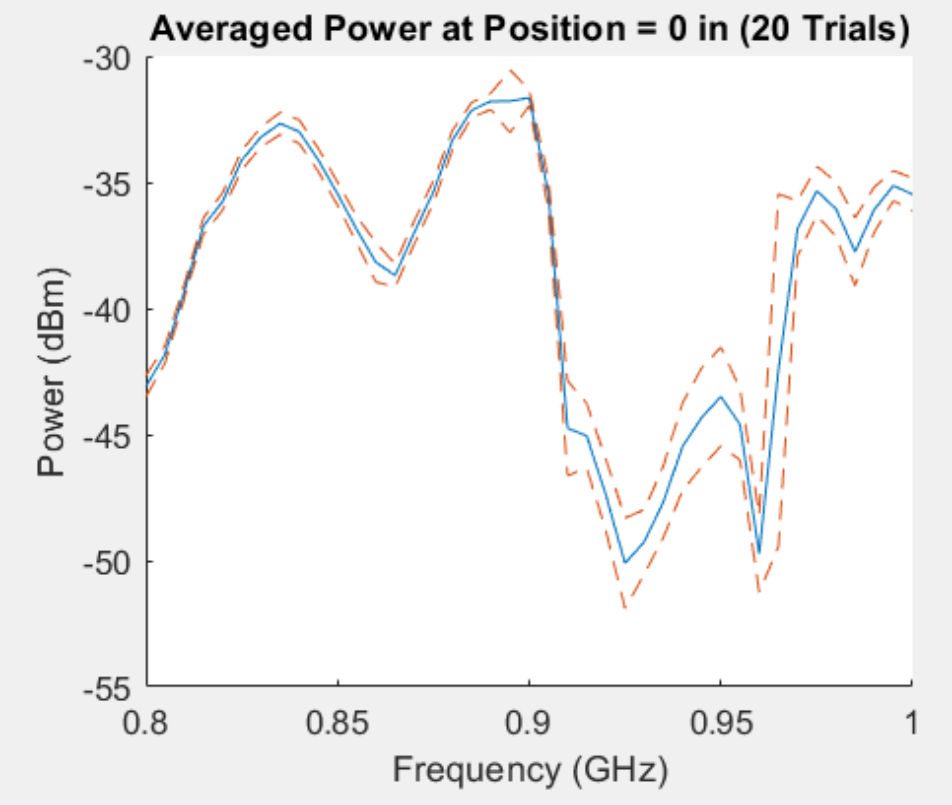
Averaged Power at Position = 0 in (20 Trials)
-30
-35
-40
-45
-50
-55
Power (dBm)
0.8
0.85
0.9
0.95
1
Frequency (GHz)

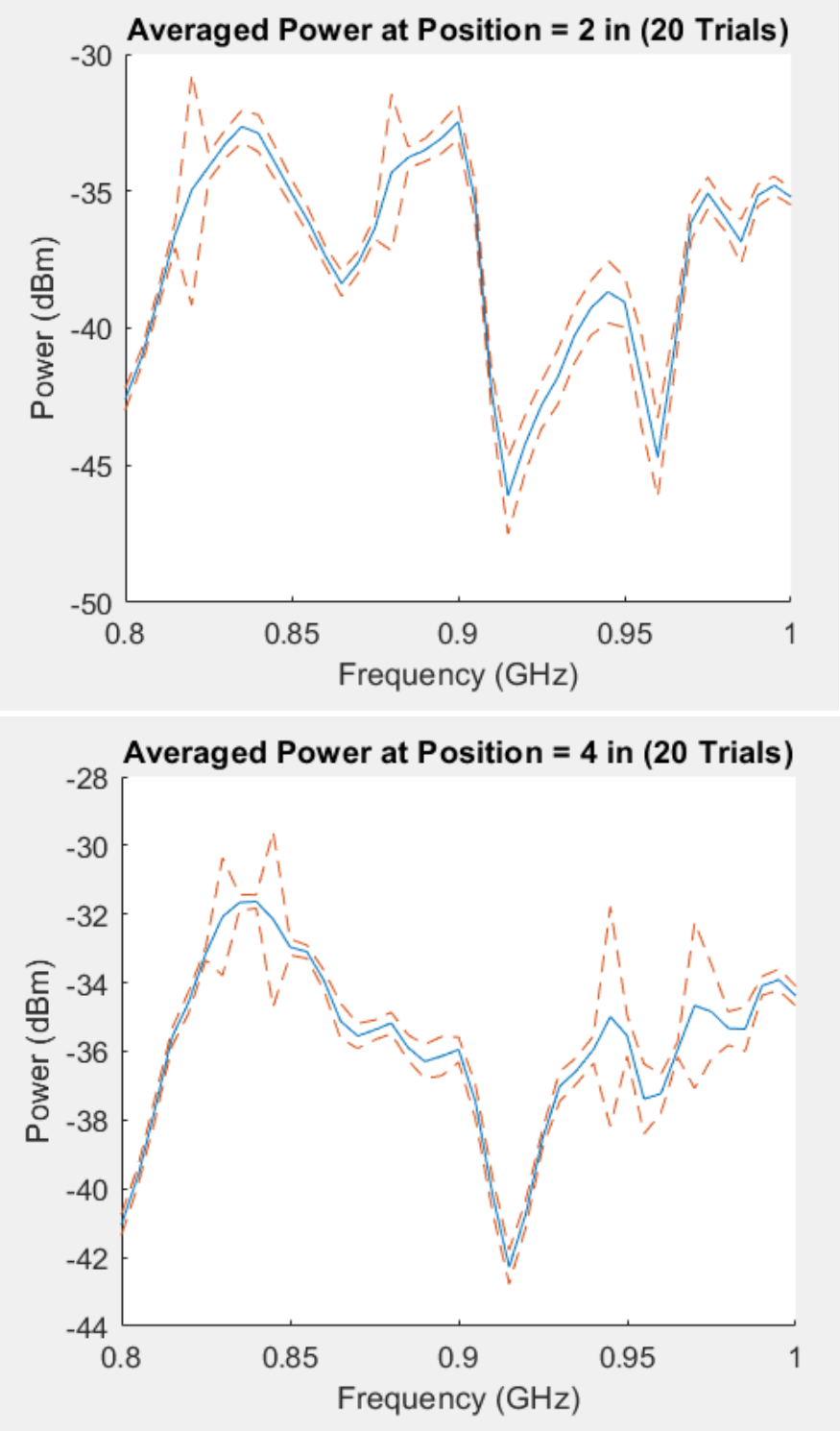

Figure 72 2-D plot for averaged power at each position

The envelopes in the plots provide new references in predicting the antenna's feasibility with the neural network. First, the definition of the confidence level suggests that the system is

stable when the confidence envelop stays narrow. In addition, when the envelope of two positions are close to each other, the two positions would be difficult to be distinguished by a neural network. For example, if we put the plot from the third and fifth position into one graph, Figure 73(a), we can see the two belts deviate from each other at most frequencies. However, if we see the third and fourth plot together, as it shown in Figure 73(b), the two belts overlap each other in a wide range, which is an undesired condition. Based on these two principles, we can choose the best antenna and then move forward.

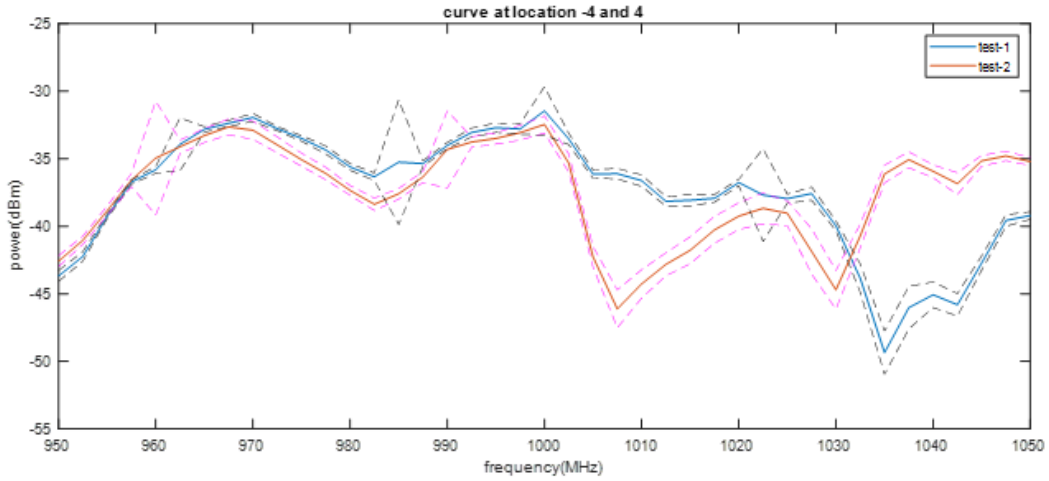

(a)

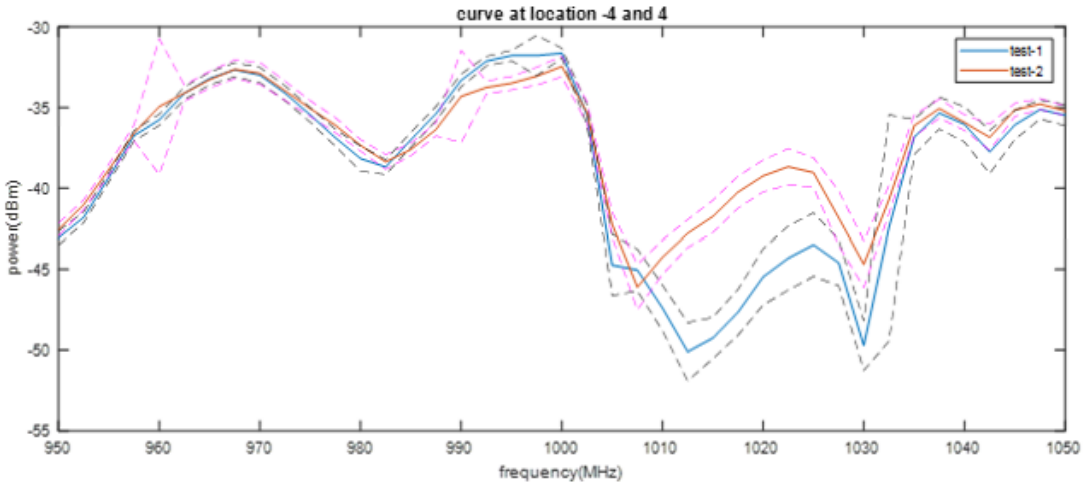

(b)

Figure 73 (a) distinguishable curve patterns (b) indistinguishable curve patterns

5.3 Predicting the Position with MATLAB Neural Network Toolbox

After a general evaluation of the 7 antennae shown in Figure 62, finally we choose the one shown in Figure 74(a) as the testing object, whose 3-D profile and 2-D average are shown in Figure 74(b) and (c). To make the prediction more convincing, the trial is repeated for a total of 150 data sets. The total sample size is 750 with 5 positions in each trial.

(a)

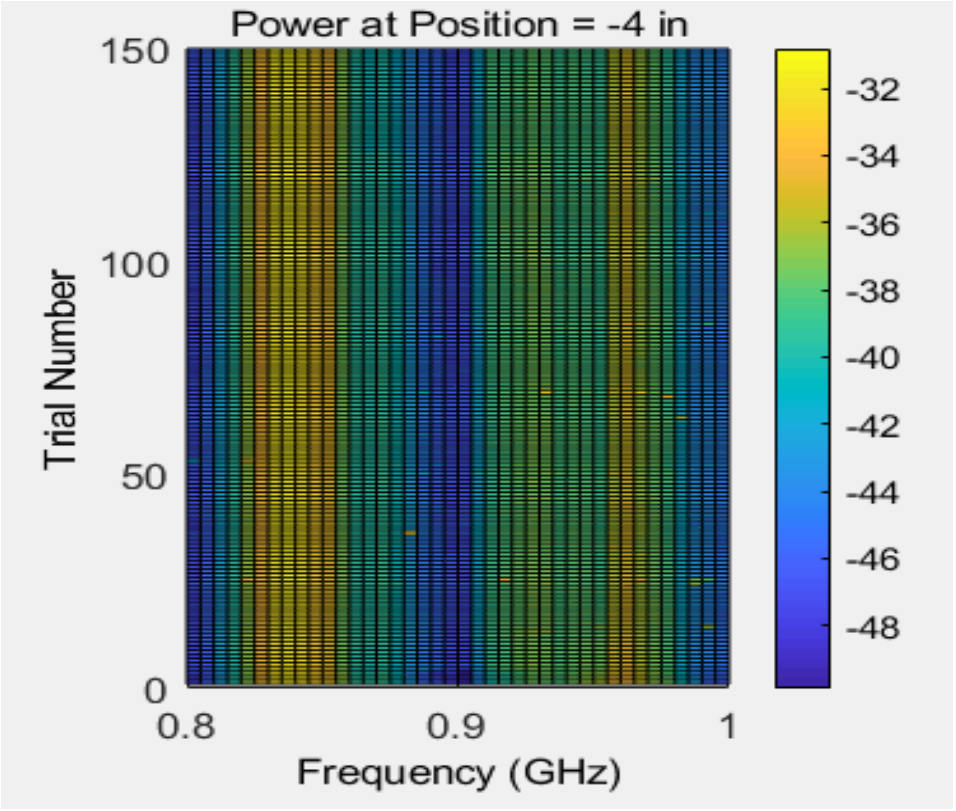
Power at Position = -4 in
150
100
50
0
Trial Number
0.8
0.9
1
Frequency (GHz)
-32
-34
-36
-38
-40
-42
-44
-46
-48

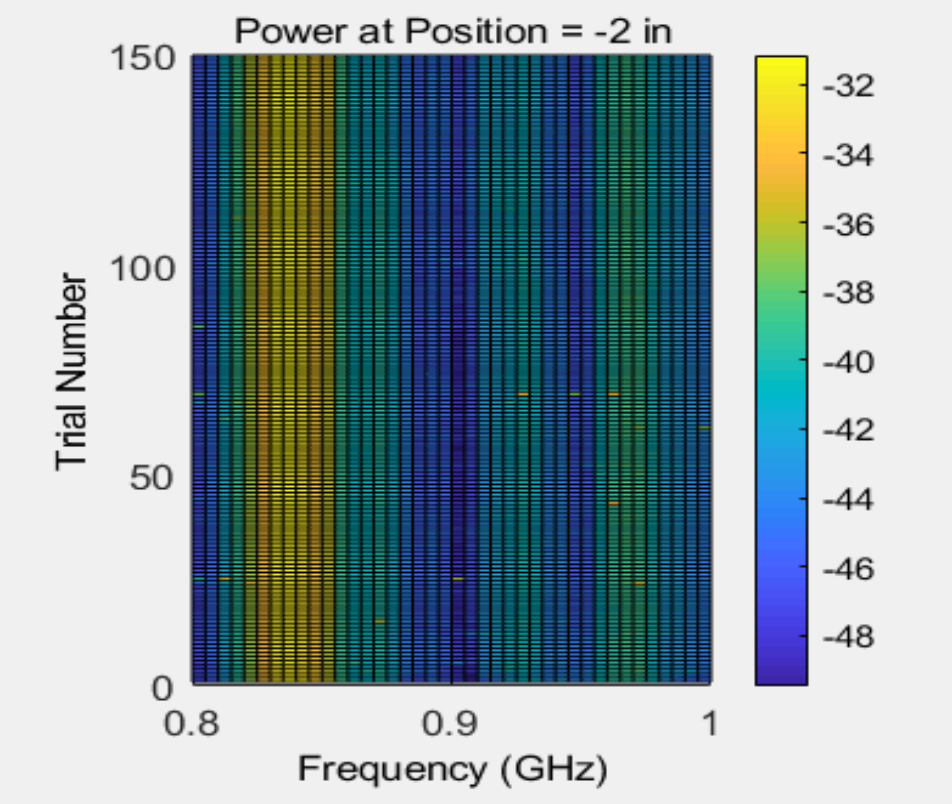
Power at Position = -2 in
150
100
50
0
Trial Number
0.8
0.9
1
Frequency (GHz)
-32
-34
-36
-38
-40
-42
-44
-46
-48

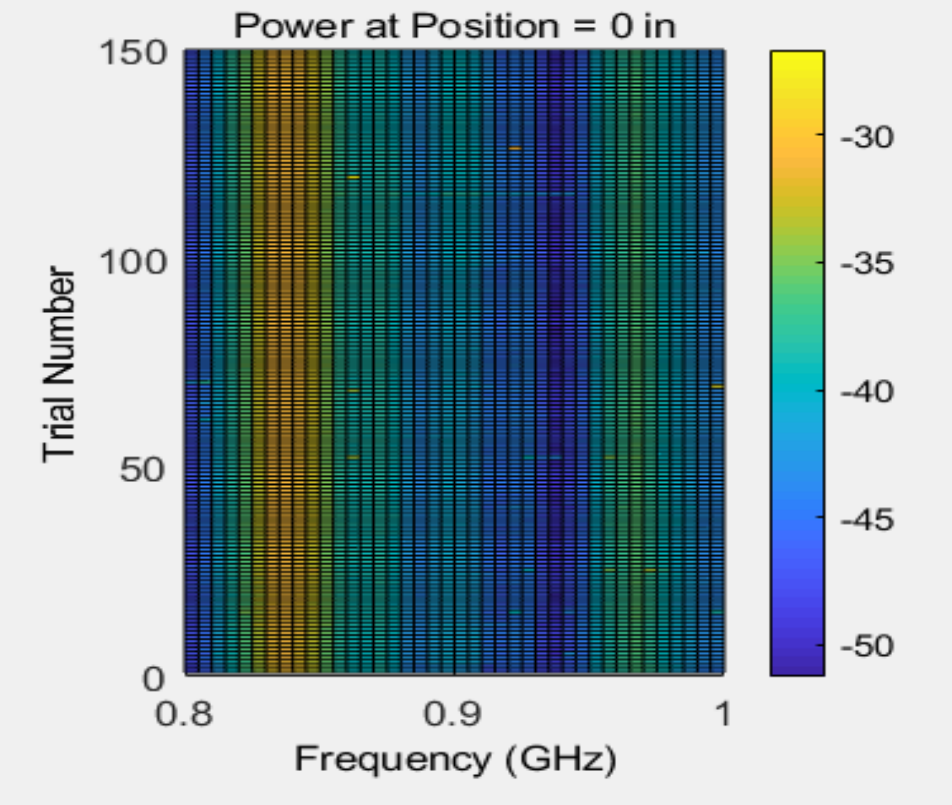
Power at Position = 0 in
150
100
50
0
Trial Number
0.8
0.9
1
Frequency (GHz)
-30
-35
-40
-45
-50

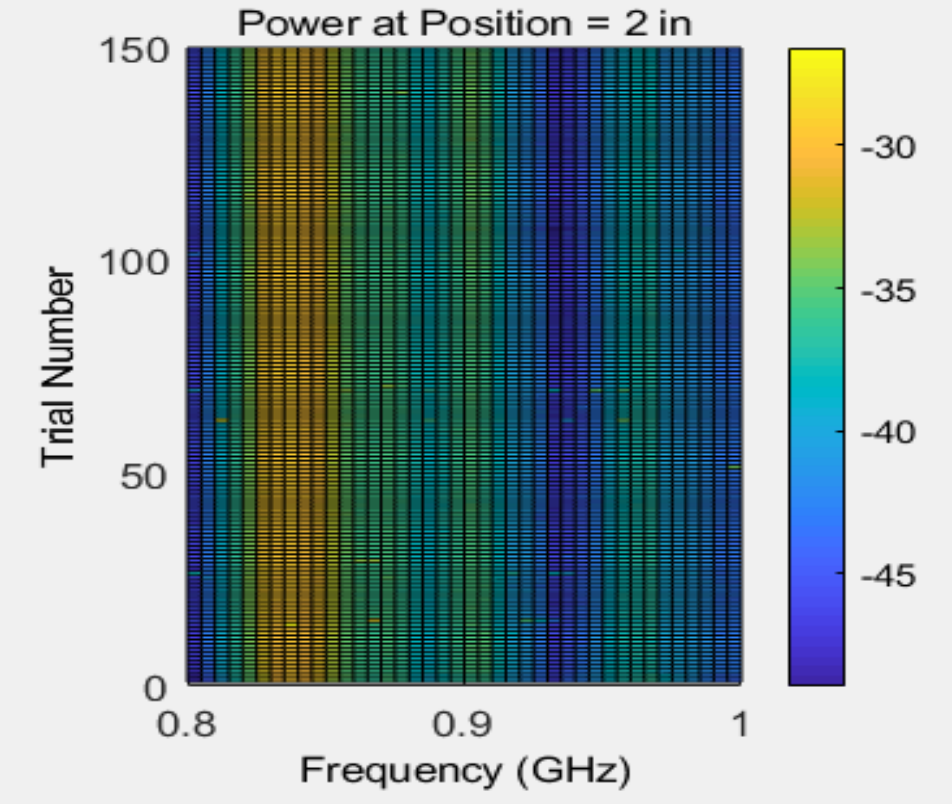
Power at Position = 2 in
150
100
50
0
Trial Number
0.8
0.9
1
Frequency (GHz)
-30
-35
-40
-45

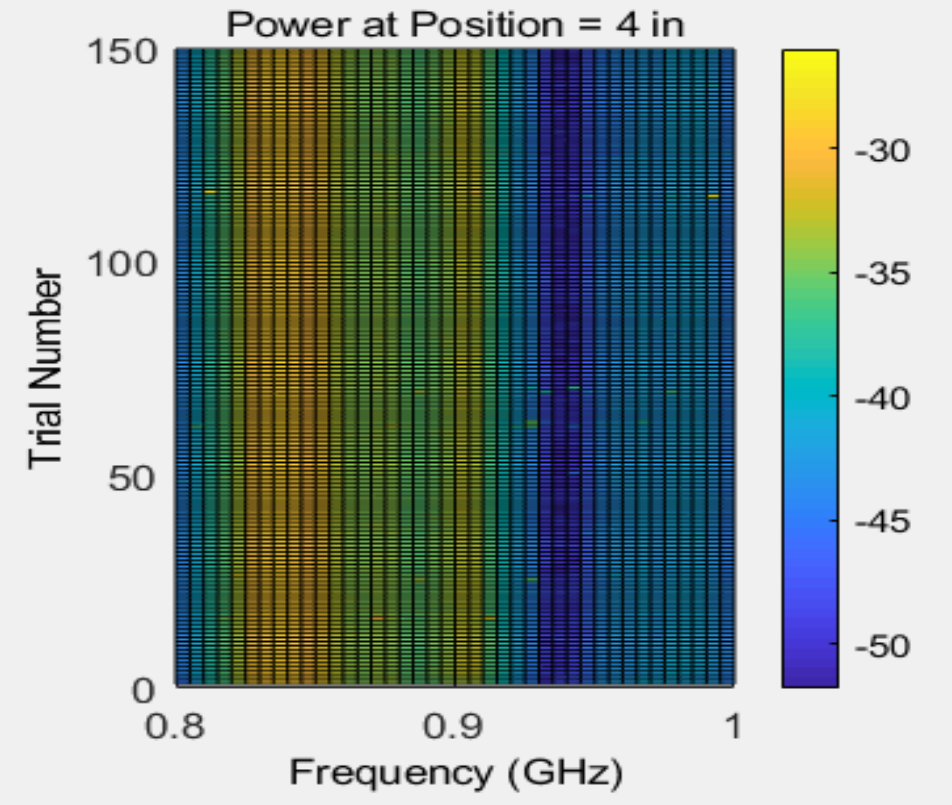
Power at Position = 4 in
150
100
50
0
Trial Number
0.8
0.9
1
Frequency (GHz)
-30
-35
-40
-45
-50

(b)

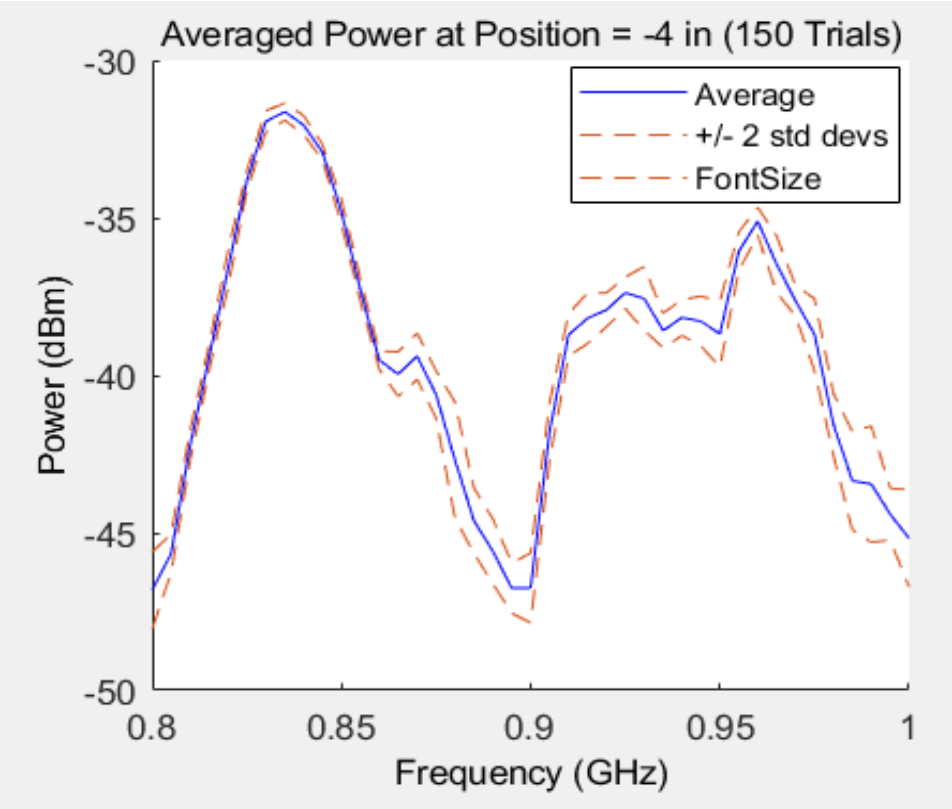
Averaged Power at Position = -4 in (150 Trials)
Average
+/- 2 std devs
FontSize
Power (dBm)
-30
-35
-40
-45
-50
0.8
0.85
0.9
0.95
1
Frequency (GHz)

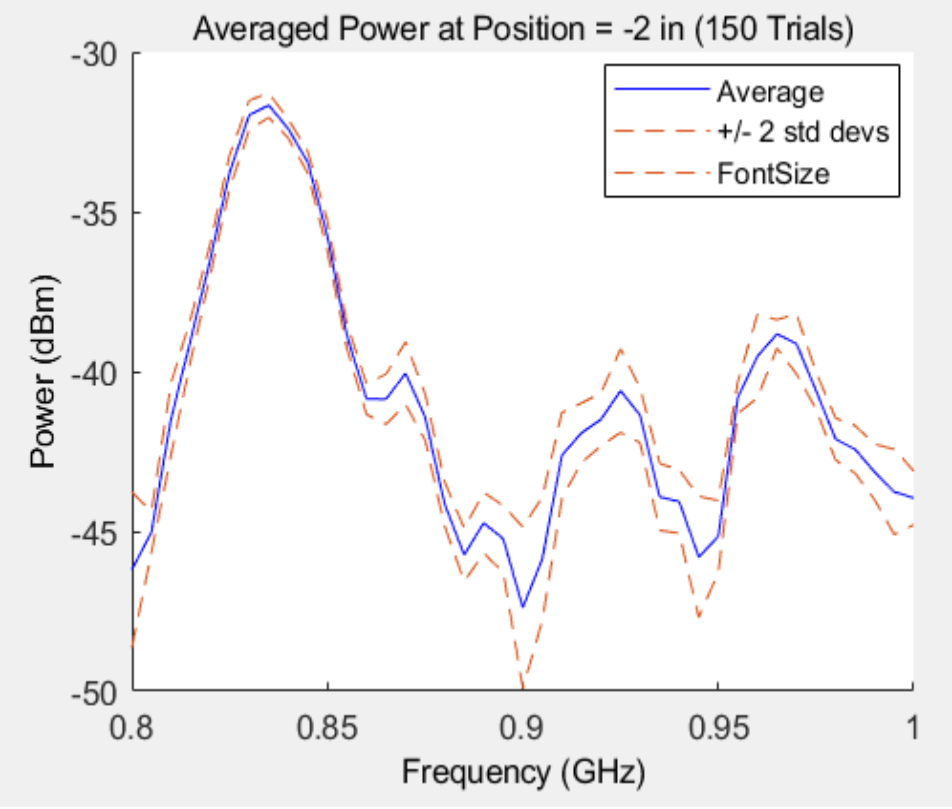
Averaged Power at Position = -2 in (150 Trials)
Average
+/- 2 std devs
FontSize
Power (dBm)
-30
-35
-40
-45
-50
0.8
0.85
0.9
0.95
1
Frequency (GHz)

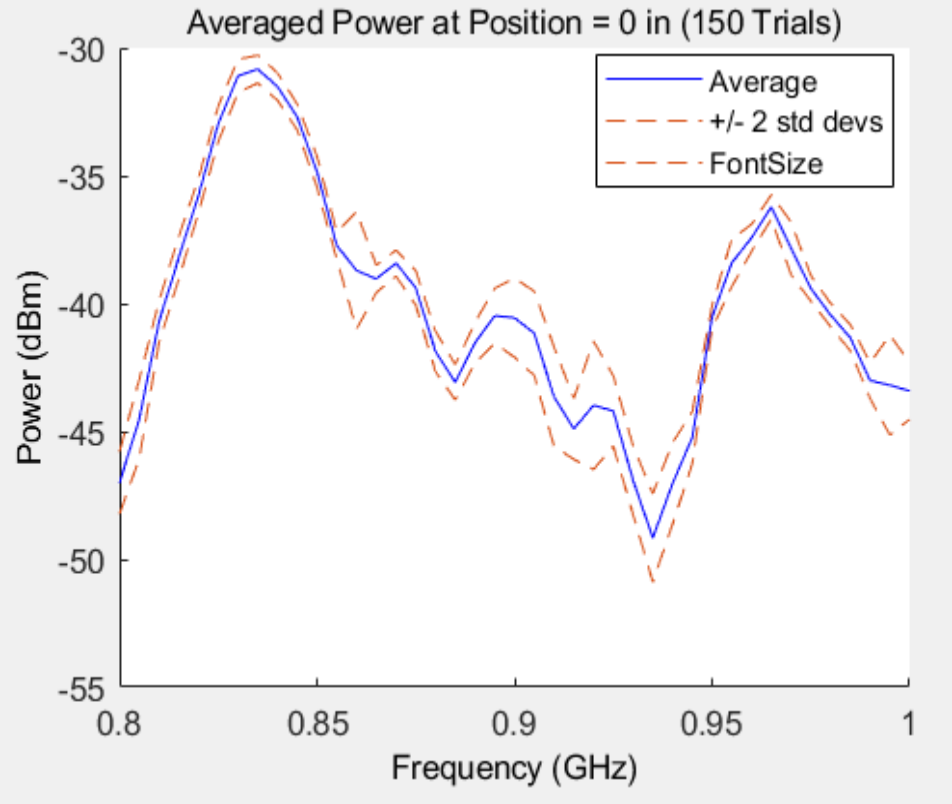
Averaged Power at Position = 0 in (150 Trials)
Average
+/- 2 std devs
FontSize
Power (dBm)
-30
-35
-40
-45
-50
-55
0.8
0.85
0.9
0.95
1
Frequency (GHz)

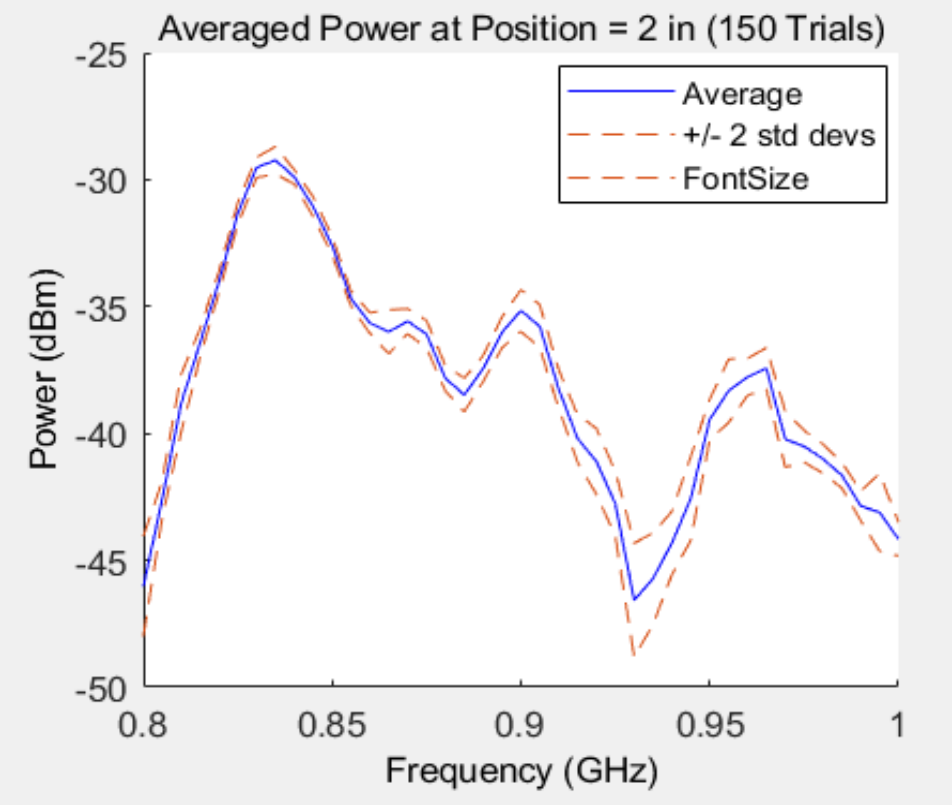
Averaged Power at Position = 2 in (150 Trials)
Average
+/- 2 std devs
FontSize
Power (dBm)
-25
-30
-35
-40
-45
-50
0.8
0.85
0.9
0.95
1
Frequency (GHz)

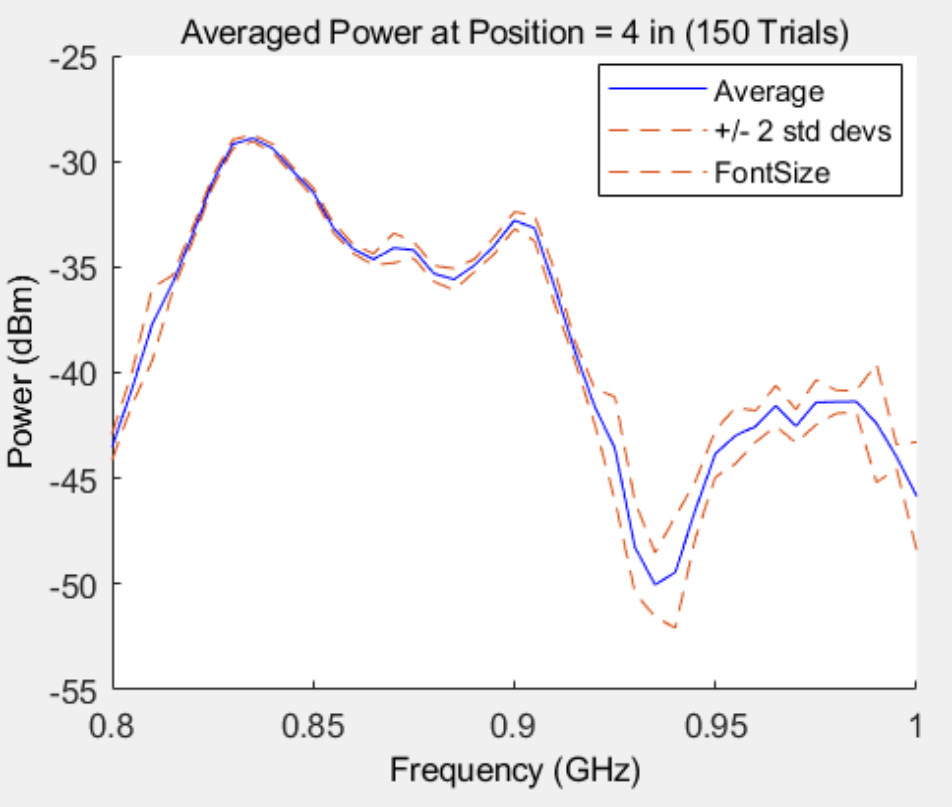

(c)

Figure 74 (a)the antenna for neural network (b)the 3-D profile (c) the 2-D averaged power

The neural network toolbox in MATLAB separates the data into three groups: training, validation and testing. The training group, usually occupying 70% of all the data, is applied to the training algorithm, and keeps updating itself according to the error. The validation group occupies 15%. This group is used as measure the network generalization on a new group unseen during training, and halts training process when the generalization stops improving. The last group also uses 15% of the data and has no effects on the training algorithm. It is an independent measure for an already trained network. (The Matworks Inc. 2017)

The classification accuracy can be clearly seen from the confusion matrix in Figure 75. The known positions -4, -2, 0, 2, 4 are classified into class 1-5. For each test, if the neural network classification (output class) is the same as the real condition (target class), it falls into

one of the green boxes on the diagonal. Incorrect classification will fall into the red boxes. For example, in the second validation confusion matrix, there is a ‘1’ that lies in the fifth row, fourth column. This suggests there is one data sample which was collected at position ‘5’, while the neural network classification is position ‘4’. Instead of the synthesis of all confusion matrices, we focus on the test confusion matrix because it is an independent measure for the trained network. Therefore, after the training is complete, the accuracy of the classification can be determined by the diagonal vs off-diagonal values in the test confusion matrix. For this antenna, it shows a high reliability of correct antenna location determination because the classification accuracy is 100%.

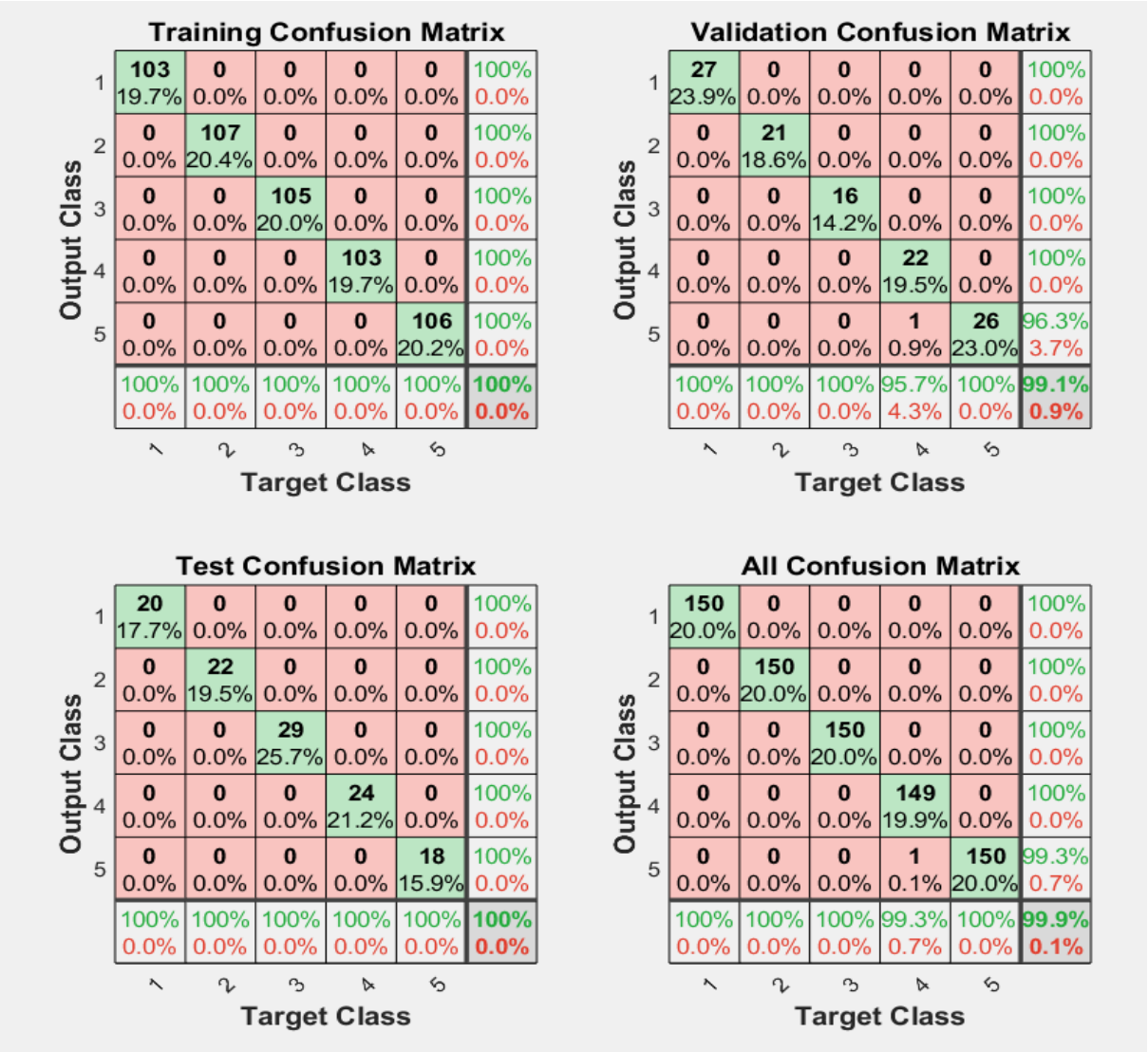

Figure 75 Confusion matrix for neural network

5.4 Problems and Future Directions

It has been shown that the neural network accuracy is almost perfect. However, the success prediction is based on many restrictions, which are difficult to achieve in practice. The first restriction is the position resolution, which is 2 inches for all the tests introduced. However, when the increment is reduced to 0.5 centimeters, according to the surgery requirements, the averaged curves tend to be the same in both shape and magnitude, as it shown in Figure 76(a). If one curve is too close to its adjacent curves, or even is located within the confidence envelop of another curve, then the neural network cannot distinguish one from another. From the confusion matrix shown in Figure 76(b), in such a case, we can see the predictions all belong to one class.

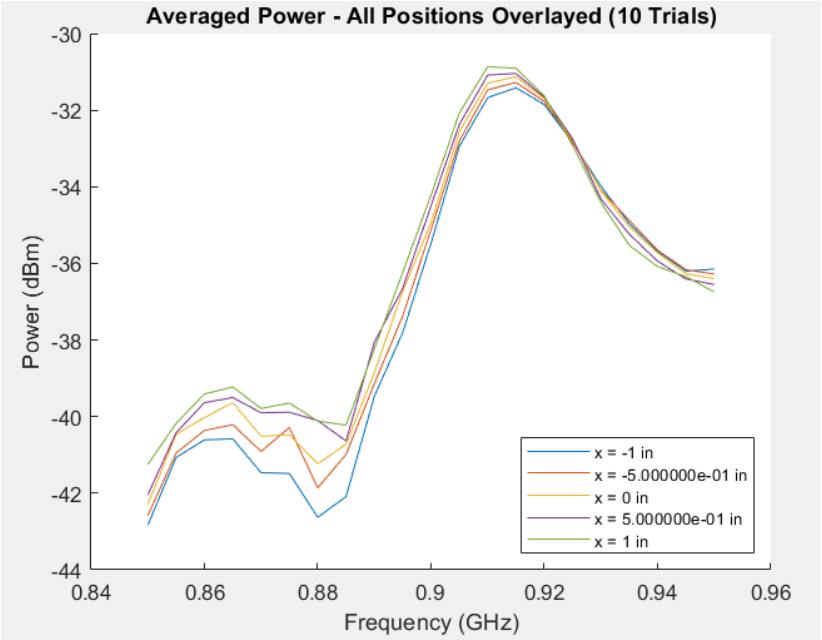

(a)

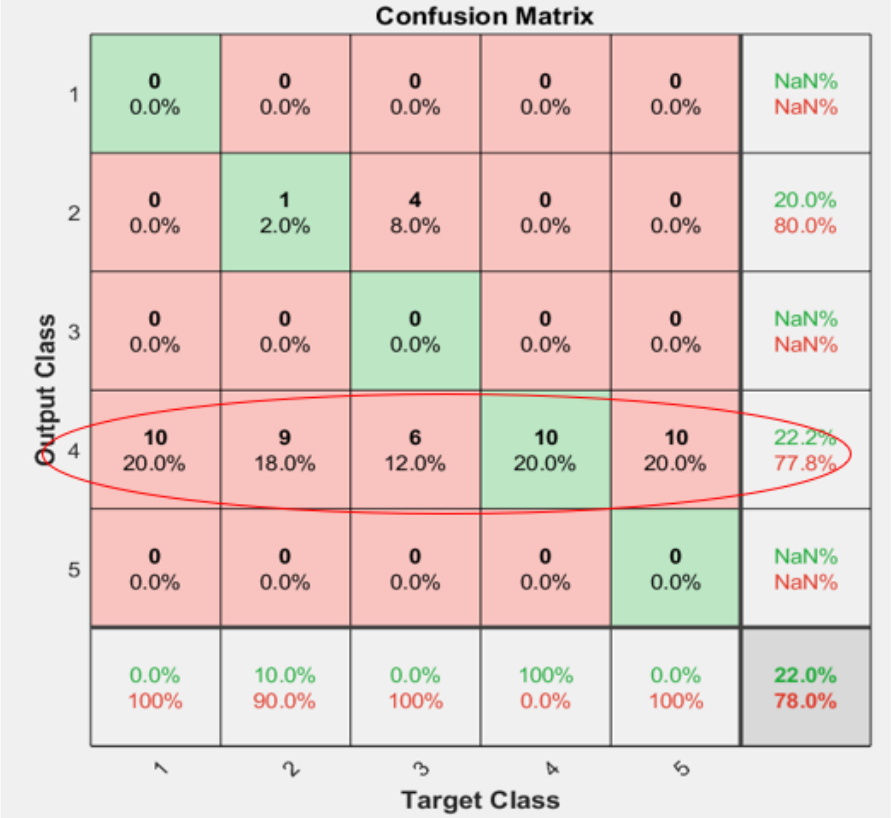

(b)

Figure 76 Test result with 0.5cm position resolution (a)averaged power curves (b)prediction result

The second problem is the susceptibility of the system. As we introduced, the automated rail creates a repeatable condition. The repeatability results in perfect prediction by applying training data and testing data come from one set of trials. However, such perfect conditions cannot be achieved in practice where the test data will be collected separately from the training data. That's why we need a certain robustness to condition changes. The patterns can become completely different with any trivial change in the system.

For example, the actual route in human artery has ups and downs instead of being straight, which is the condition for our simulation using the rail. This practical condition results in the variation of relative height between the receiver and the transmitter. Figure 77 shows the Comparison of received spectrum for a relative height difference of 1 cm. By simply

visualizing, the two curves are still similar in shape and magnitude. However, when analyzed by neural network, the accuracy drops to 42% as it shown in Figure 78.

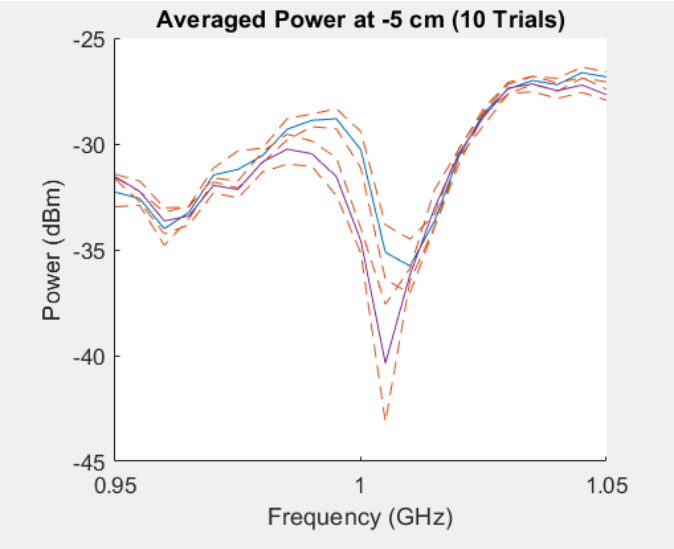

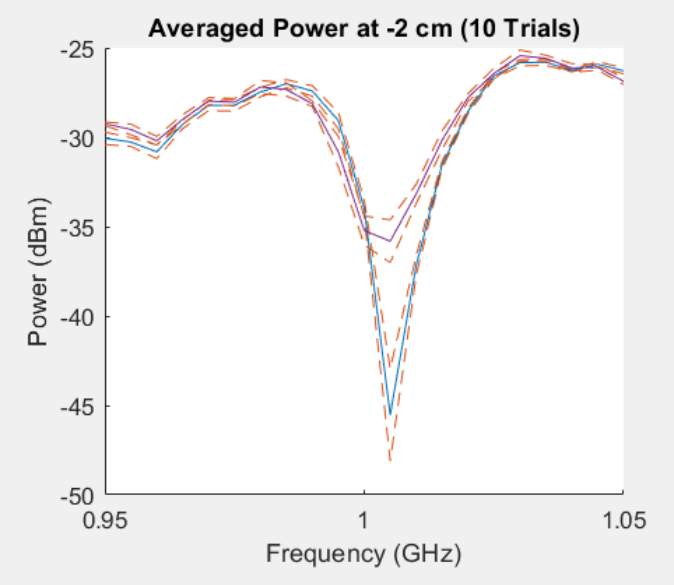

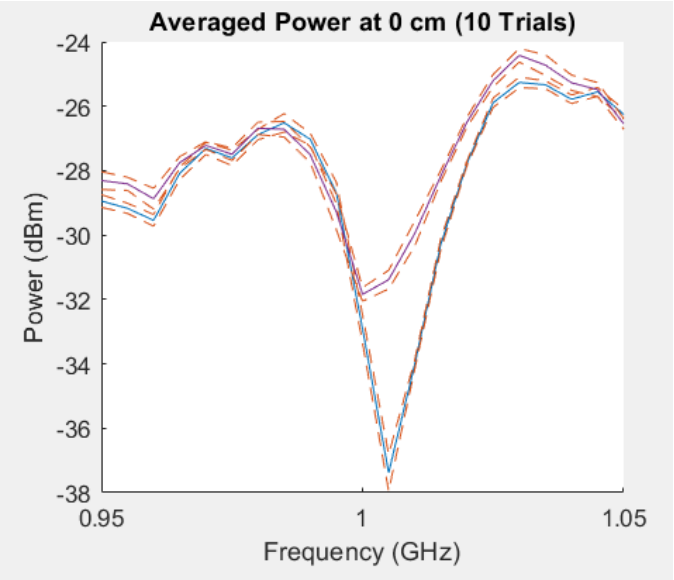
Averaged Power at 0 cm (10 Trials)
-24
-26
-28
-30
-32
-34
-36
-38
Power (dBm)
0.95
1
1.05
Frequency (GHz)

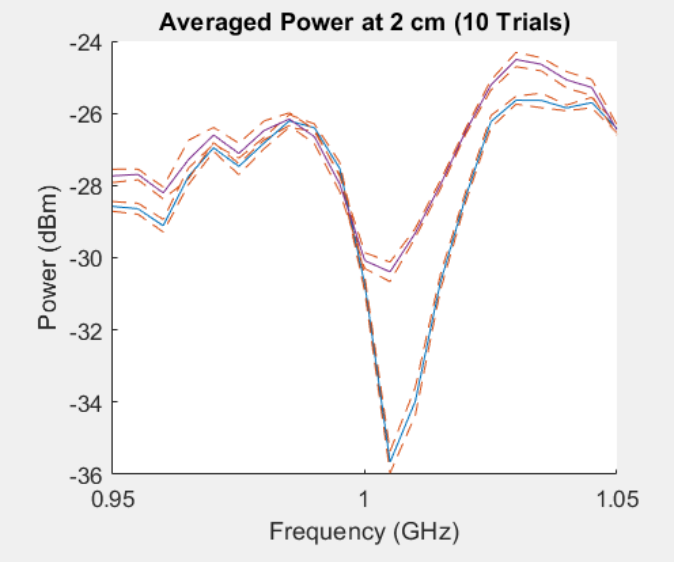
Averaged Power at 2 cm (10 Trials)
-24
-26
-28
-30
-32
-34
-36
Power (dBm)
0.95
1
1.05
Frequency (GHz)

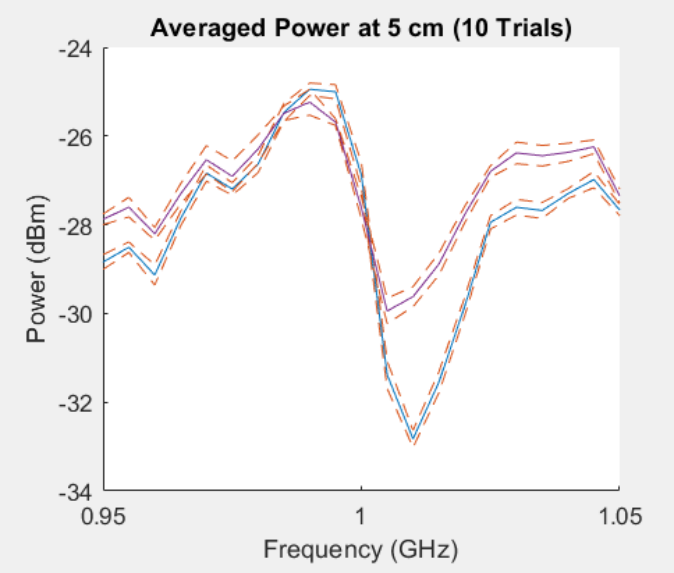

Figure 77 Relative height difference with 1cm

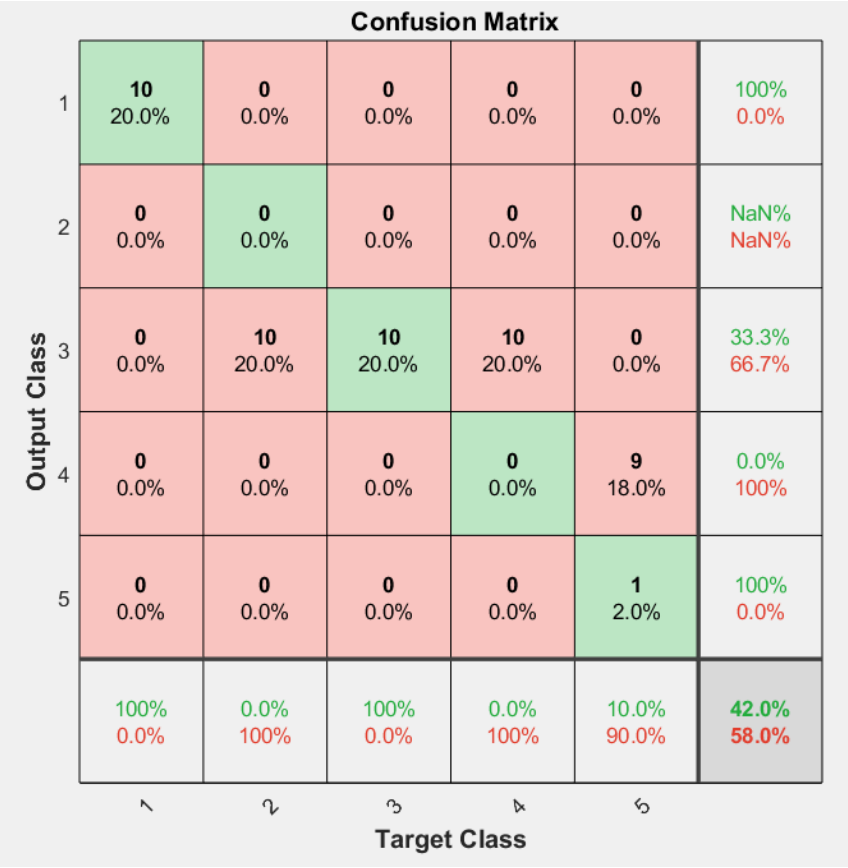

Figure 78 Classification result for two tests that different in the relative height

To solve these problems, improvements can be managed on all parts in the system. For example, except the loop antenna we kept revising, there might be antennae with more powerful and distinguishable radiation patterns like dipole, monopole, and array antenna. In addition, we can seek for other materials which are available to carry the circuit, while being more flexible for deployment.

The transmission lines have been proved to be a main source of interference signal. Two assumptions are raised to minimize its effects. The first solution is to shield the signal by wrapping the coaxial cable with RF absorbing sheets. It is simple for manipulation, though it could potentially attenuate the signal on the antenna, and results in difficulties for signal detection. The second method is to remove the cable and integrate the power source into the transmitter board. Through wireless power a remotely controlled antenna could be developed (Yakovlev et al, 2012), the difficulty is how to reduce the size of a power source into millimeter scale. Much efforts are still needed to reach the destination.

6.0 Conclusions

This thesis introduces the development of a radio frequency antenna for integration into a perfusion stent for location measurement inside the human body. The development started with a square loop antenna whose radiation is too weak to be detected, and improvements were made in all parts of the system to produce an antenna design that could penetrate the body. The system was tested and an algorithm was developed with which to determine antenna location using a neural network.

From the aspect of transmitter structure, we want it to be balanced and matched. The construction process was simulated in the ANSYS HFSS model. A balanced circuit is capable of resisting external noise and minimizing the radiation effect of the unbalanced coaxial cable. This is achieved by adding a proper balun after the antenna. A matched circuit maximizes the circuit efficiency, where the load impedance is the complex conjugate to the power impedance. There are two patterns of network used: square and L-cascaded. They both consist of capacitors, inductors and a balun. When the matching network is introduced, a peak occurs in the power gain curve because one system can only be perfectly matched at one frequency. The balanced and matched transmitter shows an evident increase in power magnitude.

Besides the circuit structure, another direction of improvement was regarding the antenna layout. Based on previous researches, the fundamental approach to increasing transmitted power is by increasing the antenna length. To expand the antenna size in its restricted space, we replaced the silicon substrate with polyamide, which could carry a longer

antenna while allowing it to be bent (rolled into a cylindrical shape) to fit into the catheter. The first improved layout started with the square loop antenna, then was extended in one direction. Based on the first one, the second layout introduced square turns along the extended sides. These two antenna layouts were combined with an L-cascaded network and were simulated at gradually increasing lengths to find the optimal length and number of added turns. The third layout was a square-wave antenna with square matching network. The last antenna design had the longest length, was shaped like fence, and was combined with a square matching network. The test result showed the first and second transmitter to have higher power than the third and fourth, which suggest the L-cascaded matching network leads to a better performance. The difference between the first and the second is minor, which means that the antenna layout is not a significant factor if they have similar size and shape.

Then we tested our flexible antenna in the pig body. The results presented in 3-D profile contains the potential relation between the received power with the transmitter location and frequency. These profiles also suggest the radiation intensity from the improved circuit boards could penetrate body tissue and deliver the information we want.

In the last stage, we developed the automated rail system to collect abundant training data with which to train and to increase the reliability of the neural network. Finally, we achieved an accuracy of over 99% in predicting the transmitter location, which means the basic propose of this thesis is accomplished.

Bibliography

Analyzer, Spectrum. 2011. “User’s Guide DSA800 Series Spectrum Analyzer.”

Astin, Angela Didomenico. 1999. “Finger Force Capability: Measurement and Prediction Using Anthropometric and Myoelectric Measures.”

Balanis, Constantine a. 2012. Electronics and Power *Antenna Theory: Analysis and Design*.

Bowick, Christopher Blyler, John Ajluni, Cheryl. *RF Circuit Design*. (September 3, 2018).

Breed, By Gary. 2008. “Improving the Bandwidth of Simple Matching Networks.” *Circuit Design*

Brohi, Karim. 2002. “Peripheral Vascular Trauma.” *CardioVascular and Interventional Radiology* 32(March):

Brownlee, Jason. 2000. “2000 Telecommunications Technology Council Report.”

Burgt, Martin J Van Der, Senior Product, Engineering Project, and Belden Electronics Division. 2003. “Coaxial Cables and Applications.”

Chow, Eric Y. et al. 2009. “High Frequency Transcutaneous Transmission Using Stents Configured as a Dipole Radiator for Cardiovascular Implantable Devices.”

Chun, Youngjae et al. 2017. “A Retrievable Rescue Stent Graft and Radiofrequency Positioning for Rapid Control of Noncompressible Hemorrhage.” *Journal of Trauma and Acute Care Surgery.*

Compton, C. 2005. “Peripheral Vascular Trauma.” *Perspectives in Vascular Surgery and Endovascular Therapy* 17.

Ding, Yicheng. 2018. “Radio Frequency Antenna Design and Test.” University of Pittsburgh.

Dsg, Guide, Series Rf, and Signal Generator. 2013. “User’s Guide DSG3000 Series RF Signal Generator.”

Finkenzeller, Klaus. 2010. RFID Handbook: Fundamentals and Applications in Contactless Smart Cards, Radio Frequency Identification and near-Field Communication

Floyd, Raymond E. 2015. “Tracking Applications.”

Foody, Giles M. 2009. “Sample Size Determination for Image Classification Accuracy Assessment and Comparison.” *International Journal of Remote Sensing*.

Heights, Columbia, N Roger, and Maple Grove. 1995. “United States Patent

Jin-Chung Shih, Kao-Lang Liu. 2005. “Temporary Balloon Occlusion of the Common Iliac Artery: New Approach to Bleeding Control during Cesarean Hysterectomy for Placenta Percreta.” *American Journal of Obstetrics and Gynecology*.

Kays, Roland et al. 2011. “Tracking Animal Location and Activity with an Automated Radio Telemetry System in a Tropical Rainforest.” *Computer Journal*.

Kim, H. S. et al. 2006. “Life-Threatening Common Carotid Artery Blowout: Rescue Treatment with a Newly Designed Self-Expanding Covered Nitinol Stent.” *British Journal of Radiology*.

Kim, Jaehoon, and Yahya Rahmat-Samii. 2004. “Implanted Antennas inside a Human Body: Simulations, Designs, and Characterizations.” *IEEE Transactions on Microwave Theory and Techniques*.

Landt, Jeremy. 2005. “The History of RFID.” *IEEE Potentials* 24(4): 8–11.

Leivre.com. 2016. “Impedance Matching Network Designer.” http://leleivre.com/rf_lcmatch.html.

Lumenistic LLC. 2012. *Light Spectrum*. http://lumenistics.com/what-is-full-spectrum-lighting.

Manjulatha, V., and K. Ch Sri Kavya. 2016. “Implantable Antennas for Biomedical Applications.” *ARPN Journal of Engineering and Applied Sciences*.

Müller, Frank C. “Compressed and Expanded Peripheral Artery Stents.”

Regulators, High-current Low-dropout, General Description, and Typical Application. 2012. “Manual for Power Detector LTC5582.”

Scavée, Vincent et al. 2001. “Pseudoaneurysm of the Internal Carotid Artery: Treatment with a Covered Stent.” *CardioVascular and Interventional Radiology*.

Simon J. Crick, Mary N. SHeppard, Siew Yen Ho. 2018. “Anatomy of the Pig Heart : Comparisons with Normal Human Cardiac Structure.”

Sparkfun. “Easy Driver Hookup Guide” https://learn.sparkfun.com/tutorials/easy-driver-hook-up-guide.

Suykens, Johan A.K. 2014. “Introduction to Machine Learning with Python: A Guide for Data Scientists.”: 765–73. http://linkinghub.elsevier.com/retrieve/pii/B9780123965028000139.

Tech, Johanson. 2008. “High Frequency Ceramic Solutions."

TEORANTA, ARAN BIOMEDICAL. “PTFE Covered Stent.”

The Matworks Inc. 2017. “Pattern Recognition Network - MATLAB Patternnet.” *1994-2017*. https://de.mathworks.com/help/nnet/ref/patternnet.html.

Thom Graves, CMI. “Carotid Angioplasty for Carotid Occlusive Disease.” *Weil Cornell Brain and Spine Center*.

Transformers, Balun. “Basics Primer.”

Vychytil, A. et al. 1999. “Tidal Peritoneal Dialysis for Home-Treated Patients: Should It Be Preferred?” *American Journal of Kidney Diseases*.

Waight, P J et al. 1999. Environmental Health Directorate Health Protection Branch *Limits of Human Exposure to Radiofrequency Electromagnetic Fields in the Frequency Range from 3 KHz to 300 GHz A. Federal Departments and Agencies*.

Well, T I S. 1966. “Available Power Gain , Noise Figure , and Noise Measure.” *Ieee Transactions On Circuit Theory*.

Wikipedia. 2015. “Nickel Titanium.” *Wikipedia*: 1–8. https://en.wikipedia.org/wiki/Nickel_titanium.

Yakovlev, Anatoly, Daniel Pivonka, Teresa Meng, and Ada Poon. 2012. “A Mm-Sized Wirelessly Powered and Remotely.” *IEEE International Solid-State Ciircuits Conference*.